

# Sediment transport under sheetflow conditions

H. Koelewijn

Graduation committee: prof. ir. K. d'Angremond  
dr. ir. J. van de Graaff  
dr. ir. J.S. Ribberink  
ir P.J. Visser

November 1994

Delft University of Technology  
Department of Civil Engineering



# Contents

List of tables . . . . .	vii
List of figures . . . . .	ix
Summary . . . . .	xi
<b>1 Introduction . . . . .</b>	<b>1</b>
1.1 General . . . . .	1
1.2 Scope and outline of the present study . . . . .	2
<b>2 Theories on sheetflow and sediment transport under combined waves and currents . . . . .</b>	<b>5</b>
2.1 Basic flow equations . . . . .	5
2.2 Theories on bed shear stress . . . . .	7
2.2.1 Introduction . . . . .	7
2.2.2 Boundary layer flow model of Al-Salem . . . . .	7
2.2.3 Simplified models for bed shear stress under combined waves and currents . . . . .	9
2.2.3.1 Introduction . . . . .	9
2.2.3.2 Model of Ribberink/Van Rijn for combined wave-current flow	11
2.2.3.3 Model of Soulsby for combined wave-current flow . . . . .	11
2.2.3.4 Comparison of bed shear stress models . . . . .	12
2.3 Theories on sediment transport . . . . .	14
2.3.1 Introduction . . . . .	14
2.3.2 Transport models using bed shear stress . . . . .	15
2.3.3 Transport models using velocity moments . . . . .	17
2.3.4 Description of the model of Dibajnia and Watanabe (1992) . . . . .	18
<b>3 Experimental set-up . . . . .</b>	<b>21</b>
3.1 Introduction . . . . .	21
3.2 Large Oscillating Water Tunnel . . . . .	21

3.3	Imposed and measured parameters . . . . .	24
3.4	Measuring facilities and measuring techniques . . . . .	25
3.5	Experimental conditions and test programme . . . . .	31
3.6	Data acquisition and storage . . . . .	34
<b>4</b>	<b>Results of experiments and comparison with other experiments . . . . .</b>	<b>37</b>
4.1	Introduction . . . . .	37
4.2	Concentration profiles . . . . .	38
4.2.1	General . . . . .	38
4.2.2	Time averaged concentration profiles . . . . .	38
4.2.3	Time dependent concentration profiles . . . . .	44
4.3	Velocity profiles . . . . .	51
4.3.1	General . . . . .	51
4.3.2	Velocity profiles in the suspension layer . . . . .	51
4.3.3	Velocity profiles in the sheetflow layer . . . . .	55
4.4	Sediment fluxes . . . . .	59
4.4.1	General . . . . .	59
4.4.2	Flux profiles in the suspension layer . . . . .	61
4.4.3	Total flux profiles . . . . .	67
4.4.4	Discussion about sediment fluxes . . . . .	72
<b>5</b>	<b>Verification of sediment transport models . . . . .</b>	<b>75</b>
5.1	Introduction . . . . .	75
5.2	Comparison of transport models . . . . .	79
5.3	Influence of the bed-roughness height on transport models . . . . .	85
5.4	Influence of the bed shear stress model . . . . .	87
5.4.1	Existing models . . . . .	87
5.4.2	Alternative formulations . . . . .	89
<b>6</b>	<b>Summary of conclusions and recommendations for future research . . . . .</b>	<b>93</b>
6.1	Experimental research . . . . .	93
6.2	Transport modelling . . . . .	95
6.3	Recommendations for further research . . . . .	97

<b>Appendices</b> . . . . .	<b>99</b>
<b>A</b> Measuring techniques - General information and calibration . . . . .	101
<b>A1</b> Laser-doppler flow meter (LDFM) . . . . .	101
<b>A2</b> Electro-magnetic flow meter (EMF) . . . . .	101
<b>A3</b> Optical concentration meter (OPCON) . . . . .	102
<b>A4</b> Conductivity concentration meter (CCM) . . . . .	106
<b>A5</b> High speed video (HSV) . . . . .	109
<b>A6</b> Mass-conservation technique . . . . .	109
<b>B</b> Important non-dimensional parameters . . . . .	113
<b>C</b> Method of Soulsby/Ockenden to calculate bed shear stress . . . . .	115
<b>D</b> Influence of the side-walls on the velocity moment . . . . .	119
<b>E</b> Input and output of the sediment transport program . . . . .	125
<b>E.1</b> Input . . . . .	125
<b>E.2</b> Output . . . . .	127
<b>F</b> Tables . . . . .	129
<b>F.1</b> Tables with fluxes . . . . .	129
<b>F.2</b> Result of High speed video analysis . . . . .	134
<b>G</b> Listing of calculation modules of transport program . . . . .	139
<b>G.1</b> Introduction . . . . .	139
<b>G.2</b> Analysis of velocities . . . . .	139
<b>G.3</b> Calculation of critical shields parameter . . . . .	140
<b>G.4</b> Calculation of bed-roughness height . . . . .	140
<b>G.5</b> Modules to calculate bed shear stress . . . . .	141
<b>G.5.1</b> Bed shear stress according to Ribberink/ Van Rijn . . . . .	141
<b>G.5.2</b> Bed shear stress according to Soulsby/ Ockenden . . . . .	142
<b>G.5.3</b> Bed shear stress imported from 1-DV model of Al-Salem . . . . .	143
<b>G.6</b> Modules to calculate sediment transport . . . . .	144
<b>G.6.1</b> Transport calculated with Al-Salem's method . . . . .	144
<b>G.6.2</b> Transport calculated with the method of Ribberink and Al-Salem . . . . .	144
<b>G.6.3</b> Transport calculated with the method of Bailard . . . . .	145
<b>G.6.4</b> Transport calculated with the new method of Ribberink . . . . .	145
<b>G.6.5</b> Transport calculated with the method of Dibajnia and Watanabe . . . . .	146
<b>References</b> . . . . .	<b>149</b>
<b>List of Symbols</b> . . . . .	<b>153</b>



## List of tables

3.1	Test conditions . . . . .	31
3.2	Measuring programme . . . . .	32
4.1	Processed data . . . . .	37
4.2	Calculated values of concentration decay parameter . . . . .	38
4.3	Sediment transport rates, average . . . . .	59
4.4	Sediment fluxes divided in bed load and suspended load transport . . . . .	73
5.1	Conditions of tests involved in testing of models . . . . .	76
5.2	Sandtransport models with choices for $k_s$ and bed shear stress model . . . . .	79
6.1	Division in concentration layers . . . . .	94
C.1	Coefficients used to calculate bed shear stress . . . . .	116
D.1	Values of $C_1$ and $C_2$ . . . . .	120
D.2	Correction factors for measured transport series E . . . . .	121
D.3	Correction factors for measured transport series C . . . . .	122
F.1.1	Velocities and concentration measurements used in calculations of sediment fluxes for E1 . . . . .	129
F.1.2	Velocities and concentration measurements used in calculations of sediment fluxes for E2 . . . . .	130
F.1.3	Velocities and concentration measurements used in calculations of sediment fluxes for E3 . . . . .	130
F.1.4	Velocities and concentration measurements used to calculate sediment fluxes for E4 . . . . .	131
F.1.5	Sediment fluxes calculated for E1 . . . . .	131
F.1.6	Sediment fluxes calculated for E2 . . . . .	132
F.1.7	Sediment fluxes calculated for E3 . . . . .	132
F.1.8	Sediment fluxes calculated for E4 . . . . .	133
F.1.9	Sediment fluxes, total, wave- and current-related . . . . .	133
F.2.1	Grain velocities estimated with HSV-analysis for E1 . . . . .	134
F.2.2	Grain velocities estimated with HSV-analysis for E3 . . . . .	134
F.2.3	Grain velocities estimated with HSV-analysis for C . . . . .	135
F.2.4	Concentrations used in calculations of fluxes for E1 . . . . .	135

<b>F.2.5</b>	Concentrations used in calculations of fluxes for E3 . . . . .	135
<b>F.2.6</b>	Concentrations used to calculations of fluxes for C . . . . .	136
<b>F.2.7</b>	Sediment fluxes in the sheetflow layer for E1 . . . . .	136
<b>F.2.8</b>	Sediment fluxes in the sheetflow layer for E3 . . . . .	136
<b>F.2.9</b>	Sediment fluxes in the sheetflow layer for C . . . . .	137
<b>F.2.10</b>	Total fluxes in the sheetflow layer for E1 . . . . .	137
<b>F.2.11</b>	Total fluxes in the sheetflow layer for E3 . . . . .	138

## List of figures

2.1	Definition sketch . . . . .	5
2.2	Bed shear stress, comparison of formulation Ribberink and Soulsby . . . . .	13
2.3	Typical velocity profile . . . . .	18
3.1	Large Oscillating Water Tunnel . . . . .	22
3.2	General outline of the recirculation system . . . . .	23
3.3	Imposed and measured parameters . . . . .	24
3.4	Transverse suction concentration meter . . . . .	27
3.5	OPCON configuration in the tunnel . . . . .	28
3.6	Electro-magnetic velocity meter . . . . .	29
3.7	Laser-beam configuration in the tunnel . . . . .	29
3.8	CCM configuration in the tunnel . . . . .	30
3.9	Grain-size distribution . . . . .	35
4.2.1	Averaged concentration profile (OPCON and suction) on log-scale . . . . .	40
4.2.2	Averaged concentration profile of CCM-measurements . . . . .	40
4.2.3	Combined averaged concentration profile of OPCON, Suction and CCM (E1-E4) . . . . .	41
4.2.4	Averaged concentration profile of all tests combined . . . . .	43
4.2.5	Ensemble averaged concentration profiles OPCON (E1-E4) . . . . .	46
4.2.6	Ensemble averaged concentration profiles CCM (E1-E4) . . . . .	48
4.2.7	Concentration profiles in the sheetflow layer . . . . .	50
4.3.1	Averaged velocity, measured by LDFM and EMF . . . . .	52
4.3.2	Ensemble averaged velocity, measured by LDFM (E1 & E3) . . . . .	53
4.3.3	Ensemble averaged velocity, measured by LDFM, wave-related part (E1 & E3) . . . . .	54
4.3.4	Time dependent velocities at various elevations in the sheetflow layer (E1, E3 & C) . . . . .	57
4.3.5	Horizontal grain velocity profiles in the sheetflow layer (E1, E3 & C) . . . . .	58
4.4.1	Averaged erosion of the bed during the experiments . . . . .	60
4.4.2	Measured sediment transport rates over the test section . . . . .	61
4.4.3	Averaged sediment fluxes, total, wave- and current-related (E1-E4) . . . . .	63

4.4.4	Combined plot of sediment fluxes in the suspension layer (total, wave- and current-related) . . . . .	64
4.4.5	Ensemble averaged sediment fluxes in the suspension layer (E1-E4) . . . .	65
4.4.6	Combined net flux profiles in sheetflow and suspension layer (E1 & E3) .	69
4.4.7	Time dependent fluxes at various elevations in the sheetflow layer (E1, E3 & C) . . . . .	70
4.4.8	Horizontal flux profiles in the sheetflow layer (E1, E3 & C) . . . . .	71
5.1.1	Schedule of sand transport program . . . . .	77
5.1.2	Calculation module of sand transport program . . . . .	78
5.2.1	Comparison sandtransport models, $k_s = D_{50}$ . Bed shear stress acc. to Ribberink/Van Rijn . . . . .	81
5.2.2	Comparison sandtransport models, $k_s = 3 \cdot D_{90}$ . Bed shear stress acc. to Ribberink/Van Rijn . . . . .	82
5.2.3	Comparison sandtransport models, $k_s = 3 \cdot D_{90}$ . Bed shear stress acc. to Soulsby/Ockenden . . . . .	83
5.2.4	Time dependent bed shear stress for some tests . . . . .	84
5.3.1	Influence of bed-roughness height on transport model of Ribberink . . . . .	86
5.4.1	Influence of bed shear stress model on transport model of Ribberink . . . .	87
5.4.2	Time dependent bed shear stress for test E3 . . . . .	88
5.4.3	Alternative formulations for bed shear stress . . . . .	90
5.4.4	Alternative model for bed shear stress applied to Ribberink's transport model . . . . .	91
5.4.5	Ribberink's transport model . . . . .	91
A3.1	Calibration OPCON - concentration . . . . .	104
A3.2	Influence of D50 on OPCON calibration . . . . .	104
A3.3	Calibration OPCON as a function of elevation . . . . .	105
A3.4	Calibration constant OPCON fitted polynomial curve . . . . .	105
A4.1	CCM calibration . . . . .	107
A4.2	Sensing volume of CCM . . . . .	108
B.1	Critical Shields parameter . . . . .	114
D.1	Measured velocity profile over cross-section . . . . .	122
D.2	Correction factors for measured sediment transport . . . . .	123

## Summary

Important changes in the coastal profile can appear in a few hours during storm conditions. During these conditions it is difficult to conduct measurements in the field, especially in the region of most interest (very near to the bed). Because of the complex physics of the problem it is not possible to make a proper scale model. Also full scale measurements in laboratories are scarce because they demand costly facilities. To fill this lack of data oscillating water tunnels were built. An oscillating water tunnel offers the possibility to simulate the near bed velocity under waves on a full scale.

During the present study experiments were conducted in the oscillating water tunnel of DELFT HYDRAULICS. The main scope of this study is to obtain data for the verification and development of sediment transport models. The series of water tunnel experiments were focused on sheetflow conditions (= flat bed) under sinusoidal waves combined with a current. Measurements were aimed on detailed time dependent research in the sheetflow and suspension layer.

The following measuring devices were used to measure concentration: a conductivity concentration meter (CCM) and an optical concentration meter (OPCON) to measure respectively in the sheetflow and in the suspension layer. Further time averaged concentrations were measured with a transverse suction system, the obtained sand samples were used to obtain a  $D_{50}$  distribution in the vertical. Velocities were measured with an electro-magnetic flow meter (EMF) and a laser-doppler flow meter (LDFM) in the suspension layer. Grain velocities in the sheetflow layer were estimated with help of a high speed video technique (HSV). Time averaged sediment transport was measured with help of a mass-conservation technique.

Four different test conditions were studied concerning sinusoidal waves combined with a net current all with approximately the same third-order velocity moment ( $\langle u^3 \rangle$ ). More than one hundred tests were executed during October and November 1993 in the laboratory of DELFT HYDRAULICS in De Voorst. The investigation was part of the EU program "Access to Large-scale Facilities and Installations". The analysis of the raw data was conducted by the different members of the research team. A complete overview of this processed data can be found in a data report (Katapodi et al, 1994).

'Intra-wave' concentrations and velocities were determined by ensemble averaging over a number of waves of the measurements data. The HSV-technique was not useful to determine very accurate velocities in the sheetflow layer, but it is a useful tool to gain qualitative insight in the processes in the sheetflow layer.

The obtained time dependent concentrations and velocities were combined to time dependent sediment fluxes. Fluxes in the suspension layer could be obtained quite accurate. Fluxes in the sheetflow layer were not very accurate because of the uncertainty in the HSV-analysis. The obtained fluxes (in sheetflow and suspension layer) lead to the conclusion that the bed load transport was dominating over the suspended load transport, although the exact distribution could not be determined. Near the bed the wave-related flux is dominating over the current-related flux.

The measured time averaged sediment transport rates were used to test sediment transport models. In this testing also former wave tunnel tests with regular asymmetric waves combined with a net current were involved.

Five different quasi-steady sediment transport models were tested, namely:

- Two bed shear stress models: The model of Al-Salem/Ribberink and the new model of Ribberink
- Models using velocity moments: The model of Al-Salem and the model of Bailard
- The model of Dibajnia and Watanabe

The sediment transport models were combined, if necessary, with three different theories for the bed shear stress:

- The model of Soulsby/ Ockenden
- The model of Ribberink/ Van Rijn
- The boundary layer flow model of Al-Salem

Different bed-roughness heights were used in the sediment transport models,  $k_s = D_{50}$ ,  $k_s = 3D_{90}$  and  $k_s = 3\theta D_{90}$ .

The transport model of Bailard and the model of Al-Salem/Ribberink were overestimating the transport rate for all combinations. Contrary the model of Dibajnia/Watanabe underestimated the transport rate. The simple transport model of Al-Salem gave a good prediction for the measured transport rates.

The transport model of Ribberink showed good behaviour in combination with the bed shear stress formulation of Ribberink/Van Rijn and  $k_s = 3\theta D_{90}$ , but generally the calculated transport was a little overestimated. To improve the transport model the wave friction factor was adapted. This led to a satisfactory transport model.

The bed shear stress model of Ribberink/Van Rijn gave better results than the model of Soulsby/Ockenden.

For the present study quasi-steady modelling of the transport led to satisfactory results. Further research should be done in situations with smaller sediment to check whether intra-wave modelling is necessary.

# 1 Introduction

## 1.1 General

The interaction between waves, currents and the coast can result in sediment movement and eventually in coastal changes. The processes leading to these morphological changes are difficult to understand. At the present state of the art it is hardly possible to make accurate predictions of coastal changes.

Normally the transport of sediment at the coast is divided into two categories, namely transport along the coast (longshore transport) and transport perpendicular to the coast (cross-shore transport).

### *Longshore transport*

The longshore transport is caused by the wave-induced and/or tidal currents along the coast. The influence of the breaking waves and the oscillatory movement of the water cause sand to go in suspension, this suspended sand is transported by the net current. For this reason the transport is generally treated with a wave averaged concept. The time-scale of interest can be several years and it is possible to test formulas with in-situ measurements of coastal changes and wave characteristics.

### *Cross-shore transport*

The modelling of the cross-shore transport is more difficult. The oscillatory water movement, which is generally almost perpendicular to the coast, in combination with cross-shore currents, is responsible for the sediment transport. The transport is dominated by the processes in the wave-boundary layer (directly above the bed). Important changes in the coast-profile can appear in a few hours during storm conditions. During these conditions it is difficult to conduct measurements in the field, especially in the region of most interest (very near to the bed). Because of the complex physics of the problem it is hardly possible to make a proper scale model. Also full scale measurements in laboratories are scarce because they demand costly facilities.

This problem can be solved by using an oscillating water tunnel. In such a facility the water movement near the sea bottom under waves can be simulated on a full scale, without reproducing the waves over the full water depth. This kind of facilities is used in different parts in the world. Some of the tunnels also have the possibility to superimpose a current on the waves.

One of these large-scale facilities is found at DELFT HYDRAULICS. Since 1992 the tunnel has been extended with a recirculation system to make it possible to add a current to the oscillatory movement. Before the extension with the recirculation system different series of tests were carried out:

- Series A was focused on bed-forms and wave cycle averaged suspended sediment concentrations under sinusoidal waves.

- Series B was focused on measuring the wave cycle averaged sediment transport rates under regular and irregular asymmetric waves (Al-Salem, 1993).
- Series C was aimed at a time dependent description of the transport process under regular asymmetric waves (Al-Salem, 1993).
- Series D was focused on the influence of the grain diameter; test conditions concerned irregular and regular asymmetric waves (Ribberink and Chen, 1993).

After 1992 experiments were carried out under combined wave/current conditions:

- Series A was carried out to obtain net current profiles under currents combined with and without waves in a fixed bed condition (Ramadan, 1993).
- Series B was aimed at studying the behaviour of bed-forms under waves alone, net current alone and combinations of waves and currents (Ramadan, 1993)
- Series C was focused on time averaged suspended concentration profiles and net sediment transport rates under asymmetric waves combined with following and opposing currents, (Ramadan, 1993 and Ribberink, 1994).
- Series D was focused on the behaviour of bed-forms under regular asymmetric waves combined with different following and opposing currents. Special attention was paid to the transition of ripples to plane-bed/sheetflow conditions (Ribberink, 1994).

## 1.2 Scope and outline of the present study

The main scope of the present experiments (series E) was to obtain a detailed dataset concerning sheetflow conditions under waves combined with a current. The description is time dependent so both 'intra-wave<sup>1</sup>' and 'quasi-steady<sup>2</sup>' sediment transport models can be tested or developed. The measurements were especially focused on detailed intra-wave research in the sheetflow layer.

More than one hundred experiments were performed in the large oscillating water tunnel of DELFT HYDRAULICS during October and November 1993. The test conditions concern four different combinations of a sinusoidal wave and a current, all with approximately the same third-order velocity moment ( $\langle u^3 \rangle =$  the time averaged value of  $u^3(t)$ ). The experimental investigation was part of the EU programme "Access to Large-scale Facilities and Installations". To make the data accessible for other researchers a detailed data report was drawn up by the research team (Katapodi et al, 1994).

---

<sup>1</sup>) The transport is described within the wave-cycle with a time-scale much smaller than the wave period. First a total time dependent description of the flow and concentrations in and above the wave boundary layer is given. Transport is calculated afterwards by multiplying velocities and concentrations (memory effects are included).

<sup>2</sup>) Sediment transport is supposed to react instantaneously on changes in the velocity. Sediment transport is described as a function of the instantaneous velocities above the wave boundary layer or the instantaneous bed shear stress (memory effects are not included) .

Instantaneous sediment concentration profiles were measured in the suspension layer (using an optical concentration meter) and in the sheetflow layer (using a conductivity concentration meter). Time averaged concentration profiles were measured with a transverse suction system. Instantaneous velocity profiles were measured in the suspension layer using a laser doppler flow meter and an electro-magnetic flow meter. Grain velocities in the sheetflow layer were estimated with the help of high speed video recordings.

In the framework of this thesis part of the data processing of the series E experiments was done. The thesis was focused on the (time dependent and time averaged) distribution of the transport in the vertical. Attention is paid to the division of the transport in a bed load and a suspended load part. Different quasi-steady transport models were tested in combination with different bed shear stress theories.

First a review of the theoretical basics of wave-current interaction is given and some models to describe the bed shear stress and the net sediment transport rate are discussed (Chapter 2).

Chapter 3 gives the experimental setup of the series E tests. In Chapter 4 experimental results are presented time averaged and intra-wave. Net sediment fluxes are obtained in the sheetflow and suspension layer by multiplying measured time dependent concentrations and velocities. Attention is paid to the distribution of the transport in the vertical. The obtained results are compared with data of former research.

Different 'quasi-steady' sediment transport models (as described within Chapter 2) are tested with the measured data as input (Chapter 5). Also data of former experiments (Ramadan, 1993; Ribberink, 1994) were used for the model testing. Attention is paid to the modelling of the bed shear stress in combined wave-current flow. A summary of conclusions and recommendations for further research can be found in Chapter 6.



## 2 Theories on sheetflow and sediment transport under combined waves and currents

### 2.1 Basic flow equations

Balance equations are used to analyse the turbulent fluid motion above a fixed bed. Of particular importance is the balance equation for momentum: the 2-DV Navier Stokes equation in the horizontal direction (see Figure 2.1):

$$\frac{\partial u}{\partial t} + \frac{\partial u^2}{\partial x} + \frac{\partial uw}{\partial z} = -\frac{1}{\rho} \frac{\partial p}{\partial x} + \nu \left\{ \frac{\partial^2 u}{\partial x^2} + \frac{\partial^2 u}{\partial z^2} \right\} \quad (2.1)$$

In which:  $w$  = vertical velocity  
 $u$  = horizontal velocity  
 $p$  = pressure  
 $\nu$  = kinematic viscosity  
 $\rho$  = density  
 $t$  = time  
 $x$  = horizontal coordinate  
 $z$  = vertical coordinate

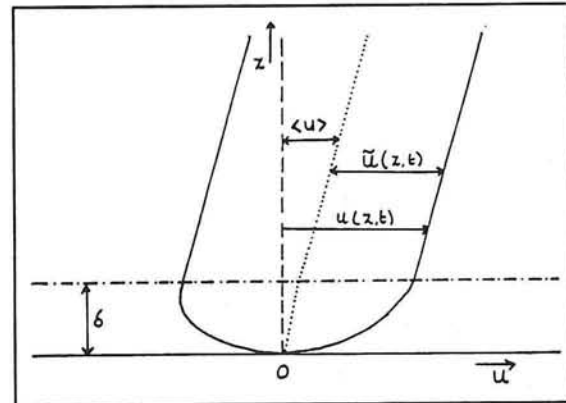


Figure 2.1 Definition sketch

Natural flows are almost always turbulent. Turbulence is brought into this equation by replacing total velocity (and pressure) by an averaged and a random part:

$$\begin{aligned} u &= \bar{u} + u' \\ w &= \bar{w} + w' \\ p &= \bar{p} + p' \end{aligned} \quad (2.2)$$

Herein:  $\bar{\dots}$  = averaged over turbulence time-scales  
 $\dots'$  = random component

Substituting this in equation 2.1 and averaging over the turbulence time-scales gives:

$$\frac{\partial \bar{u}}{\partial t} + \frac{\partial \bar{u}^2}{\partial x} + \frac{\partial \bar{u}^2}{\partial x} + \frac{\partial \bar{u} \bar{w}}{\partial z} + \frac{\partial \overline{u'w'}}{\partial z} = -\frac{1}{\rho} \frac{\partial \bar{p}}{\partial x} + \nu \left\{ \frac{\partial^2 \bar{u}}{\partial x^2} + \frac{\partial^2 \bar{u}}{\partial z^2} \right\} \quad (2.3)$$

The equation obtained is called the Reynolds equation; new in this equation are the turbulent Reynold stresses:  $-\overline{\rho u'w'}$  and  $-\overline{\rho u'^2}$ .

For the oscillating water tunnel this equation can be simplified by neglecting the horizontal derivatives  $\delta./\delta x$  of the velocity (horizontal oscillatory flow) and the knowledge that the mean velocity in z-direction is zero:

$$\rho \frac{\partial \bar{u}}{\partial t} = -\frac{\partial \bar{p}}{\partial x} - \rho \frac{\partial \overline{u'w'}}{\partial z} + \nu \rho \frac{\partial^2 \bar{u}}{\partial z^2} \quad (2.4)$$

The second term in the right part of the equation represents the turbulent Reynolds stresses:

$$\tau_{\text{turb}} = -\overline{\rho u'w'} \quad (2.5)$$

The Reynolds stresses depend on the turbulent motion; they add an extra unknown to the equation. A solution for this gives the Boussinesq hypothesis:

$$\tau_{\text{turb}} = \rho \nu_t \frac{\partial \bar{u}}{\partial z} \quad (2.6)$$

Herein:  $\nu_t$  = turbulent eddy viscosity

Using this in equation 2.4 gives:

$$\frac{\partial \bar{u}}{\partial t} = -\frac{1}{\rho} \frac{\partial \bar{p}}{\partial x} + \frac{\partial}{\partial z} \left\{ \nu_t + \nu \right\} \frac{\partial \bar{u}}{\partial z} \quad (2.7)$$

In case of turbulent boundary layer flow the turbulent eddy viscosity is much larger than the kinematic viscosity, so the next equation remains:

$$\frac{\partial \bar{u}}{\partial t} = -\frac{1}{\rho} \frac{\partial \bar{p}}{\partial x} + \frac{\partial}{\partial z} \left\{ \nu_t \frac{\partial \bar{u}}{\partial z} \right\} = -\frac{1}{\rho} \frac{\partial \bar{p}}{\partial x} + \frac{1}{\rho} \frac{\partial \tau}{\partial z} \quad (2.8)$$

For combined wave current flow  $\bar{u}$  and  $\bar{p}$  can be replaced by:

$$\begin{aligned} \bar{u} &= \bar{u} + \langle u \rangle \\ \bar{p} &= \bar{p} + \langle p \rangle \\ \tau &= \bar{\tau} + \langle \tau \rangle \end{aligned} \quad (2.9)$$

and the next equation is found in case of a steady (wave averaged) flow:

$$\rho \frac{\partial \bar{u}}{\partial t} = -\frac{\partial \langle p \rangle}{\partial x} - \frac{\partial \bar{p}}{\partial x} + \frac{\partial \langle \tau \rangle}{\partial z} + \frac{\partial \bar{\tau}}{\partial z} \quad (2.10)$$

Herein:  $\langle . \rangle$  = time averaged over a time-scale  $>$  period of oscillation

$\bar{.}$  = oscillating component

Averaging over the wave cycle gives:

$$\rho \frac{\partial \bar{u}}{\partial t} = -\frac{\partial \bar{p}}{\partial x} + \frac{\partial \bar{\tau}}{\partial z} \quad (2.11)$$

Above the wave-boundary layer ( $z > \delta$ ) the wave-related shear stress is disappearing:  $\bar{\tau} = 0$ , thus the equation can be rewritten as:

$$\rho \frac{\partial \bar{u}_\infty}{\partial t} = -\frac{\partial \bar{p}}{\partial x} \Leftrightarrow \rho \frac{\partial}{\partial t}(\bar{u} - \bar{u}_\infty) = \frac{\partial \bar{\tau}}{\partial z} \quad (2.12)$$

herein:  $u_\infty$  = velocity outside wave-boundary layer

Using the fact that time derivative of the averaged velocity is zero and filling in equation 2.12 in equation 2.10 gives finally:

$$\rho \frac{\partial}{\partial t}(\bar{u} - \bar{u}_\infty) = -\frac{\partial \langle p \rangle}{\partial x} + \frac{\partial \bar{\tau}}{\partial z} = -\frac{\partial \langle p \rangle}{\partial x} + \frac{\partial}{\partial z} \left( \nu_t \frac{\partial \bar{u}}{\partial z} \right) \quad (2.13)$$

With an additional model for  $\nu_t$  (turbulence closure) oscillatory flow velocity profiles and bed shear stress can be solved from equation 2.13 for a given net pressure gradient.

## 2.2 Theories on bed shear stress

### 2.2.1 Introduction

Some sediment transport formulas need the bed shear stress as input (see section 2.3), so it is useful to pay attention to this subject. Using the basic equations to calculate bed shear stress is time-consuming, so (semi-)empirical models were developed to estimate the bed shear stress.

Some of the theories use the momentum equation to determine the velocity profile and the shear stress distribution. An example is the 1-DV boundary layer model of Al-Salem (1993) which is discussed in section 2.2.2. Simplified models are proposed by Ribberink/Van Rijn and Soulsby/Ockenden.

### 2.2.2 Boundary layer flow model of Al-Salem

Al-Salem (1993) developed a computer model which gives a total description of the flow in the wave-boundary layer. In the present study only his results for the bed shear stress are used.

The model is distracted directly from the momentum equations as discussed in section 2.1:

$$\rho \frac{\partial}{\partial t}(u - u_{\infty}) = -\frac{\partial \langle p \rangle}{\partial x} + \frac{\partial \tau}{\partial z} \quad (2.13)$$

Al-Salem neglected the first term of the right-hand side of the equation; this term represents the driving force for the current. This is allowed if the waves dominate over the net current. The following equation remains to be solved:

$$\rho \frac{\partial}{\partial t}(u - u_{\infty}) = \frac{\partial \tau}{\partial z} \quad (2.14)$$

Two boundary conditions are needed to solve this equation, Al-Salem used:

$$\begin{aligned} -u &= 0 & \text{at } z &= k_s/30 & (k_s &= \text{Nikuradse roughness height}) \\ -u &= u_o(t) & \text{at } z &= h & (h &= \text{prescribed level outside wave-boundary layer}) \end{aligned}$$

The turbulent shear stress is supposed to be in proportion to the derivative of the velocity in the z-direction:

$$\tau = \rho \nu_t \frac{\partial u}{\partial z} \quad (2.6)$$

In which  $\nu_t$  = turbulent eddy viscosity

The eddy viscosity is modelled with the mixing length model of Prandtl (1926). Prandtl suggested that  $\nu_t$  is proportional to a mean fluctuation velocity  $V$  and a mixing length  $l_m$ :

$$\nu_t = V l_m \quad (2.15)$$

The velocity scale  $V$  is taken as:  $V = l_m \left| \frac{\partial u}{\partial z} \right|$ , and

the length scale is supposed to be proportional to the distance to the bottom:  $l_m = \kappa z$

herein  $\kappa$  = von Karman coefficient

Finally this leads to this expression for the shear stress:

$$\tau = \rho \kappa^2 z^2 \left| \frac{\partial u}{\partial z} \right| \frac{\partial u}{\partial z} \quad (2.16)$$

Substituting in the equation of motion:

$$\frac{\partial}{\partial t}(\mathbf{u}-\mathbf{u}_\omega) = \frac{\partial}{\partial z} \left\{ \kappa^2 z^2 \left| \frac{\partial \mathbf{u}}{\partial z} \right| \frac{\partial \mathbf{u}}{\partial z} \right\} \quad (2.17)$$

This equation has been solved with help of a computer model developed by Al-Salem. The bed shear stress calculated with this method is used as input for sediment transport formulas as discussed in section 2.3.

### 2.2.3 Simplified models for bed shear stress under combined waves and currents

#### 2.2.3.1 Introduction

In this section two different methods are described, both methods use separate formulations developed for waves only and currents only as basis.

*Only waves:*

Experiments of Jonsson (1966) indicate that the bed shear stress is proportional to the square of the near bed velocity. He suggested the following expression to calculate the bed shear stress:

$$\tau_b(t) = \frac{1}{2} \rho f_w |\mathbf{u}_b(t)| \mathbf{u}_b(t) \quad (2.18)$$

with  $\tau_b$  = bed shear stress  
 $\mathbf{u}_b$  = the velocity outside the wave-boundary layer  
 $f_w$  = the wave friction factor

In case of high Reynolds numbers (turbulent conditions) the wave friction factor depends on the relative roughness ( $\hat{x}/k_s$ ). To estimate this factor the formula of Swart (1974) is used:

$$f_w = \exp \left\{ -6 + 5.2 \left( \frac{\hat{x}}{k_s} \right)^{-0.19} \right\} \quad (2.19)$$

$$f_{w,max} = 0.3 \quad (2.20)$$

with  $\hat{x}$  = amplitude of the horizontal oscillatory flow near the bed

The roughness height depends on the size of the grains, characterized by  $D_{50}$  or  $D_{90}$ . For flat beds and low Shields numbers ( $\theta < 1$ )  $k_s = 3D_{90}$  (according to Van Rijn, 1993). If the Shields numbers are larger sheetflow will occur and it is generally accepted that the simple relationship for the roughness height is no longer applicable. Al-Salem (1993) suggested the use of Wilson's model (1987) for the increased roughness height. Based on Wilson's work van Rijn (1993) suggested:  $k_s = 3\theta D_{90}$  ( $\theta \geq 1$ ). Now  $k_s$  depends on  $\theta$  and  $\theta$  depends on  $k_s$ , thus an iterative procedure has to be

followed to calculate both. In the present study also other values for  $k_s$  are used, for example  $k_s = D_{50}$  or  $k_s = 2.5D_{50}$ .

### *Steady current*

In case of a steady (uniform) current the bed shear stress can be calculated with the help of the Chezy friction factor:

$$\tau_b = \rho u_*^2 = \frac{\rho g v^2}{C^2} \quad (2.21)$$

With:  $v$  = depth-averaged current velocity  
 $C$  = Chezy friction coefficient ( $= 18^{10} \log(12h/k_s)$ )  
 $u_*$  = friction velocity ( $u_* = \sqrt{\tau/\rho}$ )  
 $h$  = waterdepth

In the oscillating water tunnel a depth-averaged velocity cannot be calculated, thus the formula stated above cannot be used. Also in the field (with 3-D flow) a depth-averaged velocity is not always relevant. This problem is solved by using the knowledge that the

velocity above the bed has a logarithmic shape:  $U(z) = \frac{u_*}{\kappa} \ln\left(\frac{z}{z_0}\right)$

with:  $\kappa$  = von Karman constant ( $= 0.4$ )  
 $z_0$  =  $k_s/30$  (rough bed)

It is possible to eliminate  $u_*$  from the formula for the bed shear stress using the formula for the velocity profile:

$$\tau_b = \rho \left\{ \frac{\kappa}{\ln(z/z_0)} \right\}^2 u(z)^2 = 1/2 \rho f_c u_b^2 \quad (2.22)$$

In which:  $u_b$  = velocity at level  $z$  above the bed  
 $f_c$  = current friction factor (depending on distance above the bed!)  
 $= 2 * (\kappa / \ln(z/z_0))^2$

The result of this analysis is a similar formula for the bed shear stress for both waves and for currents. To combine these results for a situation for both waves and currents different approaches are used. Because of the non-linear relationship superposition of  $\tau_{\text{current}}$  and  $\tau_{\text{wave}}$  is not correct. The turbulence generated by the waves will affect the current and vice versa, so the combination gives a larger bed shear stress than can be expected by simply adding  $\tau_c$  and  $\tau_w$ . Below two of the suggested methods to model this enhancement are discussed.

### 2.2.3.2 Model of Ribberink/Van Rijn for combined wave-current flow

As part of the newly developed sediment transport model Ribberink assumes that for the bed shear stress the same basic assumption can be used as was used in the formulas for either waves or currents. In case of co-linear flow:

$$\tau_b(t) = \frac{1}{2}\rho f_{cw} |u_b(t)| u_b(t) \quad (2.23)$$

Herein  $f_{cw}$  is the friction factor for combined waves and currents. Jonsson (1966) suggested to use a weighted friction coefficient for currents and waves (see also Van Rijn, 1993):

$$f_{cw} = \alpha f_c + (1-\alpha) f_w \quad \text{with:} \quad \alpha = \frac{|\langle u_b \rangle|}{|\langle u_b \rangle| + \hat{u}_b} \quad (2.24)$$

Herein:  $\langle u_b \rangle$  = time averaged near bed velocity (at level z)

$\hat{u}_b$  = velocity amplitude of the oscillatory flow (without mean current)

To compute this bed shear stress first the roughness height  $k_s$  has to be known. In case of sheetflow,  $k_s$  depends on the Shields parameter and thus varies during the wave cycle. To make things not too complicated this variation is neglected and  $k_s$  is calculated using the average Shields parameter during the wave cycle. The following procedure is followed:

1) Estimate the mean magnitude of the bed shear stress with  $k_s = 3D_{90}$  as input, by using the individual formulas for only waves and only currents, in case of sinusoidal waves:

$$\langle |\tau_b| \rangle = \frac{1}{4}\rho f_w \hat{u}_b^2 + \frac{1}{2}\rho f_c \langle u_b \rangle^2 \quad (2.25)$$

2) Calculate the Shields parameter and estimate  $k_s$  using  $k_s = 3\theta D_{90}$

3) Repeat with the new value of  $k_s$  until  $k_s$  becomes (almost) constant.

### 2.2.3.3 Model of Soulsby for combined wave-current flow

The starting point of this model is the parameterization of boundary layer models as inter-compared within the MAST G6M Coastal Morphodynamics project (Soulsby et al, 1993). This parameterization gives the mean and the maximum value of the bed shear stress (respectively  $\langle \tau_b \rangle$  and  $\tau_{b,max}$ ). Soulsby and Ockenden (1994) used this mean and maximum to calculate a time dependent shear stress.

As originally proposed by Christoffersen and Jonsson (1985) the bed shear stress is assumed to consist of a part caused by the waves and a part caused by the net current, both contributions enhanced by the interaction of waves and currents:

$$\tau_b(t) = \tau_c^+ + \tau_w^+(t) = \frac{1}{2}\rho f_c^+ |\langle \mathbf{u}_b \rangle| \langle \mathbf{u}_b \rangle + \frac{1}{2}\rho f_w^+ |\tilde{\mathbf{u}}_b(t)| \tilde{\mathbf{u}}_b(t) \quad (2.26)$$

in which:  $f_c^+$  = current friction factor enhanced by waves  
 $\tau_c^+$  = current-related bed shear stress enhanced by waves  
 $f_w^+$  = wave friction factor enhanced by the current  
 $\tau_w^+$  = wave related bed shear stress enhanced by the current  
 $\tilde{\mathbf{u}}_b(t)$  = oscillatory component of the near bed velocity  
 $\langle \mathbf{u}_b \rangle$  = net (wave averaged) near bed velocity

With the mean ( $\langle \tau_b \rangle$ ) and maximum value ( $\tau_{b,max}$ ) of the bed shear stress as input  $f_c^+$  and  $f_w^+$  can be calculated. Assuming sinusoidal waves ( $\tau_c^+ = \langle \tau_b \rangle$ ):

$$\langle \tau_b(t) \rangle = \frac{1}{2}\rho f_c^+ |\langle \mathbf{u}_b \rangle| \langle \mathbf{u}_b \rangle \Leftrightarrow f_c^+ = \frac{\langle \tau_b \rangle}{\frac{1}{2}\rho |\langle \mathbf{u}_b \rangle| \langle \mathbf{u}_b \rangle} \quad (2.27)$$

and:

$$\tau_{b,max} = |\langle \tau_b \rangle| + \frac{1}{2}\rho f_w^+ \hat{u}_b^2 \Leftrightarrow f_w^+ = \frac{\tau_{b,max} - |\langle \tau_b \rangle|}{\frac{1}{2}\rho \hat{u}_b^2} \quad (2.28)$$

See appendix C for an overview of the method to calculate the mean and maximum values of the bed shear stress from the parameterized boundary layer model. In the present study the parameterization of the boundary layer flow model of Fredsoe was used as input.

#### 2.2.3.4 Comparison of bed shear stress models

A comparison between the two models was made for different combinations of important parameters ( $z_0/h = 10^{-4}$  and  $10^{-3}$ ,  $\hat{x}/z_0 = 10^4$  and  $10^5$ ). In Figure 2.2 the mean and the maximum shear stress are plotted against the current-related bed shear stress. Both are made dimensionless by dividing by  $\tau_c + \tau_w$ . ( $\tau_c$  and  $\tau_w$  represent the bed shear stress for respectively only currents and only waves.) The dotted lines represent the mean and maximum shear stress in case no enhancement would be present.

As can be expected the model of Soulsby/Ockenden shows good agreement with output from the parameterized 1-DV model (Soulsby, 1993). The model of Ribberink/van Rijn gives more enhancement especially with larger additional currents.

It is not possible to make a choice for one model based on this analysis. To judge which model is to prefer, the calculated time dependent bed shear stress should be compared with measurements of the bed shear stress.

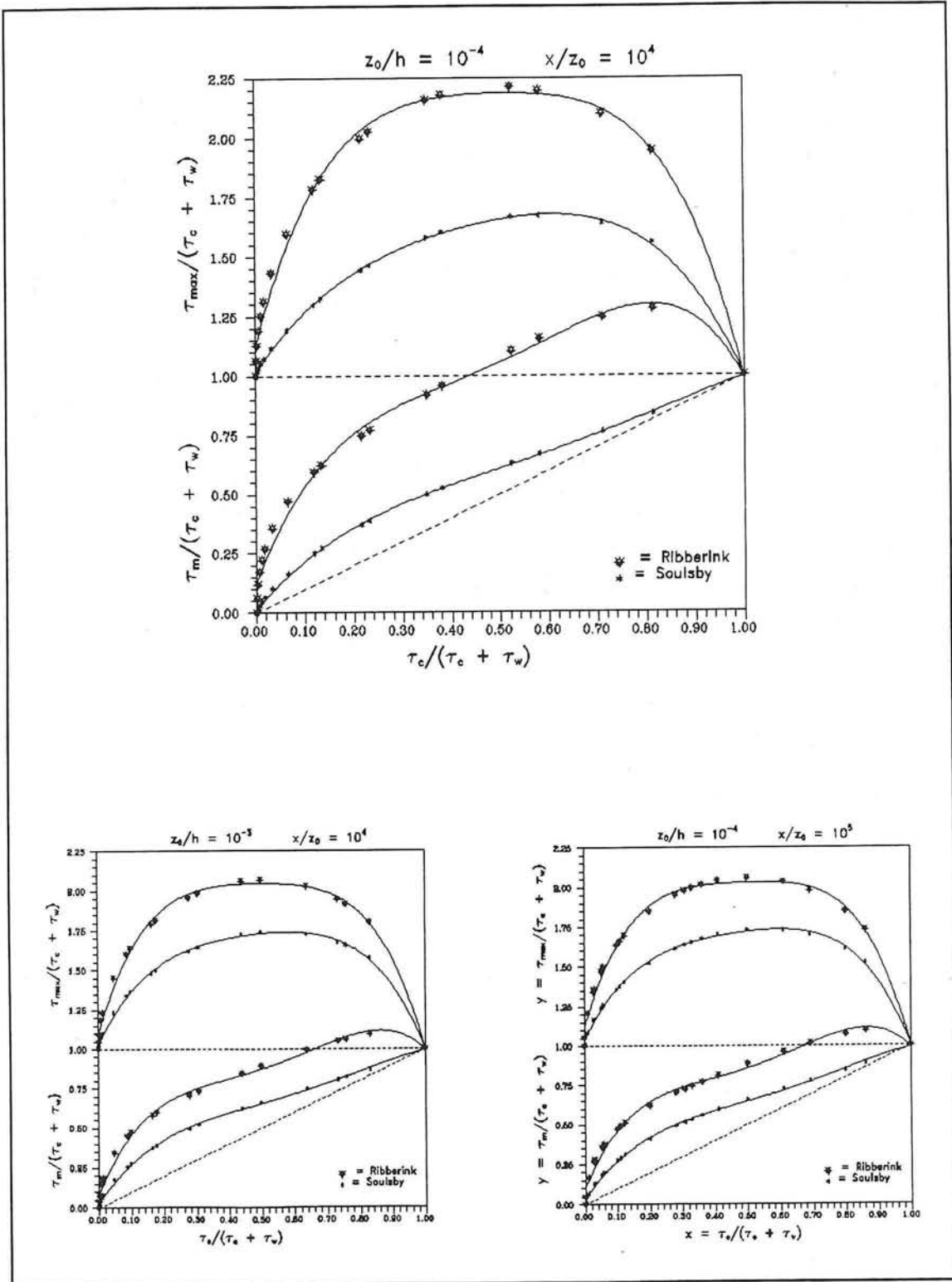


Figure 2.2 Bed shear stress, comparison of formulation Ribberink and Soulsby

## 2.3 Theories on sediment transport

### 2.3.1 Introduction

Different sediment transport formulas are used to predict the rate of sediment transport. They can roughly be divided into two groups; models which use the bed shear stress as input, and models which use the velocity signal directly. A disadvantage of the last group of methods is that the transport becomes dependent on the height above the bed where the velocity signal is specified.

As already mentioned in the first Chapter the present experiments are focused on sheetflow conditions, thus before concentrating on the transport theories a description of sheetflow is given.

#### *Sheetflow*

Under storm conditions high bed shear stresses will occur, the ripples formed under lower stresses disappear and sediment is transported in a layer above the bed. In this thin (sheetflow) layer near the bed very high concentrations of sediment occur, so it is suggested that large transport rates will occur near the bed. In the present experiments attention was paid to the relative contribution of the sheetflow layer and the higher suspension layer to the total transport rate.

Different criteria were formulated to describe the transition between rippled-bed and the sheetflow regime. Horikawa et al (1982) mentioned three of them:

$$\text{Manohar:} \quad \Psi > \frac{2 \cdot 10^3}{\sqrt{\text{Re}}} \quad (2.29)$$

$$\text{Komar-Miller:} \quad \Theta > \frac{4.4}{\text{Re}^{1/3}} \quad (2.30)$$

$$\text{Dingler-Inman:} \quad \Psi > 240 \quad (2.31)$$

Herein:  $\text{Re} = \frac{\hat{u} D_{50}}{\nu}$  = Reynolds number based on grain-size.

$$\Psi = \frac{\hat{u}^2}{\Delta D_{50} g} = \text{Sediment mobility number}$$

$$\Theta = \frac{1/2 f_w \hat{u}^2}{\Delta D_{50} g} = \frac{1/2 \rho f_w \hat{u}^2}{(\rho_s - \rho) g D_{50}} = \frac{\tau_{b,\max}}{(\rho_s - \rho) g D_{50}} = \text{Maximum Shields parameter}$$

In which:  $D_{50}$  = median grain diameter  
 $\hat{u}$  = maximum orbital velocity  
 $\tau_{b,max}$  = maximum bed shear stress  
 $f_w$  = wave friction factor  
 $\rho_s$  = density of sediment  
 $g$  = gravity acceleration

The last parameter is equal to the maximum Shields parameter during the wave cycle and can be adapted easily for situations with both waves and currents.

Horikawa concluded that the criteria of Manohar and Komar-Miller are both forecasting the transition quite well, and that the formulation of Manohar is better than the one of Komar-Miller. All the criteria were developed for situations with waves only. An additional current will lead to sheetflow for lower values of the orbital velocity (see also Ramadan, 1993).

### 2.3.2 Transport models using bed shear stress

This group of formulas does not use the near bed velocity directly as input, but the bed shear stress. This bed shear stress is calculated with the help of the velocity above the bed. In theory the height on which the velocity is specified is not important anymore and velocities measured on different heights above the bed should give the same bed shear stress. A problem is that no agreement exists on which formula for bed shear stress gives the best results.

#### *Model of Al-Salem and Ribberink*

This formula for total transport was originally developed for situations with only waves. It is adapted in the present study by using an appropriate manner to calculate the bed shear stress for combined wave-current flow. When the formula of Ribberink/Van Rijn is used the only adaption is replacing the wave friction factor by a combined wave-current friction coefficient. When the bed shear stress formulation of Soulsby/Ockenden is used (which does not have a wave friction coefficient) the bed shear stress itself is necessary as input.

$$\frac{q_s(t)}{W_s D_{50}} = 4 \frac{u_*^3(t)}{W_s^3} \quad (2.32)$$

$$\text{herein: } u_*(t) = \frac{|\tau_b(t)|}{\tau_b(t)} \sqrt{\frac{|\tau_b(t)|}{\rho}} = \sqrt{\frac{f_{cw}}{2}} u_b(t)$$

In which:  $q_s$  = sediment transport in real volume per unit time and width  
 $u_*$  = friction velocity  
 $W_s$  = fall velocity of the sediment

Al-Salem tested the formula for different  $D_{50}$ . The formula has proven to be applicable for  $D_{50}$  between 0.20 and 1.10 mm (Al-Salem, 1993). Originally the calibration factor was 5 instead of 4, but a factor 4 shows better agreement with the measurements (see Ribberink and Al-Salem, 1994). For very fine sand ( $D_{50} < 0.2$  mm) the formula is not valid as has been shown by experiments conducted by Chen in the same large water tunnel of DELFT HYDRAULICS (Ribberink and Chen, 1993).

#### *New model of Ribberink*

This model, which is still under development at DELFT HYDRAULICS, tries to describe the bed load transport with a basic concept usable for all conditions (only waves, only a current or a combination of both). The basic concept was tested for waves only as well as for currents only and showed good agreement with measured data for a wide range of conditions.

In the present study it is investigated whether this formulation can also be applied to waves and currents together.

The basic time dependent formulation is:

$$\Phi_b(t) = m \{ |\theta(t) - \theta_c| \}^n \frac{\theta(t)}{|\theta(t)|} \quad (2.33)$$

herein:  $\Phi_b$  = non-dimensional transport rate parameter  
 $\theta$  = non-dimensional sediment forcing parameter  
 $\theta_c$  = critical Shields parameter, representing the threshold of motion of the sand grains  
 $m$  = empirical coefficient  
 $n$  = empirical exponent

The transport is made dimensionless by dividing  $q_b$  by the square-root of a parameter representing the under-water weight of sand grains:

$$\Phi_{bd}(t) = \frac{q_b(t)}{\sqrt{\Delta g D_{50}^3}} \quad (2.34)$$

The Shields parameter ( $\theta$ ) is used as sediment forcing parameter:

$$\theta(t) = \frac{\tau_b(t)}{(\rho_s - \rho)gD_{50}} \quad (2.35)$$

The critical Shields parameter depends on the non-dimensional grain-size (see appen.

$$B): D_* = D_{50}[g\Delta / \nu^2]^{1/3}$$

herein:  $\theta(t)$  = Shields parameter based on skin-friction  
 $\tau_b$  = bed shear stress

- $q_b$  = bed load transport rate in volume per unit time and width  
 $\rho_s$  = density of sand  
 $\rho$  = density of water  
 $g$  = gravity acceleration  
 $\Delta$  = relative density =  $(\rho_s - \rho)/\rho$   
 $\nu$  = kinematic viscosity of water

Averaging over the wave cycle gives:

$$\langle \Phi_{bd}(t) \rangle = \left\langle m \{ |\theta(t) - \theta_c|^n \frac{\theta(t)}{|\theta(t)|} \} \right\rangle \quad (2.36)$$

To make it possible to compare waves and currents a representative Shields parameter is defined:

$$\{ |\theta_{repr} - \theta_c|^n \frac{\theta_{repr}}{|\theta_{repr}|} \} = \left\langle \{ |\theta(t) - \theta_c|^n \frac{\theta(t)}{|\theta(t)|} \} \right\rangle \quad (2.37)$$

After curve fitting with a large number of data Ribberink proposed to take  $m = 9.1$  and  $n = 1.78$ .

### 2.3.3 Transport models using velocity moments

#### *Model of Al-Salem*

The most simple formula is described by Al-Salem (1993), who found from wave tunnel experiments with asymmetric waves that the rate of sediment transport is proportional to the third-order velocity moment of the free stream velocity:

$$\langle q_s \rangle = A \langle u^3(t) \rangle \quad \text{with } A = \text{calibration factor.} \quad (2.38)$$

A disadvantage of such a formula is that the calibration factor is only known for Al-Salem's experiments ( $D_{50} = 0.21$  mm); in reality 'A' is not even a constant but is still depending on variables as the particle diameter, the wave period etc.

#### *Model of Bailard*

The Bailard model is based on the energetics approach of Bagnold (1963,1966). The model consists of separate formulas for bed load and suspended load transport. For waves only and horizontal bed.

$$\text{bed load transport: } q_b(t) = \frac{1/2 f_w \epsilon_b}{\Delta g \tan \phi} u^3(t) \quad (2.39)$$

$$\text{suspended load transport: } q_s(t) = \frac{1/2 f_w \epsilon_s}{\Delta g W_s} |u^3(t)| u(t) \quad (2.40)$$

in which:  $\epsilon_b$  = bed load efficiency factor (= 0.1)  
 $\epsilon_s$  = suspended load efficiency factor (= 0.02)  
 $\phi$  = angle of internal friction of the sediment  
 $W_s$  = fall velocity of sediment particles

Al-Salem (1993) tested the Bailard formula for situations with only waves and sheetflow conditions, using the model of Jonsson to calculate the wave friction factor, using  $k_s = D_{50}$ . The agreement between calculated and measured transport was quite good (within a factor 2).

To adapt the formula for situations with waves and currents in the present study the wave friction factor is replaced by a friction factor for combined wave-current flow, calculated by:

$$f_{cw} = \frac{|\tau_{b,max}|}{\frac{1}{2}\rho u_{b,max}^2} \quad (2.41)$$

The maximum bed shear stress can be calculated by a suitable method, see section 2.2.

### 2.3.4 Description of the model of Dibajnia and Watanabe (1992)

This total load transport model takes the delayed behaviour of the suspended sediment into account; sediment brought into suspension during the negative part of the wave cycle will partly remain in suspension and will be transported by the positive part of the wave cycle and vice versa. A non-dimensional parameter  $\Gamma$  is defined to represent the net (non-dimensional) transport rate:

$$\Gamma = \frac{u_c T_c (\Omega_c^3 + \Omega_t^3) - u_t T_t (\Omega_t^3 + \Omega_c^3)}{(u_c + u_t) T} \quad (2.42)$$

In which:

$T_c/T_t$  = period of the positive/negative part of the wave cycle (see Figure 2.3)

$u_c/u_t$  = equivalent sinusoidal velocity profiles for the positive and negative parts of the velocity

$\dots_c$  = parameter related to the positive part of the wave cycle

$\dots_t$  = parameter related to the negative part of the wave cycle

$\Omega_c$ ,  $\Omega_t$ ,  $\Omega_c'$  and  $\Omega_t'$  are non-dimensional parameters.

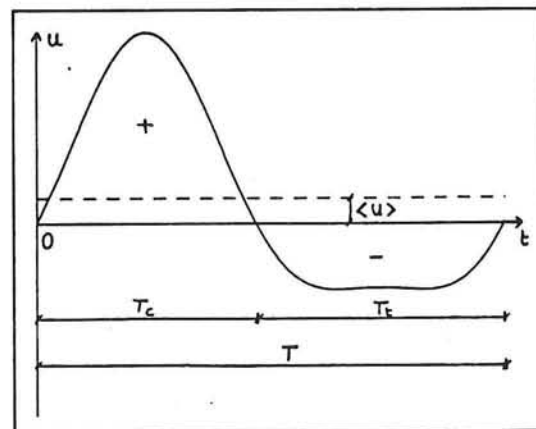


Figure 2.3 Typical velocity profile

The parameters  $\Omega_c^3$  and  $\Omega_t^3$  represent the amount of sediment brought into suspension by and transported during respectively the positive and negative part of the wave cycle. The parameters  $\Omega_c'^3$  and  $\Omega_t'^3$  represent the amount of sediment remaining in suspension from the previous half cycle and transported by the other half of the cycle.

$\Omega$  and  $\Omega'$  depends on the ratio between the time required for a particle to reach the bed (settling time) and the duration of the positive and negative part of the wave cycle:  $T_{fall}/T_c$  and  $T_{fall}/T_t$ . If the settling time is larger than  $T_c$  or  $T_t$  sediment will remain in suspension to be carried during the next part of the wave cycle ( $\Omega_c' > 0$  or  $\Omega_t' > 0$ ). Opposite if  $T_{fall} < T_i$  ( $i = c$  or  $t$ ) then all sediment will settle again before flow-reversal ( $\Omega_i' = 0$ ).

$T_{fall}$  is estimated by first calculating the thickness of the sheetflow layer with the help of an energetic concept and then dividing this distance by the fall velocity of the sediment, during the positive and negative part of the wave cycle:

$$T_{fall,c} = \frac{\Delta_s}{W_s} = \frac{1}{2} \frac{u_c^2}{\Delta g W_s} \quad \text{and} \quad T_{fall,t} = \frac{\Delta_s}{W_s} = \frac{1}{2} \frac{u_t^2}{\Delta g W_s} \quad (2.43)$$

Herein:  $\Delta_s$  = thickness of sheetflow layer  
 $u_c, u_t$  are equivalent sinusoidal velocity amplitudes for the positive and negative parts of the velocity profile:

$$u_c^2 = \frac{2}{T_c} \int_0^{T_c} u^2 dt \quad \text{and} \quad u_t^2 = \frac{2}{T_t} \int_{T_c}^T u^2 dt \quad (2.44)$$

The ratio between the settling time and the period of the positive and negative part reads:

$$\omega_c = \frac{1}{2} \frac{u_c^2}{\Delta g W_s T_c} \quad \text{and} \quad \omega_t = \frac{1}{2} \frac{u_t^2}{\Delta g W_s T_t} \quad (2.45)$$

As mentioned before if  $\omega_i$  is smaller than one, no sand will remain in suspension to be transported by the other half of the wave cycle. A larger value of  $\omega_i$  indicates a more important role for the suspension mechanism, so more sediment will remain from one part of the wave cycle to be transported by the other part. The following relations are used to estimate  $\Omega_c$  and  $\Omega_t$ :

$$\text{If } \omega_i \leq 1 \text{ then: } \Omega_i = 2 \omega_i \frac{W_s T_i}{D_{50}} \quad \text{and} \quad \Omega_i' = 0 \quad (i = c, t)$$

$$\text{If } \omega_i > 1 \text{ then: } \Omega_i = 2 \frac{W_s T_i}{D_{50}} \quad \text{and} \quad \Omega_i' = 2(\omega_i - 1) \frac{W_s T_i}{D_{50}} \quad (i = c, t)$$

The obtained relationship between  $\Gamma$  and  $\Phi_{bw}$  (= non-dimensional transport rate) is as follows:

$$\Phi_{bw} = 0.001 \cdot |\Gamma|^{0.55} \frac{\Gamma}{|\Gamma|} \quad (2.46)$$

herein  $\Phi_{bw} = \frac{\langle q \rangle}{W_s \cdot D_{50}} \quad (2.47)$

Dibajnia and Watanabe claim that this method is applicable to estimate transport in a wide range of conditions regarding sheetflow or transport over ripples, also the direction of the transport can be predicted with this method.

## 3 Experimental set-up

### 3.1 Introduction

In this Chapter the experimental set-up of the present oscillating water tunnel experiments (series E) is described. The experiments were conducted during October and November 1993 by an international research team. The principal investigator was I. Katapodi. A list of all members of the research team can be found in the data report (Katapodi et al, 1994). The main scope of these experiments was to obtain a detailed dataset concerning sheetflow conditions under waves combined with a current.

### 3.2 Large Oscillating Water Tunnel

The measurements were conducted in the Large Oscillating Water Tunnel (LOWT) of DELFT HYDRAULICS. In Figure 3.1 the general outline of the tunnel is shown. The tunnel has the shape of a vertical U-tube with a long rectangular horizontal section (test section length 14 m) and two vertical cylindrical risers on either end. The desired oscillatory water motion inside the test section is imposed by a steel piston in one of the risers. The other riser is open to the atmosphere. The piston is in direct contact with the water and is driven by a hydraulic servo-cylinder mounted on top of the riser. An electro/hydraulic valve controls the piston motion on the basis of the measured difference between the (measured) actual piston position and the desired piston position (feedback system). The test section is 14 m long, 1.1 m high and 0.3 m wide and is provided with flow straighteners on either end. A 30 cm thick sand bed can be brought into the test section, leaving 0.8 m height for the oscillatory flow above the bed.

The side-walls of the test section consist of thick glass windows supported by steel I-beams. The maximum piston amplitude is 0.75 m, which means a maximum semi-excursion length of the water particles in the test section of 2.45 m. The range of velocity amplitudes is 0.2-1.8 m/s and the range of oscillation periods is 4-15 seconds. An extensive description of the water tunnel can be found in Ribberink (1989).

In 1992 the tunnel was extended with a recirculating flow system connected to the cylindrical risers, so that a steady current can be superimposed to the oscillatory motion. The recirculating flow system is provided with a sand trap consisting of a 12 meter long pipe with a diameter of 1.2 meter that is connected with the downstream cylindrical riser by a pipe with a diameter of 0.3 meter (see Figure 3.2). The trap was designed for trapping 90% of the suspended sediments (minimum grain-size 100 microns) at maximum flow discharge. Downstream of the trap two pumps are installed for generating a net current. The maximum capacity of the larger pump is 100 l/s and of the smaller 20 l/s. The maximum superimposed current velocity in the test section of the tunnel is approximately 0.45 m/s.

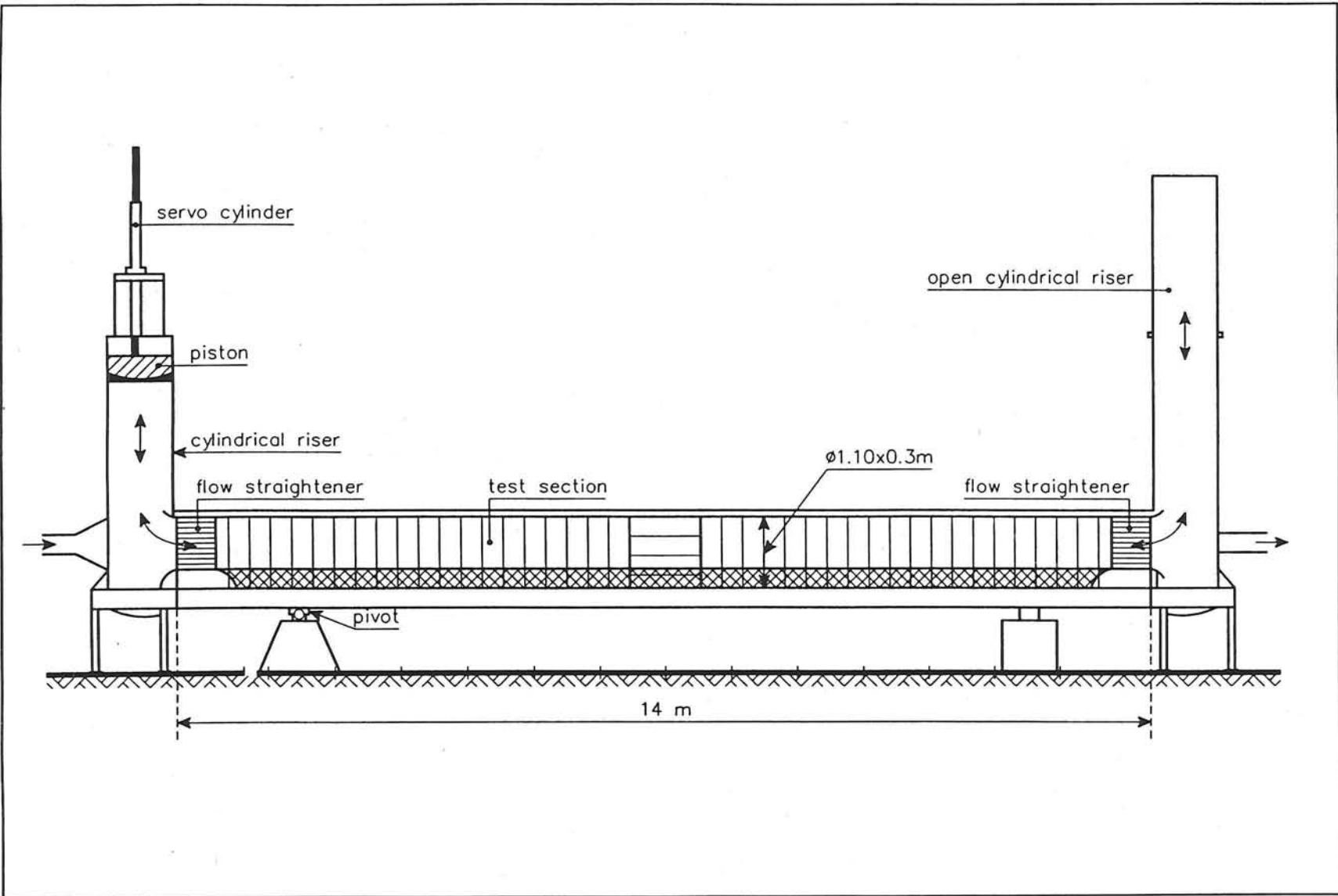


Figure 3.1 Large Oscillating Water Tunnel

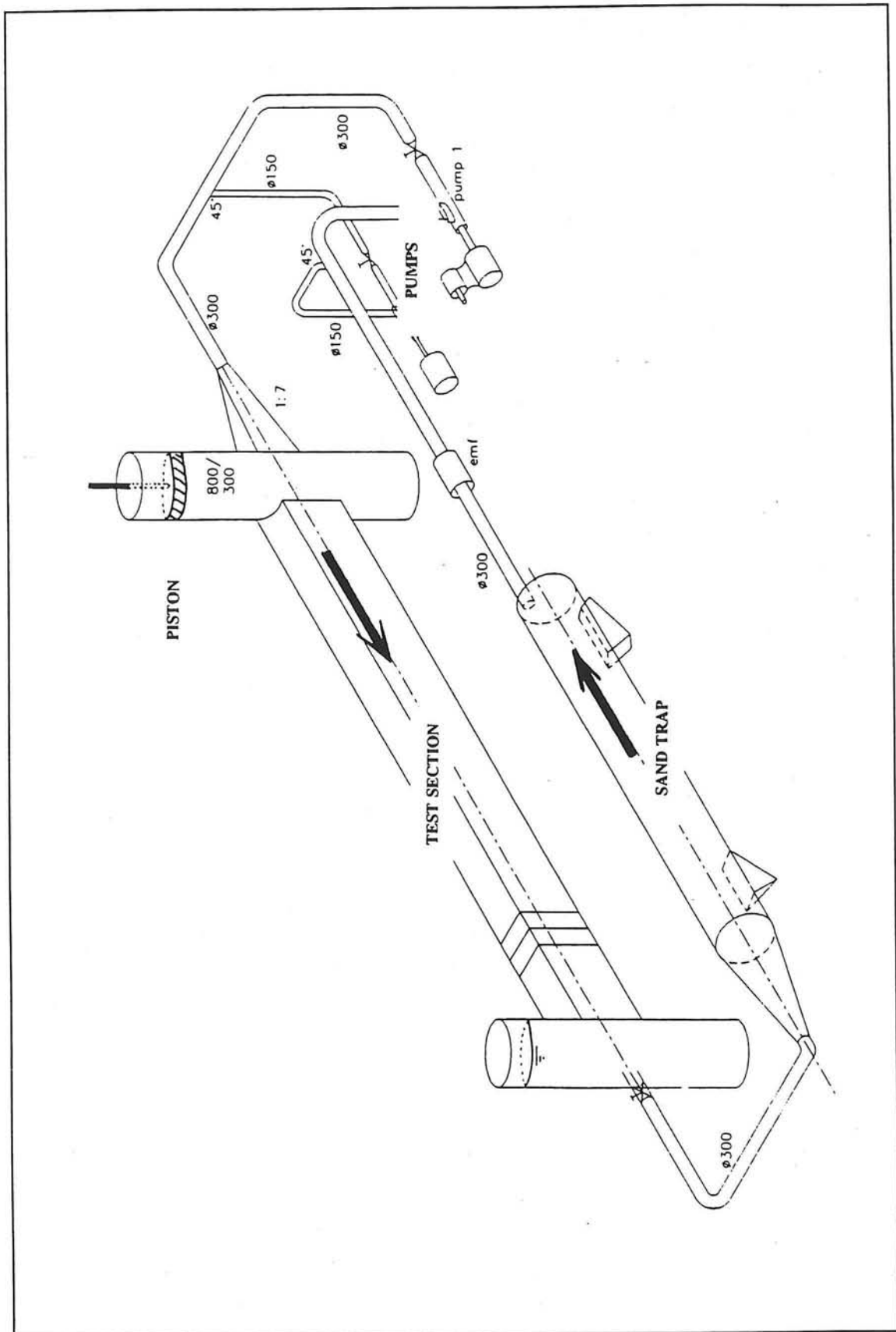


Figure 3.2 General outline of the recirculation system

### 3.3 Imposed and measured parameters

Four combinations of sinusoidal waves and steady currents were realized in the tunnel (see also Section 3.5) by imposing a required piston movement and pump discharge.

The following parameters were measured (See also Figure 3.3 for an overview of imposed and measured parameters):

- Time averaged suspended sediment concentration  $C(z)$  in the suspension layer (for  $z > 1$  cm);
- Time dependent sediment concentration  $C(z,t)$  both in the suspension layer (for  $z > 0.5$  cm) and in the sheetflow layer;
- Time dependent flow velocities  $U(z,t)$  and  $W(z,t)$ ;
- Bed levels and sand trap volumes for the estimation of the sediment transport rates;
- Sand grain velocities in the sheetflow and suspension layer.

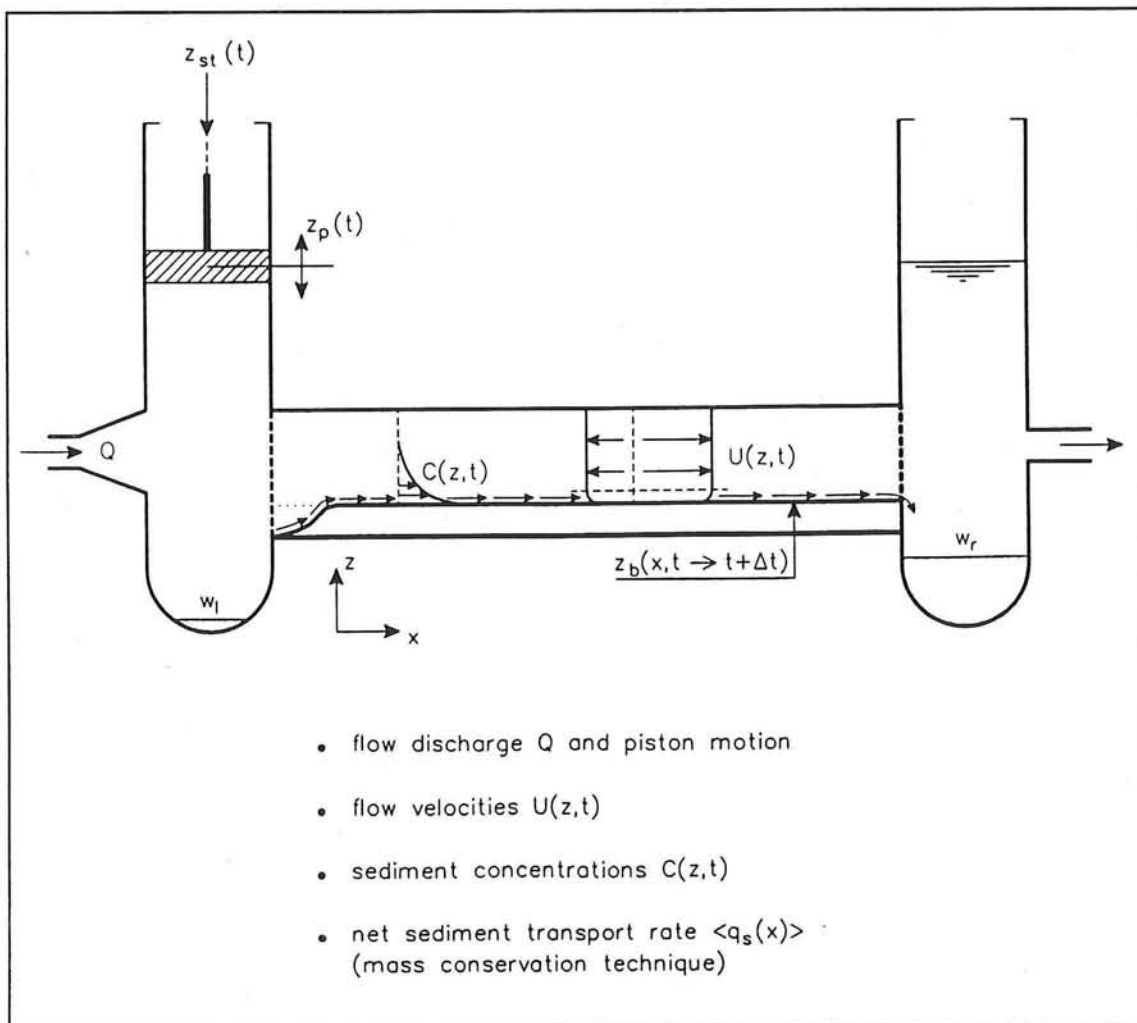


Figure 3.3 Imposed and measured parameters

### 3.4 Measuring facilities and measuring techniques

The following measuring techniques were used (see also appendix A):

#### *Transverse suction system*

A transverse suction system described by Bosman et al (1987), was used for measuring the time averaged concentration profile of the suspended sediment concentration.

The transverse suction is performed by extracting samples in a direction normal to the flow. The transverse suction system consists of 10 intake nozzles with inner diameter of 3 mm. The suction is driven by 10 peristaltic pumps. The sand samples are collected in buckets and the sand content is measured using calibrated tubes. The sand height is converted into sand mass using the sand density and the porosity of loosely packed sand.

Figure 3.4 shows an outline of the transverse suction probe. The distance of the lowest nozzle from the bed was about 1 cm. The calibration of the suction is determined by the trapping efficiency  $\alpha$  defined as the sediment concentration in the sucked sample and the concentration in the flow. The value of the trapping efficiency depends on the nozzle dimensions, their orientation relative to the flow, the ratio of the intake velocity over the ambient flow, the sediment particle characteristics and the relative density. In the present experiments the trapping efficiency was set to 0.68.

#### *Mass-conservation technique*

A mass-conservation technique was used for the estimation of the time and wave averaged sediment transport rates in the test section. The bed level along the test section was measured through the glass window before and after each run. Then the sediment continuity equation was solved twice (starting either from the left or the right trap) using as boundary conditions the sand volumes collected in the sand traps (given the sand porosity). The mean value of the two computations is used.

#### *Optical concentration meter (OPCON)*

Time dependent suspended sediment concentrations were measured using an optical concentration meter (OPCON). The OPCON measures volume concentration in the range of 0.1-50 g/l and is based on the extinction of the infra-red light. The height of its sensing volume is 2.6 mm. The OPCON configuration in the tunnel is shown in Figure 3.5. The orientation of the light beam between transmitter and receiver is horizontal and perpendicular to the oscillatory flow. The lowest point measured was at about 0.5 cm from the bed.

*Electro-magnetic Flow Meter (EMF)*

The velocities near the bed could not be measured with the LDFM due to heavy suspension that interrupted the signal. In this layer a four quadrant electro-magnetic flow meter (EMF) was used for the measurement of the horizontal velocities. The EMF employs Faraday's Induction Law for the measurement of the velocity of a conductive liquid moving across a magnetic field. The diameter of the ellipsoid sensor probe was 11 x 33 mm and the height of the sensing volume 3-5 mm. Figure 3.6 gives an outline of the EMF configuration. The lowest point measured was at about 1 cm above the bed.

*Laser Doppler System (LDFM)*

A forward scatter laser doppler system (LDFM) was used for the measurement of the horizontal and vertical velocity components of the water particles. The height of the sensing volume of LDFM is 0.3 mm. In Figure 3.7 the configuration of the laser system in the tunnel is shown. The velocities were measured from 40 cm above the bed until the closest possible point near the bed (2-4 cm depending on the condition).

*Conductivity Concentration Meter (CCM)*

The concentration in the sheetflow layer and inside the bed was measured using a Conductivity Concentration Meter. The instrument measures large sand concentrations (5-50 volume per cent, 100-1500 g/l) with a four point electro-resistance method. The height of the sensing volume of the CCM is 1 mm. In Figure 3.8 the CCM configuration in the tunnel is shown. The probe is brought into the test section from below through the tunnel bottom and the sand bed in order to minimize flow disturbances. In the framework of the present thesis a recalibration of the CCM was carried out, see appendix A4.

*High Speed Video (HSV)*

The sand grain velocities in the suspension and sheetflow layer were estimated from high speed video recordings, using a speed of 500 frames/s and a shutter time 1/5000 s. The window was 1.2 x 1.6 cm and the focus plane at about 2 cm inside the tunnel.

In Appendix A more information can be found about the measuring methods and the calibration of the instruments.

During all tests the free stream velocity at about 20 cm above the bed was measured with the LDFM in order to check (together with the piston position etc) whether the desired flow conditions were imposed.

Because the bed level was changing during the tests (mostly erosion), the elevation of each instrument relative to the bed was also changing. So the bed level used to derive the instrument elevation was measured after each level measurement. The realized instrument elevation was taken as the mean value of measured elevations before and after the measurement. A member of the research team measured by ruler the highest bed level during the wave period, i.e. at minimum fluid motion. Readings are accurate to 1 mm.

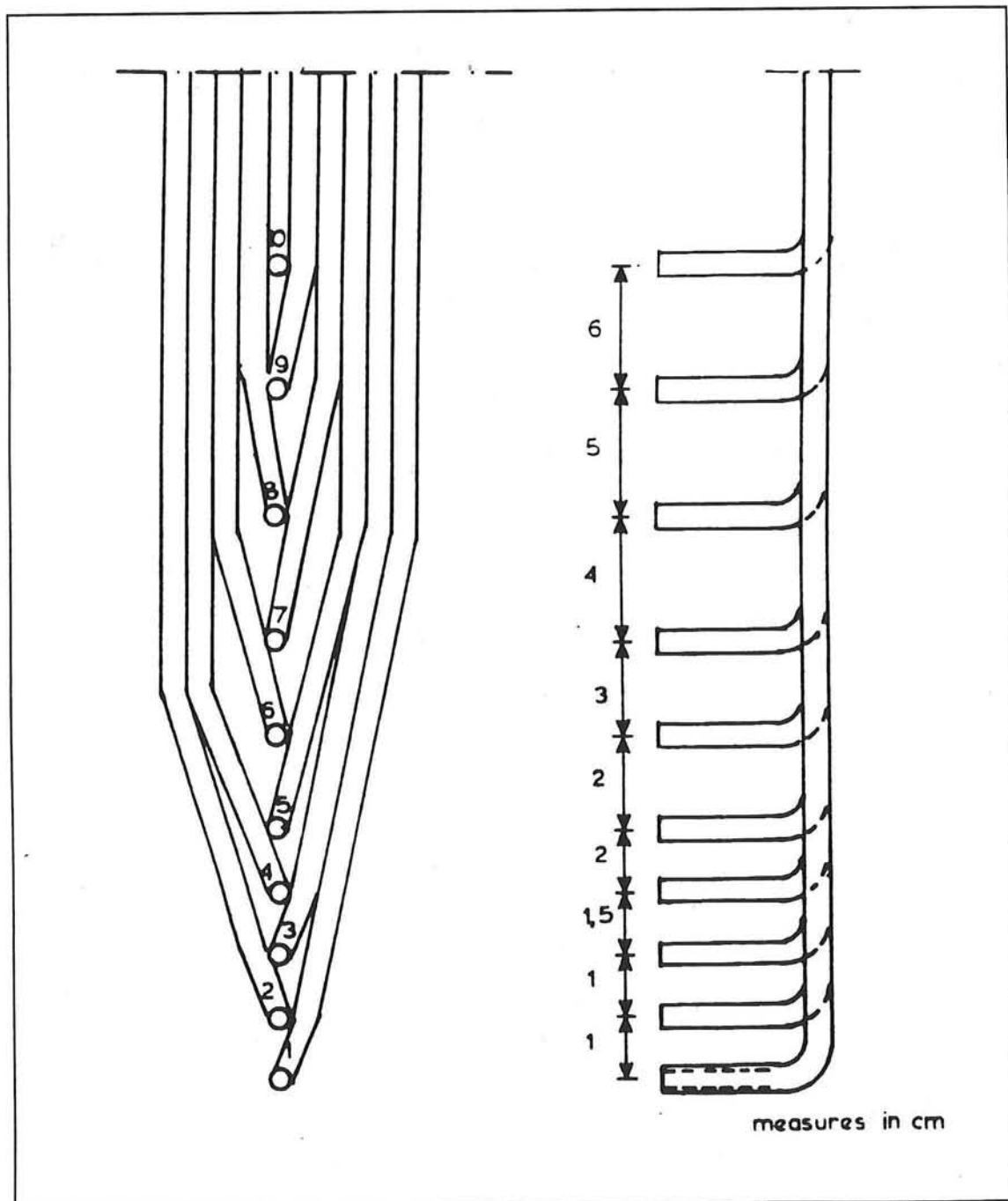


Figure 3.4 Transverse suction concentration meter

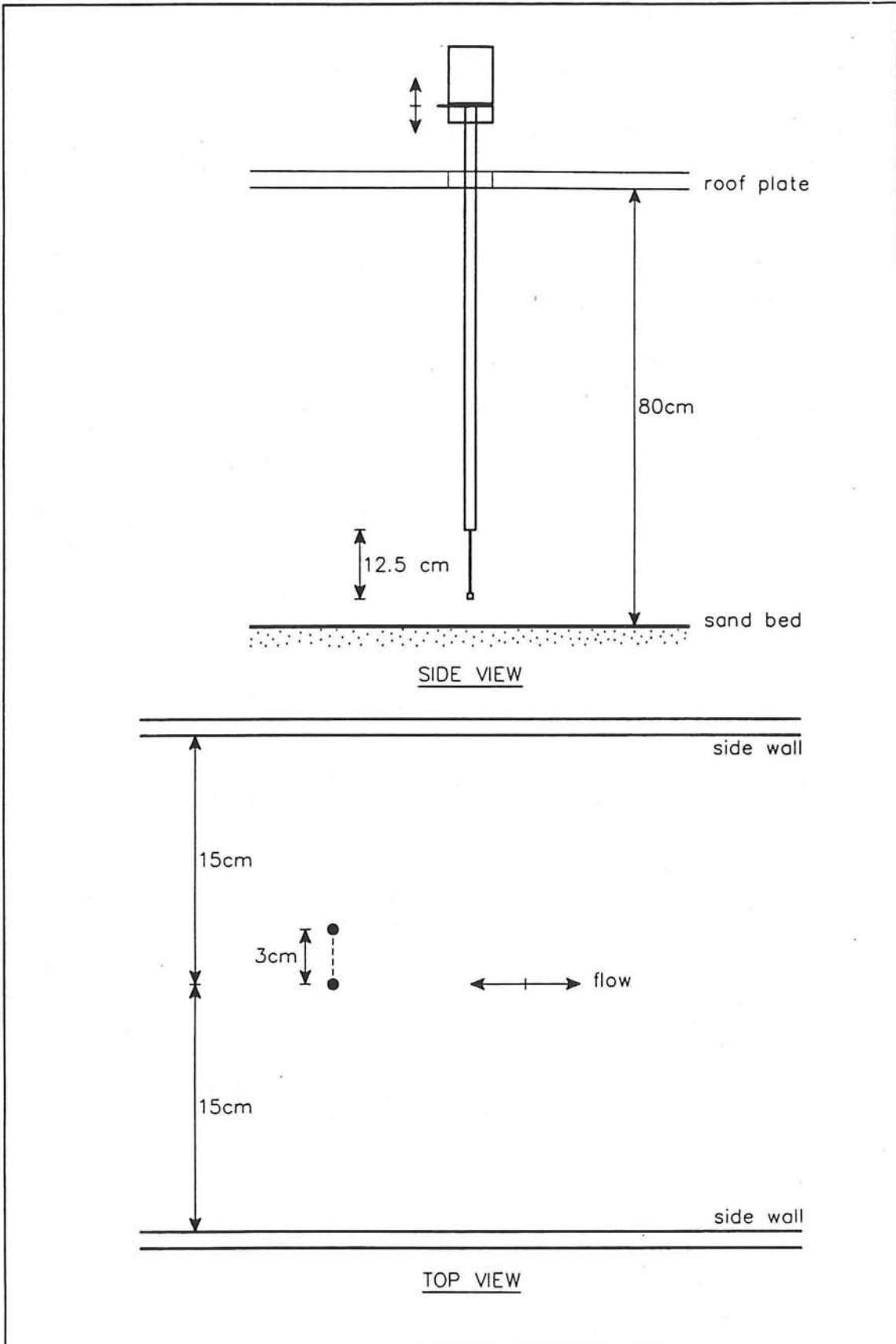


Figure 3.5 OPCON configuration in the tunnel

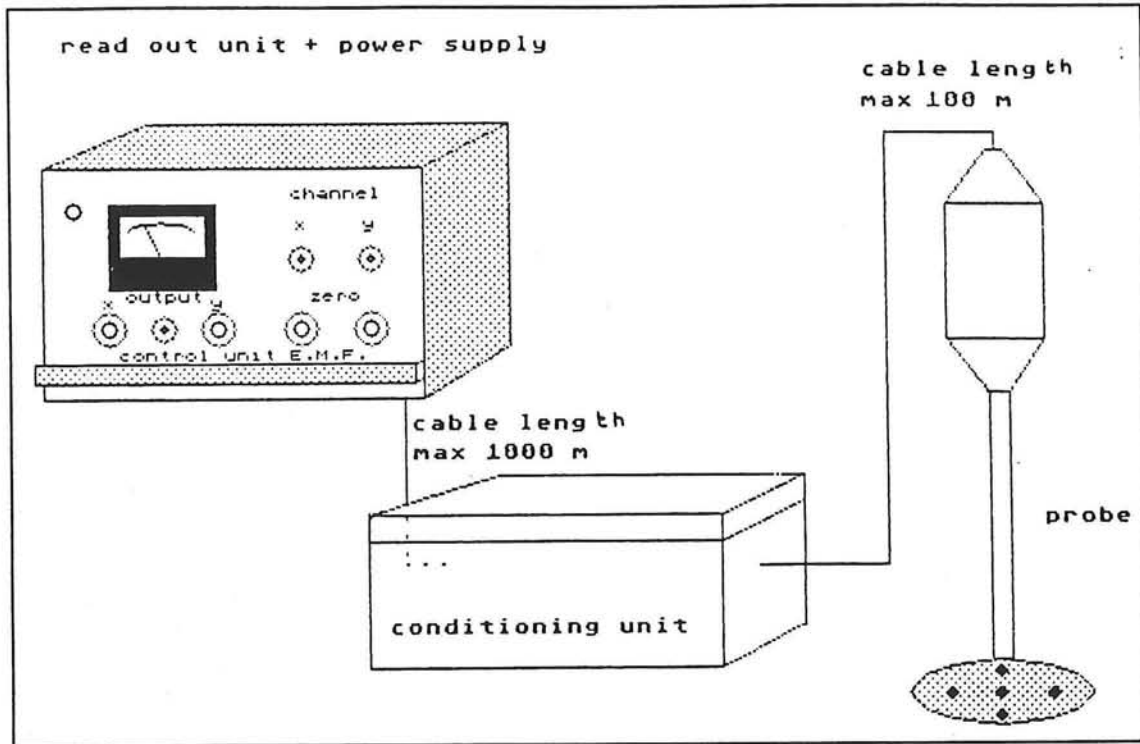


Figure 3.6 Electro-magnetic velocity meter

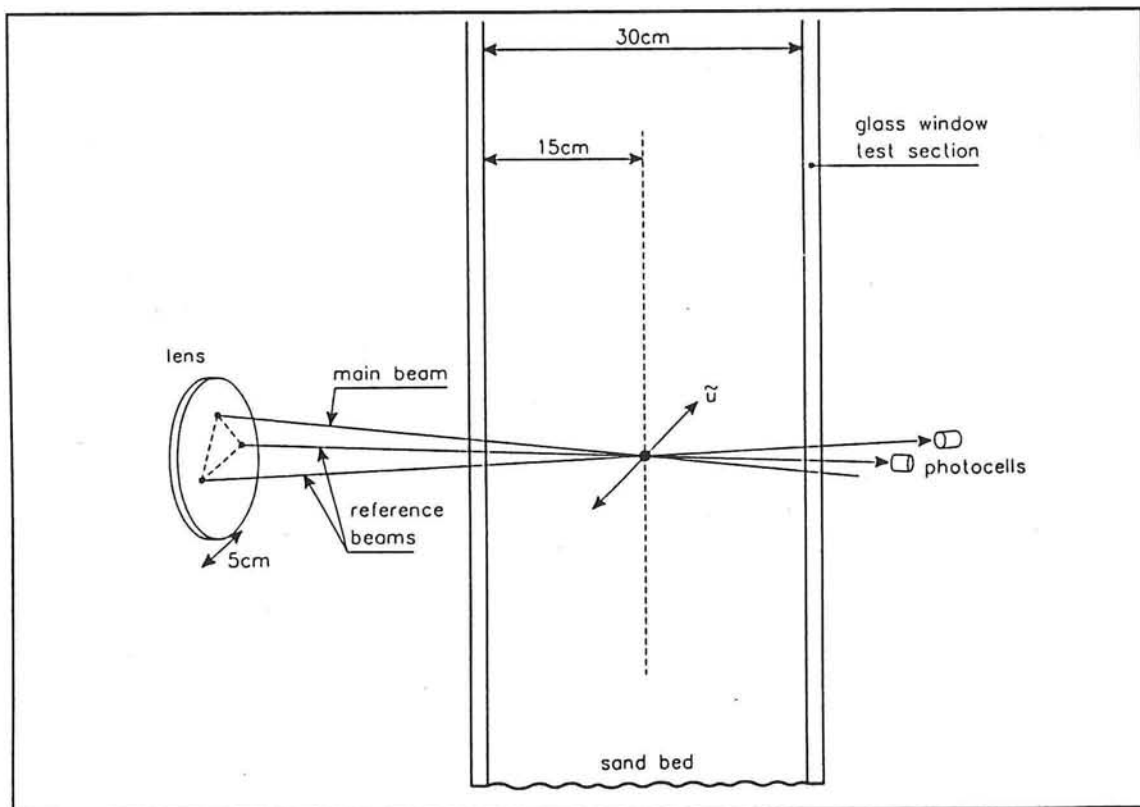
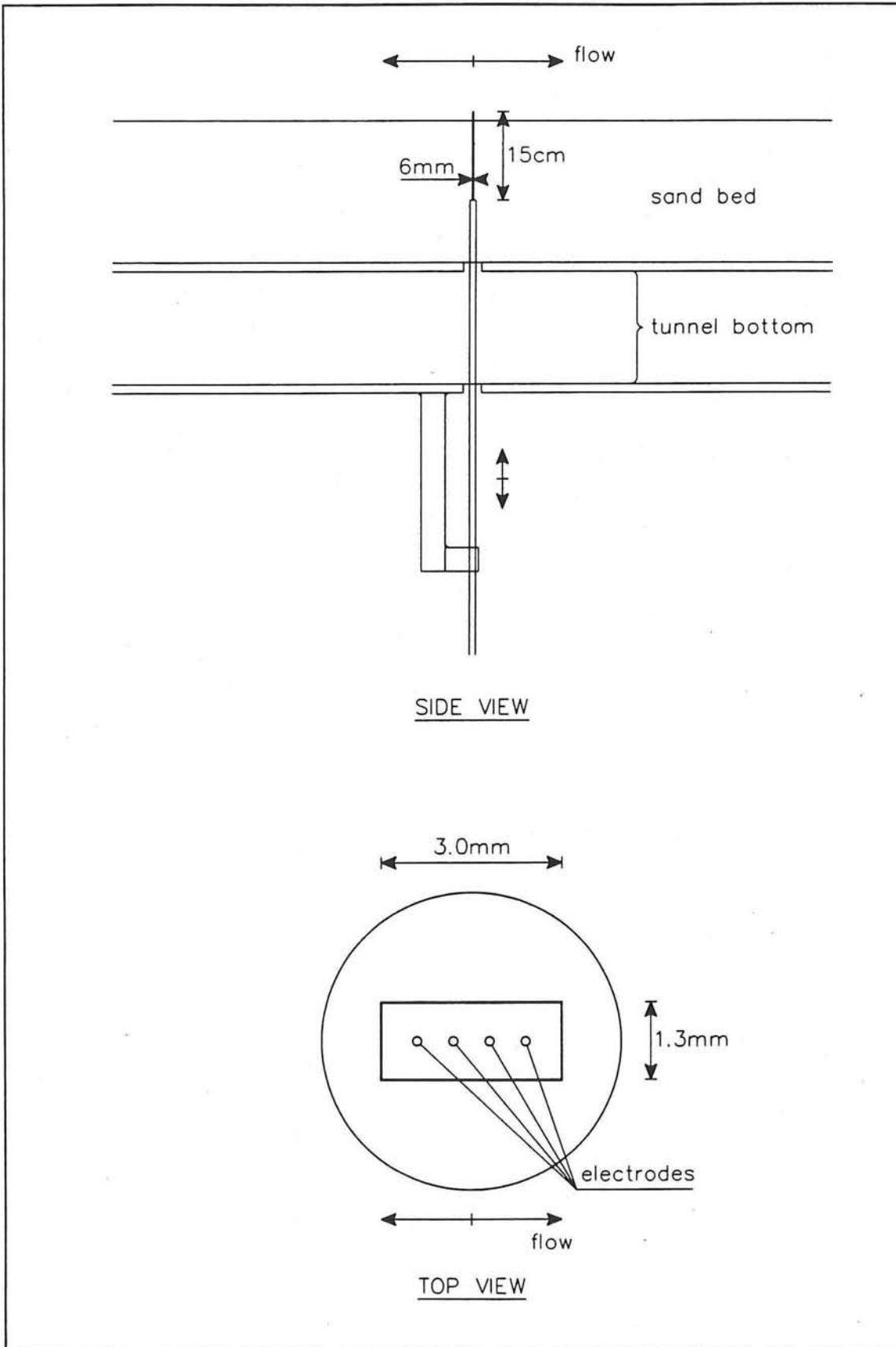


Figure 3.7 Laser-beam configuration in the tunnel



*Figure 3.8 CCM configuration in the tunnel*

### 3.5 Experimental conditions and test programme

The experimental programme consisted of 4 combined sinusoidal wave/net current conditions (E<sub>i</sub>, i = 1,4). With increasing condition number the imposed net current increases and the amplitude of the sinusoidal oscillatory motion decreases. Due to the presence of a net current all four conditions concern asymmetric flow. The flow asymmetry increases with condition number. The wave/net current conditions were chosen such that they all fall in the sheetflow regime.

For the experimental conditions see Table 3.1. In this Table the net current ( $\langle \bar{u} \rangle$ ) and associated discharge (Q), sinusoidal velocity amplitude ( $\hat{u}$ ) and associated percentage of the maximum piston position amplitude (A) and the wave period (T) can be found.

Condition	net current		wave (sine)		
	$\langle \bar{u} \rangle$ (m/s)	Q (m <sup>3</sup> /s)	$\hat{u}$ (m/s)	A (%)	T (s)
E1	0.15	0.036	1.60	72	7.2
E2	0.20	0.048	1.35	63	
E3	0.30	0.072	1.10	48	
E4	0.40	0.096	0.90	40	

Table 3.1 Test conditions

The used sand had the following characteristics:  $D_{10} = 0.15$  mm,  $D_{50} = 0.21$  mm and  $D_{90} = 0.32$  mm (for the grain-size distribution see Figure 3.9).

Ribberink and Al-Salem (1991) showed that there is a very consistent relation of the net sediment transport rate with the third-order near bed velocity moment  $\langle U^3 \rangle$  (for asymmetric waves). In order to investigate the validity of this relation for the situation of waves + currents the four conditions were chosen such that the third-order velocity moment is almost the same.

During five series of experiments 115 tests (tunnel runs) were carried out with different measuring techniques. The complete measuring programme with the number of tests per condition and per instrument and the position of the instruments along the test section can be found in Table 3.2. The centre of the test section is indicated with  $x = 0.0$  m. The positive x-axis ( $x > 0$ ) is in downstream direction. A vertical upward z-axis is used with  $z = 0$  representing the (initial) bed level without sediment/water motion before a test starts.

Series	Measuring techniques	Height above bed (cm)	Number of Tests				Total
			E1	E2	E3	E4	
I	SUCTION (x = 0 & 2.35 m) Mass-conservation LDFM (x = -2.0 & 2.0 m)	1 - 25 xxx 20	5	5	5	4	19
II	OPCON (x = 2.05 m) LDFM (x = -2.0 m)	0.5 - 10 20	10	10	10	10	40
III	EMF (x = 2.05 m) LDFM (x = -2.0 m)	1.5 - 9 20	4	4	4	5	17
IV	LDFM x = 0.00 & m CCM x = m	3 - 20 -0.6 - 0.8	9	8	8	8	33
V	HSV (x = 0 & 2.05 m) LDFM (x = 0 m)	-0.8 - 2.8 20	3	1	1	1	6
Total number of tests			31	28	28	28	115

Table 3.2 Measuring programme

The tests carried out were:

#### Series I

Transverse suction was used for the measurement of time averaged suspended sediment concentration profiles. The concentration was measured simultaneously at ten elevations. The range of the transverse suction measurements was from  $\pm 25$  cm until  $\pm 1$  cm from the bed (see Figure 3.4 for the distances between the nozzles). The horizontal position of the transverse suction system was either  $x = 0.0$  m or  $x = 2.35$  m. In every second test the sand samples were stored in order to be analyzed later for the grain-size characteristics.

Simultaneously, information to be used for the mass-conservation technique was collected (bed levels, weight of sand in the sand traps).

Four tests per condition (test codes Ei-01...Ei-04) were realized. The test duration was 8 minutes (5 litres of water-sand mixture were extracted from the flow). One extra test (code Ei-30, for the three first conditions) was done after the scheduled runs had finished, with duration 10 minutes. The water/sand mixture extraction started after the first two minutes to avoid the effect of the strong initial erosion caused by some flow disturbance of the suction probe .

*Series II*

An optical/electronic instrument (OPCON) was used for the measurement of the time-dependent (intra-wave) suspended sediment concentration (for  $z > 0.5$  cm). The sampling frequency was 40 Hz. The instrument was positioned at  $x = 2.00$  m. The range of elevations of the measurements was from 10 cm from the bed down to 0.5 cm.

Three concentration verticals with each 9 measuring elevations were obtained. Each level measurement took 3 minutes thus it was possible to do three measurements each tunnelrun ( $\pm 10$  minutes), so 9 tests per condition were necessary. Because during the first OPCON elevation measurement of each test the bed level erosion was generally too strong (too strong decay of the OPCON signal during the first three minutes), it was decided to repeat the first three elevations in one test per condition. During the first two minutes of these 11 minute test (code Ei-14) no measurement was taken. The measurement started after the first two minutes of the test.

Due to the failure of OPCON or because the desired flow conditions were not realized, some tests had to be repeated. The new tests had a duration of 11 minutes. The OPCON elevation above the bed was measured after each level measurement (i.e. 3 times per test).

*Series III*

An electro-magnetic flow meter (EMF) was used for the measurement of the time dependent horizontal velocities especially near the bottom where this was not possible by LDFM (see Series IV). The sampling frequency was 10 Hz. The instrument was positioned at  $x = 2.00$  m. The range of the EMF measurements was from 9 cm from the bed down to 1.5 cm.

Four tests (tunnel runs) per condition were realized (codes Ei-15...Ei-18). Especially for condition E4 an extra test was made with emphasis in the region  $z = \pm 2$  cm where a first analysis showed that in previous tests relatively large variations occurred (code E4-19). During each test (duration 10 min) the velocities at three elevations were measured. The EMF elevation was measured before and after each measurement (similar to OPCON).

*Series IV*

During this series of tests the time dependent horizontal and vertical velocities using a forward scatter laser system (LDFM) and the time dependent concentrations in the sheetflow layer using a conductivity concentration meter (CCM) were measured. The sampling frequency was 40 Hz. The CCM was positioned at  $x = 2.05$  m while the laser was positioned at  $x = 0.0$  m and at  $x = 2.0$  m in order to judge the uniformity of the velocity profile along the tunnel. The velocity measurements were conducted from 20 cm above the bed down to 3 cm. The CCM elevations covered the region from 9 mm

above the bed until about 6 mm inside the bed. To prevent aliasing effects analogue low pass filters (cut-off frequency 20 Hz) were applied to all channels before analogue-digital (A-D) conversion.

Eight tests per condition were carried out (codes Ei-20...Ei-27). For condition E1 an additional test (code E1-28) was made. During each test (duration 12 minutes) the velocities were measured at three elevations while the CCM elevation was sometimes changed more than three times per test depending on the steadiness of the bed. The bed level at the laser position was measured three times per test while at the CCM position it was measured every minute.

### *Series V*

During series V high speed video recordings were made to be used for the measurement of the sand grain velocities. The camera was focused at the horizontal position  $x = 2.05$  m. The depth range covered was from -8 mm to 28 mm with respect to the initial bed level.

Three tests for condition E1 (codes E1-HSV-1 ...E1-HSV-3) and one for the other three conditions (codes Ei-HSV) were realized. Three repetitions were done for condition E1 due to the strong bed erosion. The recording duration of each test was 8 min (the tunnel was run for 6.5 min). During each test 6 video recordings at different elevations were made. A normal video camera was focused at a fixed position to serve as a reference. A transparent grid was placed in the recording area. The bed level was measured every thirty seconds.

Apart from the tests of the measuring programme, a number of additional tests were carried out in order to check calibrations, laser support, filter use, etc. In Table 2.8 of the data report the additional tests, their purpose and outcome are listed.

### **3.6 Data acquisition and storage**

During each test the following time dependent parameters were stored on computer files using a PC data acquisition system: the steering signal, the measured piston position, piston velocity, piston pressure, pump discharge, horizontal and vertical velocity measured by a laser at a fixed elevation (normally at 20 cm) and the signal of the measured quantity. The measured analogue signals were digitized by means of an analog to digital (A/D) converter and stored to the PC in a binary format (two files for each test, a binary with extension .dat and an ASCII with extension .seq). All the measured signals were also recorded on paper. The bed level measurements and the sand heights in the measuring tubes (used for the calculation of the time averaged concentration) were recorded on measuring forms and later transformed to ASCII files.

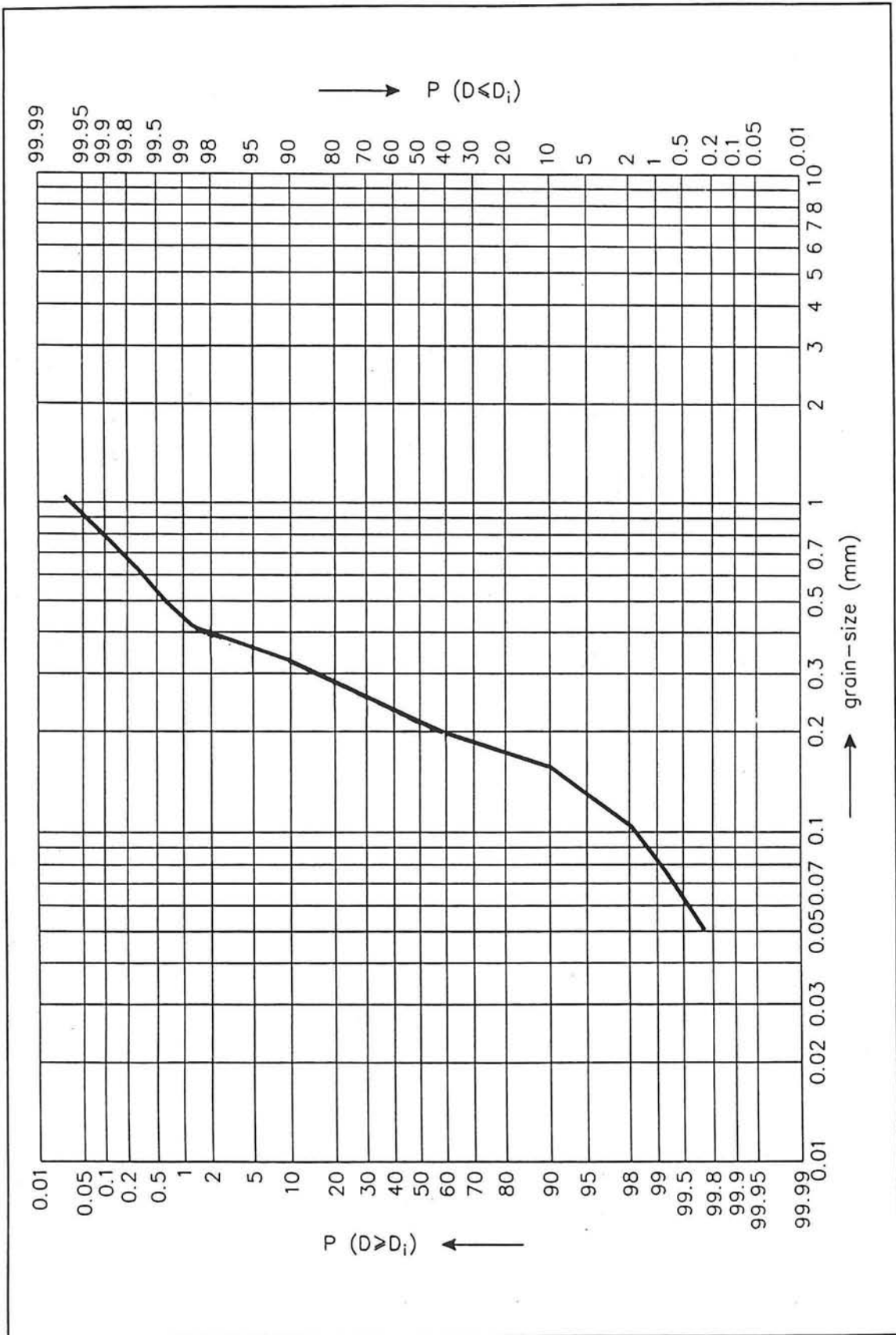


Figure 3.9 Grain-size distribution



## 4 Results of experiments and comparison with other experiments

### 4.1 Introduction

The data processing was done by different members of the research team during and after the execution of the tests. A total overview of the processed raw data can be found in the data report (Katapodi et al, 1994). In this report the main results of this analysis are given, and some further data processing and analysis is carried out. The main effort was focused on the derivation of the time dependent and time averaged sediment fluxes and the measured transport rates.

In table 4.1 an overview is given of the processed data. In the first column the type of processed data is given (which instrument, time averaged or time dependent if relevant). In the second column it is stated which of the data can be found in the data report. In the last column is stated whether the data processing was done as part of this thesis.

Instrument/ subject	Data report	Thesis
Transport	yes	yes
SUCTION	yes	no
EMF - time averaged	yes	no
EMF - intra-wave	yes (only E1/E3)	no
OPCON - time averaged	yes	partly
OPCON - intra-wave	yes	no
LDFM - time averaged	yes	partly
LDFM - intra-wave	partly (only E1/E3)	partly
CCM - time averaged	yes	yes
CCM - intra-wave	yes	yes
HSV - intra-wave	yes (E1/E3)	partly
flux - time averaged	no	yes
flux - intra-wave	no	yes

*Table 4.1 Processed data*

Results of the data processing are compared with previous research, like former water tunnel tests at DELFT HYDRAULICS and tests performed by Dick and Sleath (1991,1992). This comparison does not claim to give a complete review of relevant literature.

This chapter is divided into four sections. The introduction (section 4.1), concentration measurements (section 4.2), velocity measurements (section 4.3) and sediment fluxes (section 4.4).

## 4.2 Concentration profiles

### 4.2.1 General

Concentrations were measured using three different instruments: an optical concentration meter (OPCON), a conductivity concentration meter (CCM) and a transverse suction system. The latter is only suitable to measure time averaged concentrations, but it has the advantage that the grain-size distribution in the vertical can be determined. The OPCON and the suction system are used to measure concentrations in the suspension layer, the CCM for measuring concentrations in the sheetflow layer and below the initial bed level. The suspension layer starts approximately 1 cm above the bed (the initial bed, without motion, is defined at level  $z = 0$ ). The measuring frequency of both OPCON and CCM was 40 Hz. In this section concentrations are given in grams/litre, a concentration of 26.5 g/l is equal to one volume percent.

First the time averaged results are presented and second the time dependent concentration profiles.

### 4.2.2 Time averaged concentration profiles

The OPCON and the suction system give comparable results. Plotted on a log-log scale it is possible to draw a straight line through the points (see Figure 4.2.1). This was also found by Ribberink and Al-Salem (1992) who suggested the following relationship for situations with plane-bed conditions (only waves).

$$\langle C \rangle = C_a \left( \frac{Z_a}{z} \right)^\alpha \quad (4.1)$$

herein:  $\alpha$  = concentration decay parameter

$C_a$  = reference concentration at  $Z = Z_a$

Ribberink and Al-Salem found that the concentration decay parameter was constant for a wide range of velocities and wave periods ( $\alpha = 2.1 \pm 0.1$ ). Also for waves combined with a current the same relationship was obtained but with a smaller  $\alpha$  (see Ramadan, 1993). For the present tests the following values for  $\alpha$  were obtained (including all the results of OPCON and SUCTION):

Condition	E1	E2	E3	E4
$\alpha$	2.2	2.2	2.4	1.9

Table 4.2 Calculated values of concentration decay parameter

Closer to the bed (in the sheetflow layer) and inside the bed ( $z < 0$ ) concentrations were measured with the CCM. Inside the bed an almost constant mean concentration of about 1100 - 1400 g/lit was measured (42 - 53 %). Just above the bed (in the sheetflow layer) a straight line can be fitted through the points if they are plotted on a log-linear scale (see Figure 4.2.2). Concentrations are increasing with increasing wave height.

The three different zones as described above (suspension layer, upper sheetflow layer and pick-up layer, as observed before by Ribberink/ Al-Salem, 1992) can be seen clearly on the combined plots in Figure 4.2.3. All the measured concentrations (OPCON, SUCTION and CCM) are plotted in this Figure on a log-linear scale. The sheetflow layer is defined as the layer where concentrations are larger than 1 volume percent (26.5 g/litre). In case of E1 (the largest waves) the sheetflow zone extends up to  $\pm 14$  mm above the bed. The thickness of this layer is decreasing with decreasing wave. For E2 the sheetflow layer extends up to approximately 10 mm above the bed, for E3 up to 5.5 mm and for E4 up to 5 mm. In Figure 4.2.4 all results are plotted together on a log-linear scale. In all three regions the concentrations are increasing with increasing wave height (E1  $\rightarrow$  E4). Apparently the waves are dominating.

Dick and Sleath (1991) performed tests in a small-scale wave tunnel and also measured concentrations with another type conduction measuring probe. Perspex grains with a density of 1141 kg/m<sup>3</sup> and a median diameter of 0.7 mm were used instead of sand. The test conditions concerned waves with a velocity amplitude between 0.3 and 0.9 m/s and periods between 2.5 and 4.5 seconds and no current. They suggest the following relationship for the concentration in the sheetflow layer:

$$\langle C \rangle = C_0 \exp\left(\frac{-z}{\ell}\right) \quad (4.2)$$

herein:  $\langle C \rangle$  = time averaged concentration  
 $z$  = height above the bed  
 $C_0$  = concentration at  $z = 0$   
 $\ell$  = constant, for sheetflow  $\ell = 30 \cdot D_{50}$

Applying this formula to the measured concentrations of the present experiments (see Figure 4.2.2, elevations greater than 0 cm or Figure 4.2.3, elevations between 0 and 1 cm) learns that the assumption of an exponential distribution is correct, only the choice of  $\ell$  should be different. First this value is not constant, it differs with the condition, a reduction of maximum velocity (E1  $\rightarrow$  E4) gives a lower value of  $\ell$ . Second the values of  $\ell$  are smaller than  $30 \cdot D_{50}$  (between  $30 \cdot D_{50}$  and  $5 \cdot D_{50}$ ). This difference can probably be explained by the low density particles as used by Dick and Sleath. This low density particles have a low settling velocity  $W_s$  and thus a higher ratio of friction velocity  $u_*$  and settling velocity  $W_s$  (more mixing) than in the present experiments. This assumption is confirmed by the fact that during the present experiments  $\ell$  is decreasing if the maximum velocity is decreasing. Increasing velocity means increasing  $u_*$  and thus more mixing.

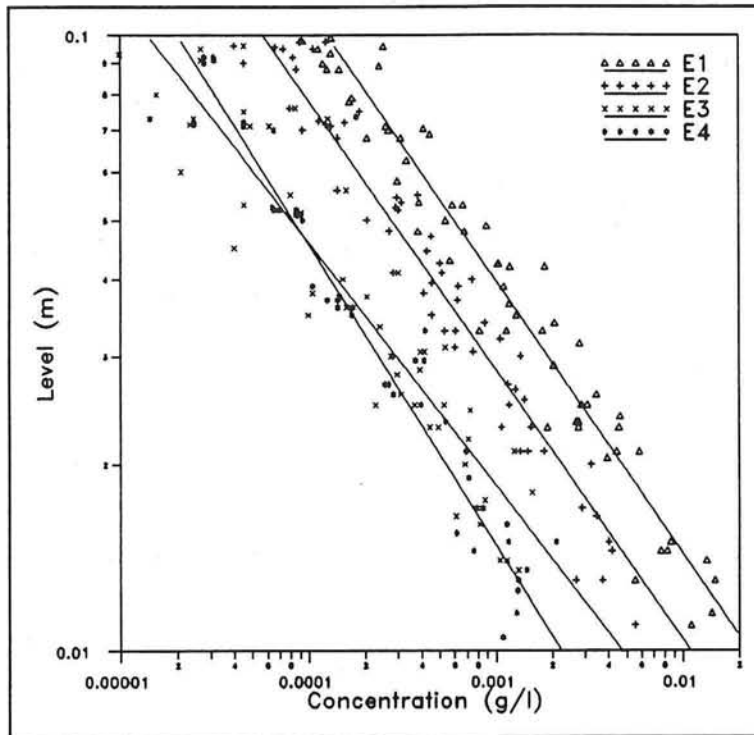


Figure 4.2.1 Averaged concentration profile (OPCON and suction) on log-scale

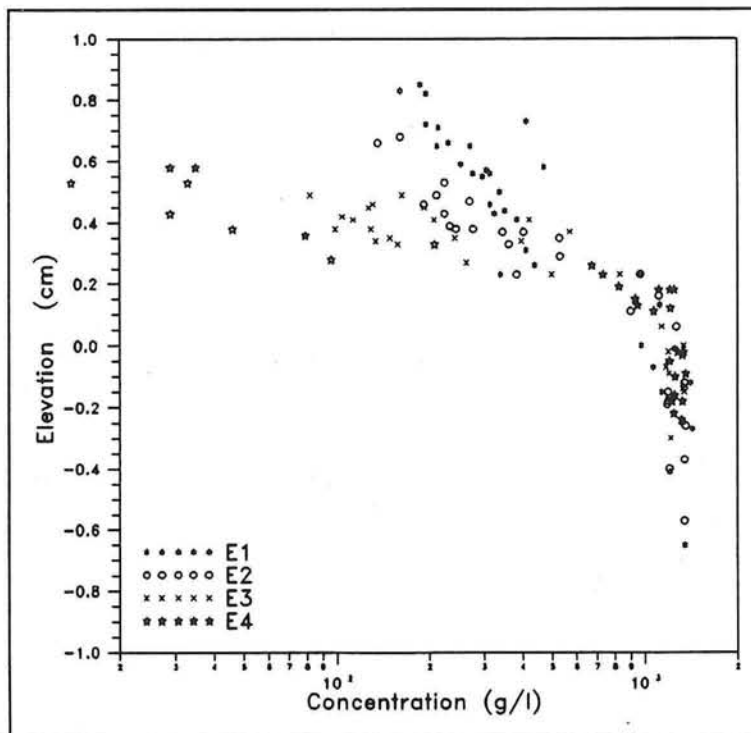


Figure 4.2.2 Averaged concentration profile of CCM-measurements

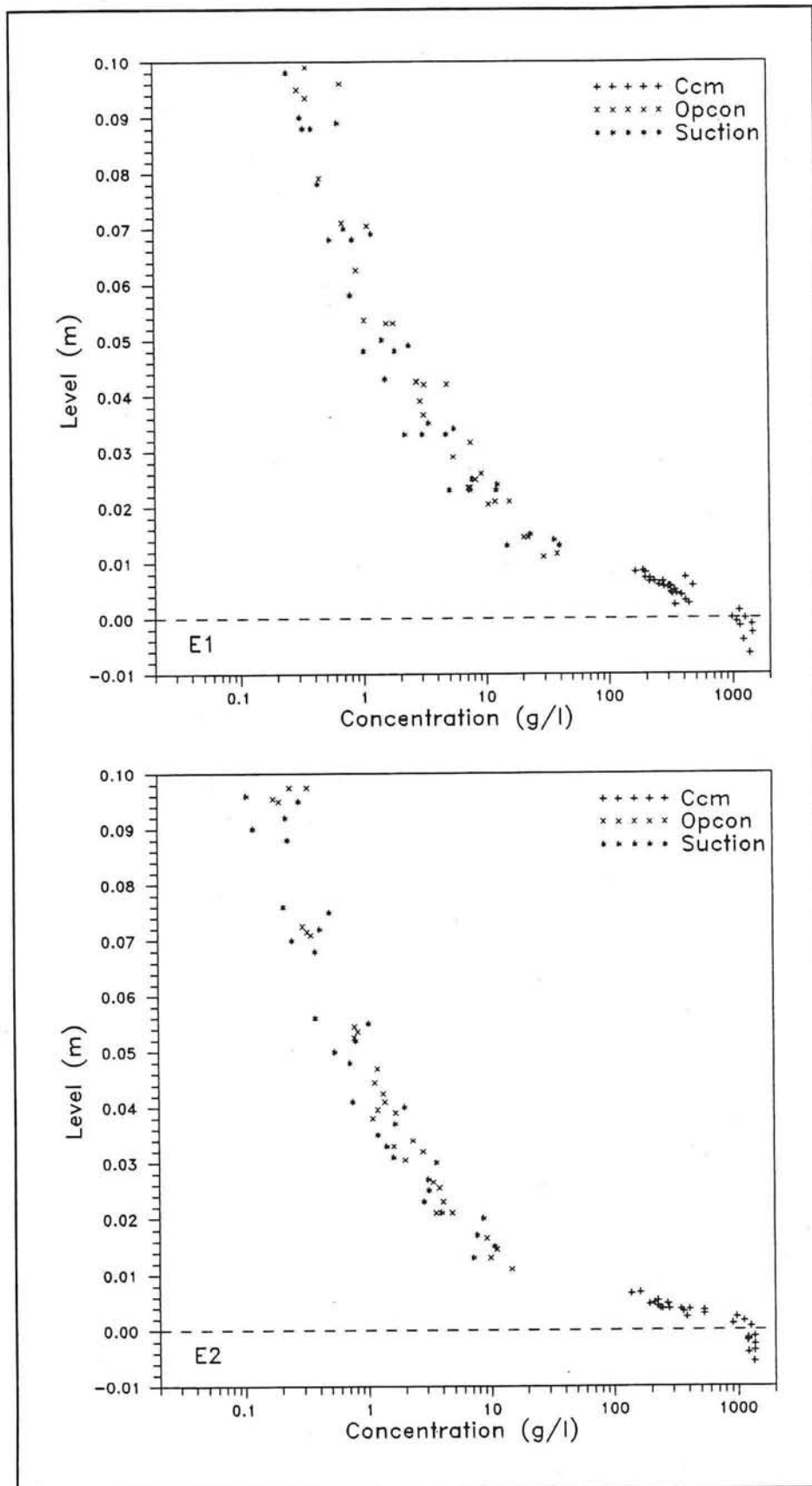


Figure 4.2.3a Combined averaged concentration profile of OPCON, Suction and CCM (E1-E2)

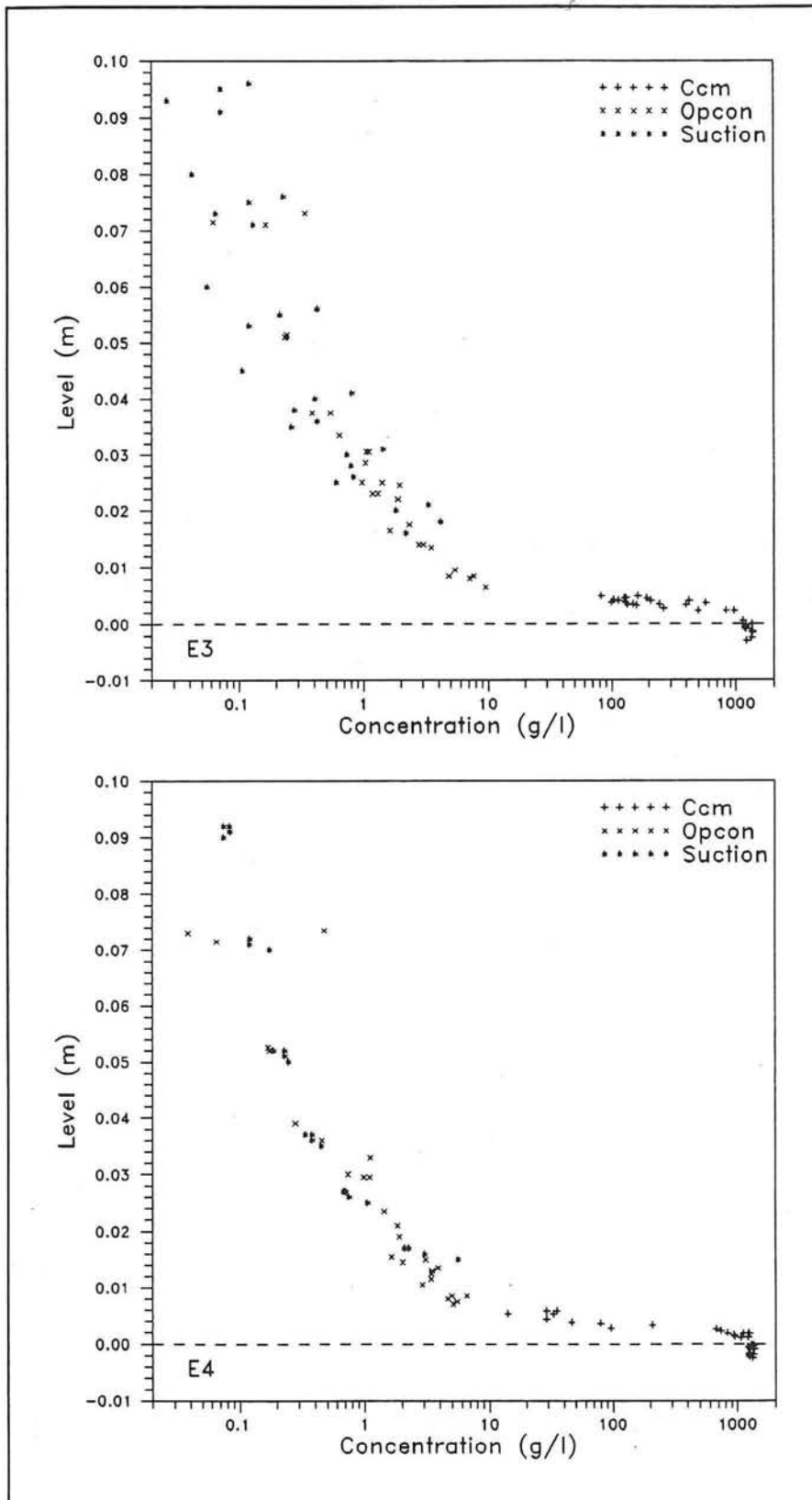


Figure 4.2.3b Combined averaged concentration profile of OPCON, Suction and CCM (E3-E4)

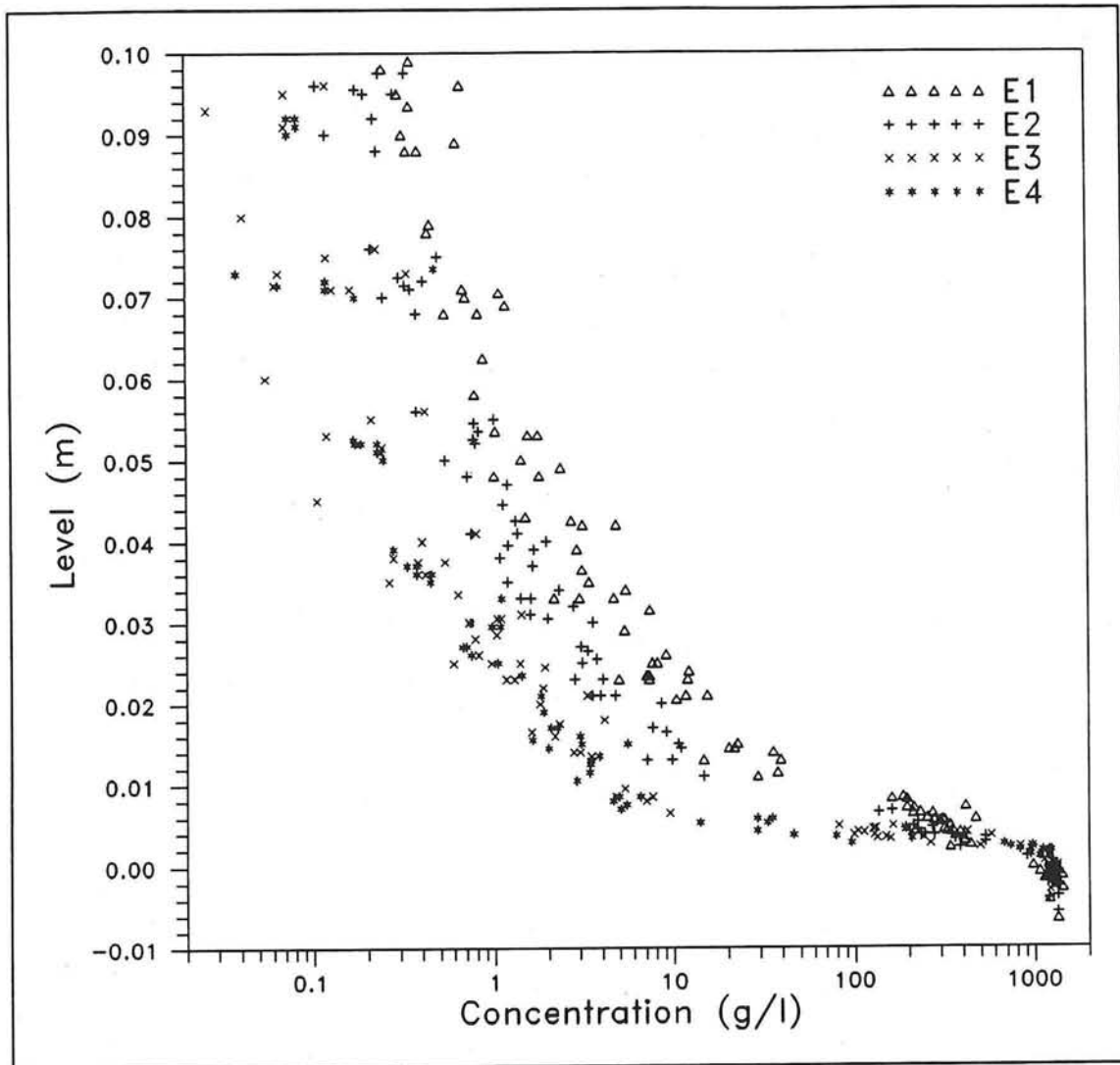


Figure 4.2.4 Averaged concentration profile of all tests combined

### 4.2.3 Time dependent concentration profiles

The measured time dependent concentrations in the suspension and sheetflow layer were ensemble averaged over a number of waves (between 7 and 28). The averaging period was chosen in such a way that the conditions were stable (small erosion rate).

In Figure 4.2.5 the time dependent concentrations measured by OPCON are presented. Clear peaks are present just after the maximum and minimum value of the free stream velocity for the tests E1, E2 and E3. For test E4 (with the smallest wave amplitude, and thus the highest asymmetry) the concentration peak during the negative part of the wave cycle has almost disappeared. Also smaller peaks are present just after the zero crossing of the velocity. Higher in the suspension layer the peaks are less sharp and they appear later: a phase-lag is present.

Time dependent concentrations in the sheetflow layer can be found in Figure 4.2.6. Clearly two zones are visible in the sheetflow layer: concentrations measured in the bed (pick-up layer) and concentrations measured above the bed (upper sheetflow layer). Above the bed the concentrations show the same behaviour as in the suspension layer. Peaks are present during maximum and minimum velocity and at flow reversal (only tests E1 and E2). The peaks measured at flow reversal (tests E1 and E2) are now larger and sharper than the peaks measured during maximum velocity. Now these peaks occur just before the flow reversal, thus earlier than in the suspension layer. Test E3 shows only a small peak at flow reversal and test E4 shows no peak at all at this point.

The concentration behaviour in the pick-up layer is just opposite to the behaviour of the upper sheetflow layer, only the peak at flow reversal is not present at all. The transition between both layers is very sharp. See for example the measurements of E3 in Figure 4.2.6b. Two measurements on  $z = 0.23$  cm (height above the bed) are shown. One behaves as pick-up layer, the other shows the behaviour of the layer just above the bed. Taking in consideration a mistake in the measured level of about 0.5 mm, a transition layer with a thickness of approximately 1 mm is found. The other graphs confirm this assumption.

Maybe the appearance of peaks at flow reversal can be explained by a higher turbulence level occurring during flow reversal. This turbulence was clearly visible at the high speed video recordings which were made during the tests. Just before flow reversal horizontal velocities became very small, thus  $\theta < \theta_c$  ( $\theta_c$  = critical Shields number). Horizontal displacement of grains stops and grains move downwards. A few tenths of seconds later, after the zero crossing, fluid velocity is accelerating again and  $\theta > \theta_c$ . Sediment grains are now moving first vertical and then again horizontal (in opposite direction). The phase-lead of the near bed boundary layer flow causes this process to start at the bed and propagating upward in the sheetflow layer within half a second.

The flow reversal peaks in the sheetflow layer were not found in former water tunnel tests with only waves (Ribberink et al, 1992). Maybe this can be explained by the small duration of these peaks and the smaller measuring frequency during the former tests (10 Hz in stead of 40 Hz).

In Figure 4.2.7 time dependent concentration verticals of three tests are shown (E1, E3 and C). Test C is treated here because the analysis of the high speed video recordings of this test was done as part of this report. This test was executed by Al-Salem in 1992 with condition 1 mentioned in table 2.1 in the report of Ribberink/ Al-Salem, 1992. The test conditions concerned a regular 2<sup>nd</sup> order Stokes wave,  $u_{rms}$  of about 0.58 m/s and an asymmetry of 0.66 (asymmetry =  $u_c/(u_c + u_r)$ ), the wave period was 6.5 seconds and no current was added. In this graph  $t = 0$  is at a zero crossing of the velocity at  $z = 20$  cm (in case of E1 and E2 the zero-down crossing, in case of C the zero-up crossing). In the plots of E1 and E3 the two upper points and in the plot of C the three upper points represent concentrations measured by OPCON, the other concentrations are measured by CCM. Again straight lines can be drawn through the points in the sheetflow layer.

The time dependent results of Dick and Sleath (as mentioned in the section before) are not comparable with the present tests. They found that minimum concentration corresponded with maximum velocity, and maximum concentration occurred at flow reversal. This different behaviour can probably be explained by the fact that they used less dense particles (perspex) with a lower fall velocity. Thus adaption of concentrations in case of changing velocities will take place slowly, and larger phase-lags will occur.

Staub et al (1984) used a 'carousel sampler' to measure concentrations in a large-scale oscillating water tunnel. The carousel sampler consisted of a suction system combined with a rotating wheel with 18 cups. They used normal sand with median diameters of 0.19 and 0.38 mm. Wave periods were 9.1 and 6.8 seconds and maximum velocities 1.3 and 1.9 m/s. The used measuring device did not allow detailed measurements and measurements very near and in the bed. They report maximum concentrations during maximum positive and negative velocities and minimum concentrations during flow reversal, comparable with the OPCON results of the present experiments.

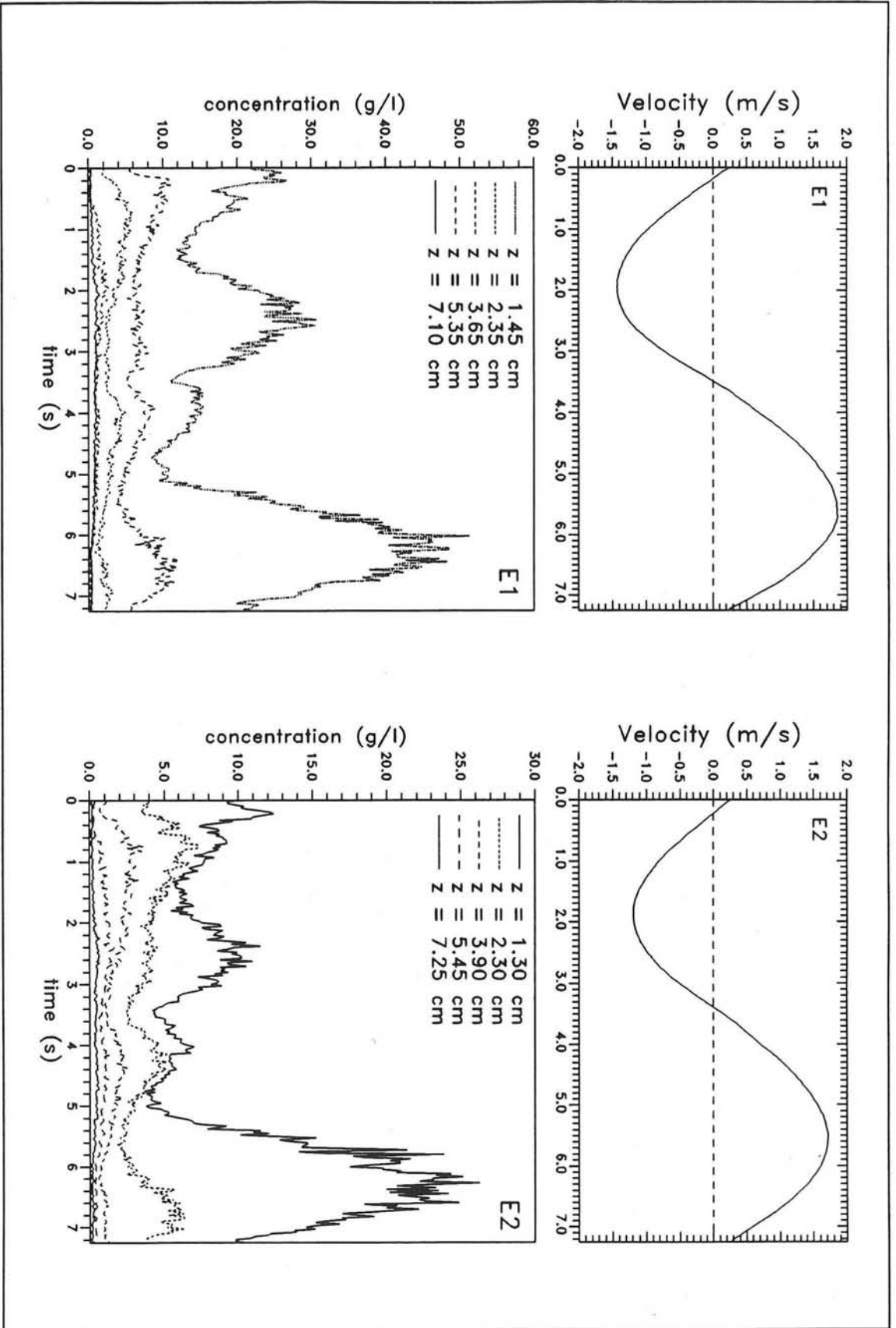
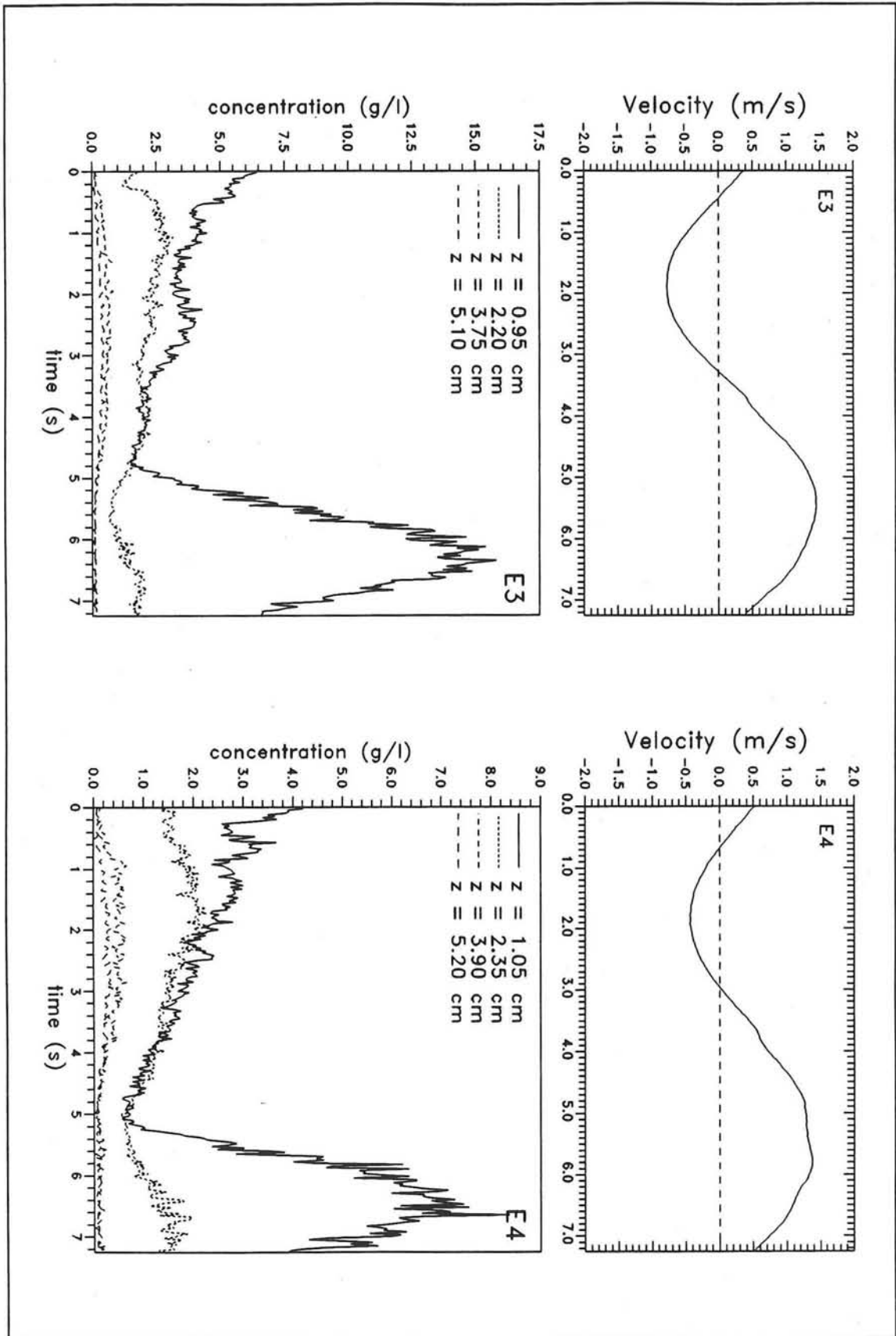


Figure 4.2.5a Ensemble averaged concentration profiles OPCON (E1-E2)

Figure 4.2.5b Ensemble averaged concentration profiles OPCON (E3-E4)



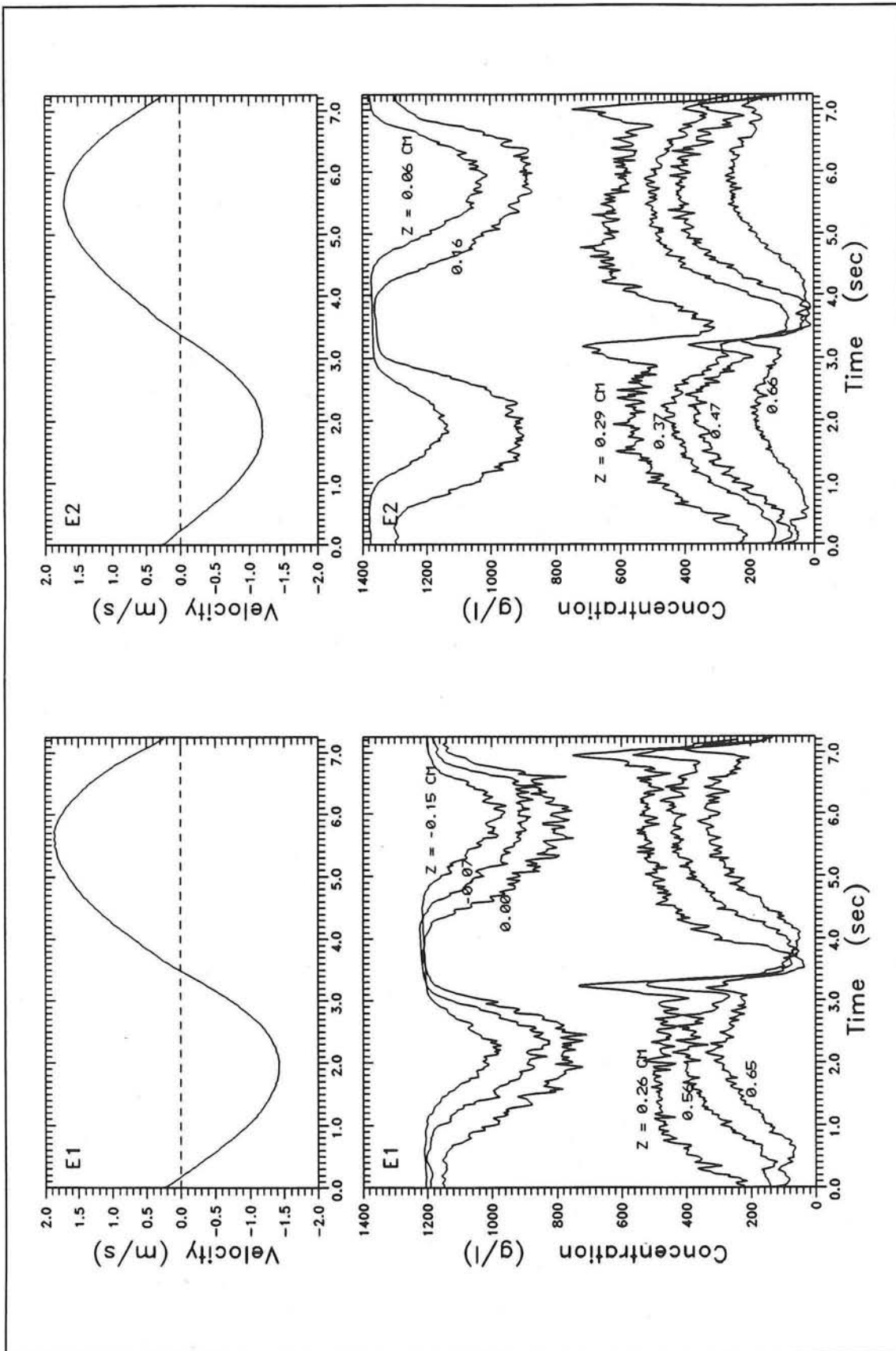


Figure 4.2.6a Ensemble averaged concentration profiles ccm (E1-E2)

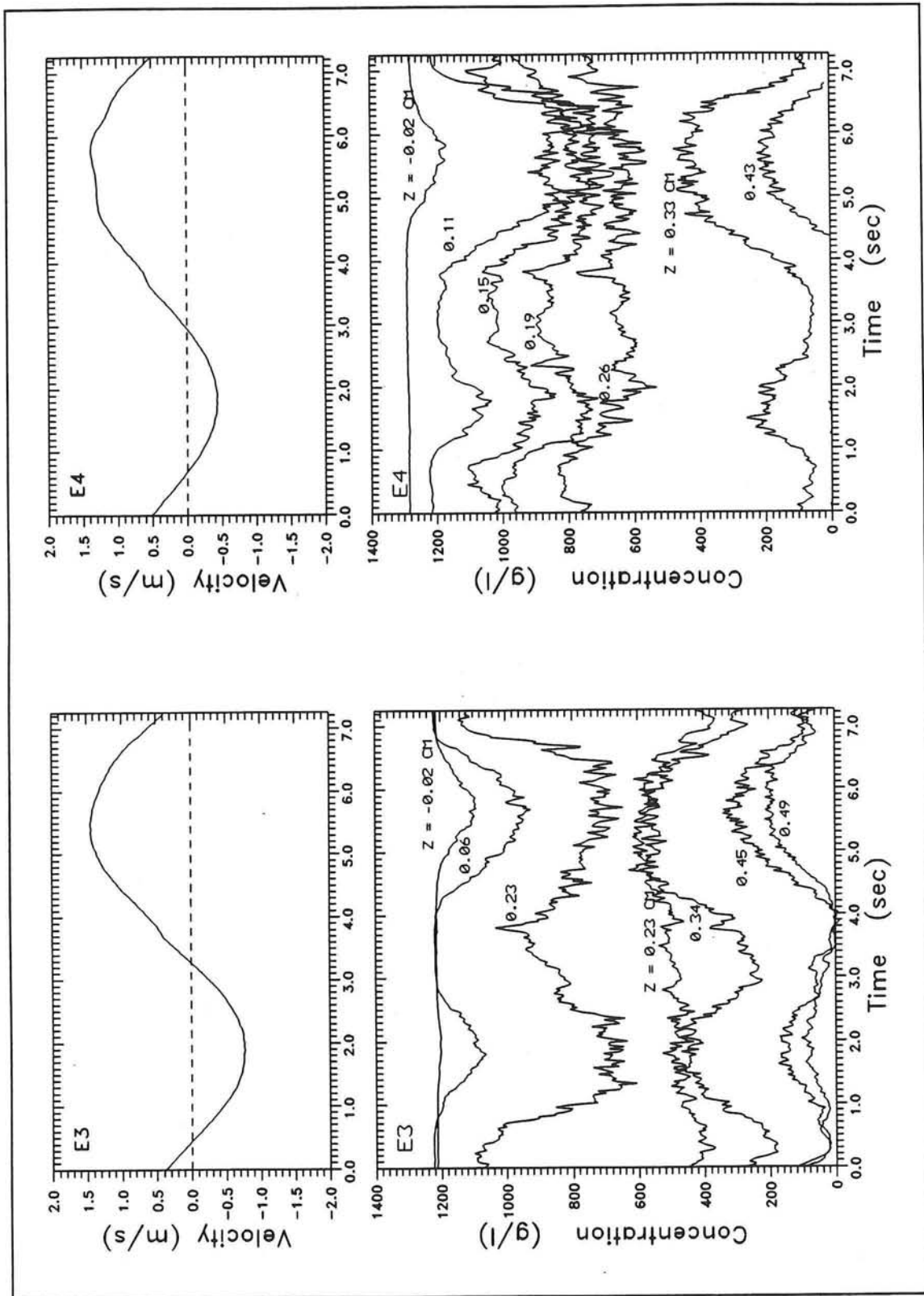


Figure 4.2.6b Ensemble averaged concentration profiles CCM (E3-E4)

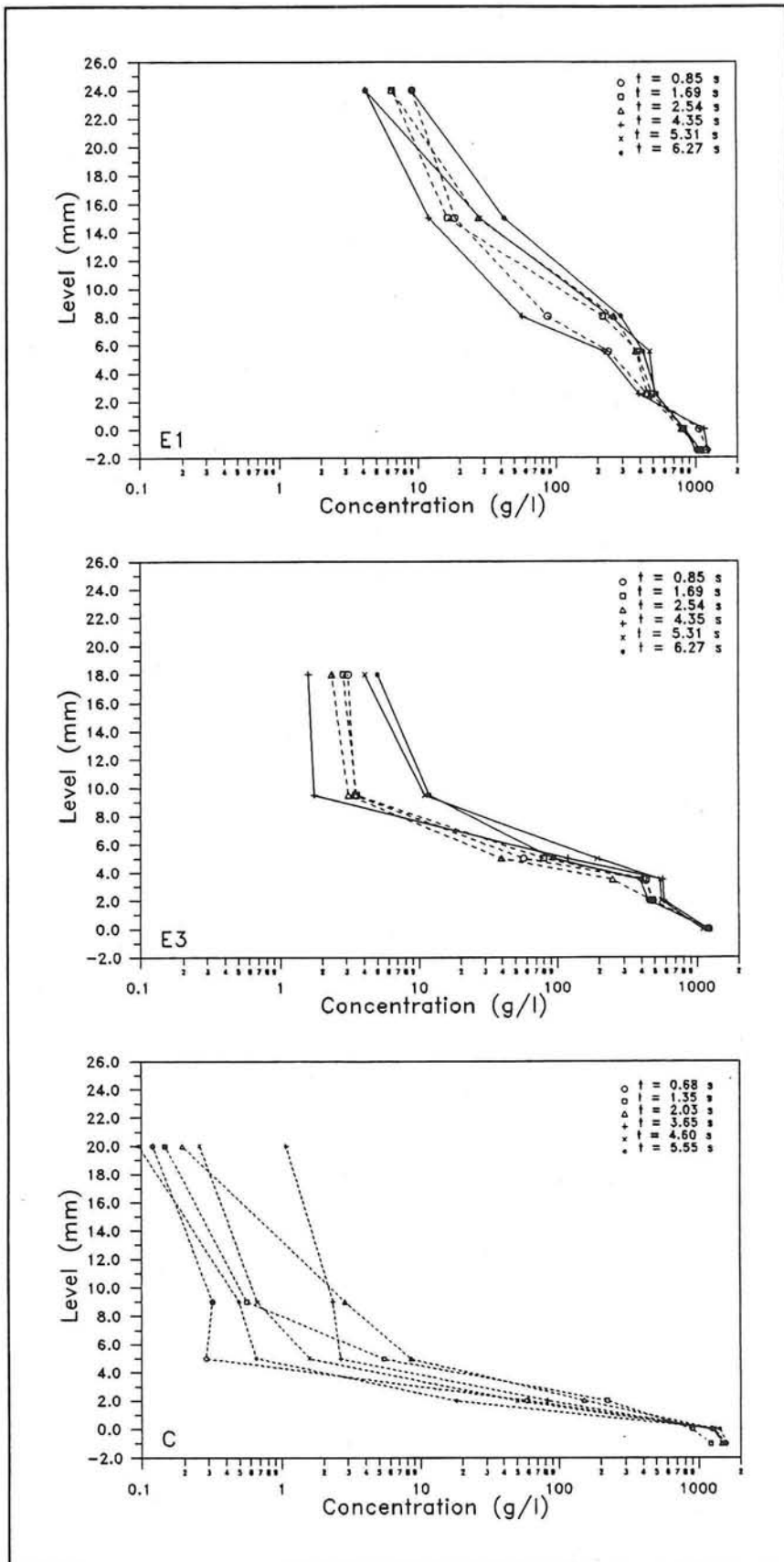


Figure 4.2.7 Concentration profiles in the sheetflow layer

### 4.3 Velocity profiles

#### 4.3.1 General

Flow velocities were measured in the suspension layer by the LDFM (laser) and the EMF. The EMF is less accurate than the LDFM but is also less hindered by suspended sand particles (thus it is possible to measure nearer to the bed than with the LDFM). Not all the data are yet analyzed, time dependent horizontal velocities are only available for E1 and E3 (EMF and LDFM, but only LDFM results are presented). Time averaged horizontal velocities are present for all the tests for both EMF and LDFM measurements. The EMF measurements started at about 1 cm above the bed, LDFM measurements started between 5 cm (E1) and 3 cm (E4) above the bed (depending on the sediment concentration).

#### 4.3.2 Velocity profiles in the suspension layer

##### *Time averaged velocity profiles*

Time averaged velocity profiles are plotted in Figure 4.3.1 on a log-linear scale. All points of one test condition are marked with the same symbol; for the EMF an open symbol is used and for the LDFM a closed symbol. All profiles show a logarithmic distribution with a slope ( $du/dz$ ) which does not show a large variation for the different conditions.

Most characteristic in this Figure is the deviation between the EMF and the LDFM measurements. On the same height above the bed the EMF gives consequently higher velocities than the LDFM. In the data report also the ensemble averaged horizontal velocities of LDFM and EMF are compared. It appears that the difference is considerable when the velocity is negative and minor when the velocity is positive. This asymmetric behaviour of the difference between LDFM and EMF is responsible for the found difference in the mean velocity.

A good explanation for this difference was not found, also a recalibration of the EMF after the experiments by DELFT HYDRAULICS did not make it fully clear. Comparison with earlier calibrations showed that a variation of  $\pm 1\%$  is possible. Also high velocities ( $> 1.6$  m/s) are overestimated (using a linear calibration relation) with a maximum of 2 cm/s and underestimation (-1 to -2 cm/s) occurs in a lower velocity range ( $< 0.8 - 1.4$  m/s). This may lead to a maximum error of about 4 cm/s in case of large velocities. A more extensive analysis of the observed difference is given in section 3.5.4 of the data report.

##### *Time dependent velocities*

In Figure 4.3.2 time dependent velocities on different heights above the bed are plotted (E1 and E3). It is chosen to add only plots of the LDFM measurements because they are the most reliable (see section 3.5.4 of the data report). To make it possible to observe

phase differences of the oscillatory flow part the velocities are plotted again after subtracting the mean velocity, see Figure 4.3.3. The phase-lag between 5 and 20 cm above the bed is approximately 0.1 seconds. The phase difference seems to be a little larger in case of E3, but the difference is too small to draw conclusions.

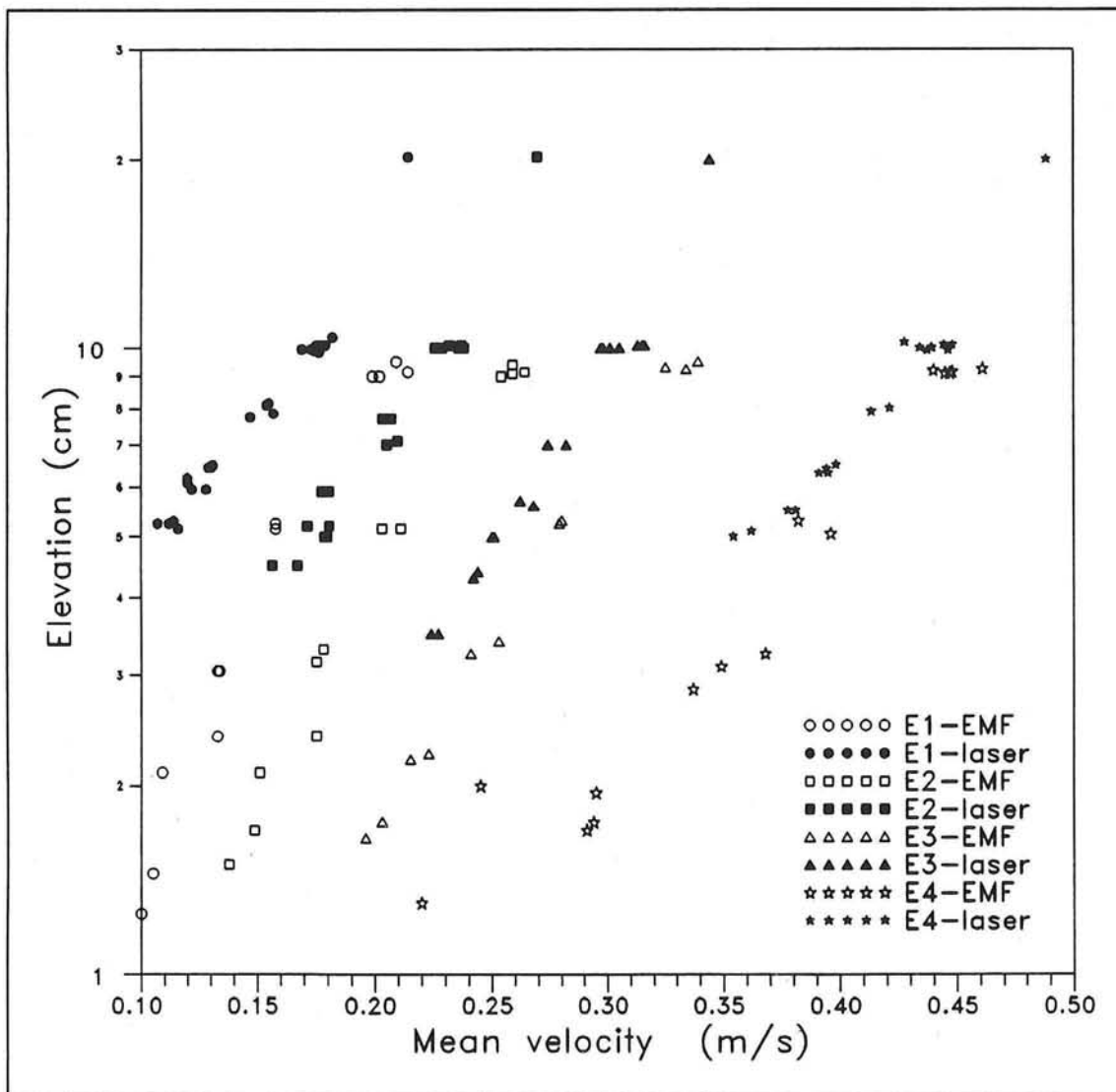


Figure 4.3.1 Averaged velocity, measured by LDFM and EMF

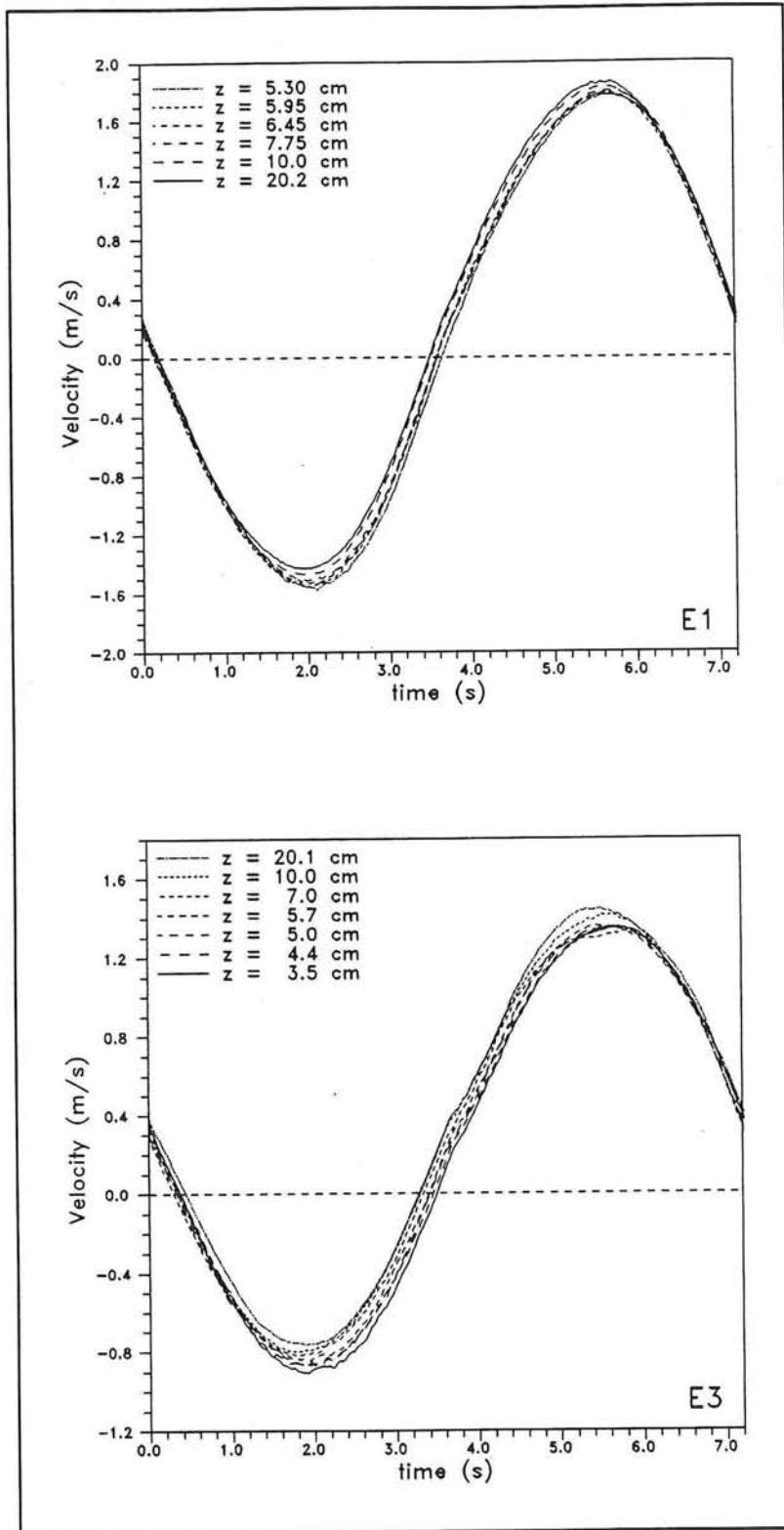


Figure 4.3.2 Ensemble averaged velocity, measured by LDFM (E1 & E3)

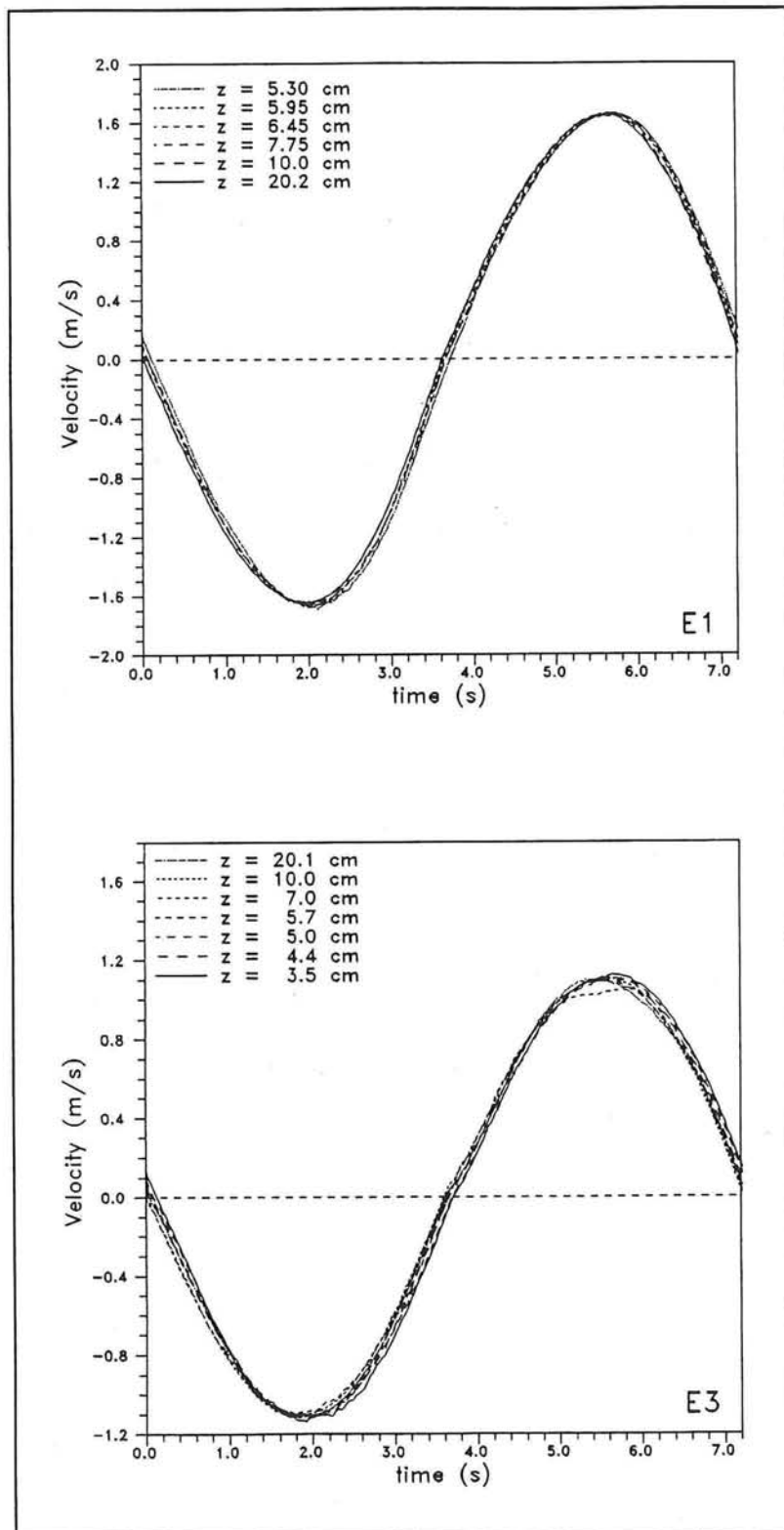


Figure 4.3.3 Ensemble averaged velocity, measured by LDFM, wave-related part (E1 & E3)

### 4.3.3 Velocity profiles in the sheetflow layer

The EMF and the LDFM are not suitable to measure velocities inside the sheetflow layer. To obtain some information about velocities in this layer, high speed video recordings were made and used to estimate grain velocities. This technique was used before by Horikawa et al (1982). Because of the time-consuming analysis not all the tests are yet analyzed, so far only E1 and E3 are ready. E1 was analyzed by me by hand and by S. Longo on a more automatized way. E3 was analyzed by C.M. Janssen and me together. In this section also my hand analysis of a test C of Al-Salem (1992) is presented.

The high speed video recordings were made through the glass side-wall of the test section, using a speed of 500 frames/second. The frame size was 1.2 x 1.6 cm and the focus plane at about 2 cm inside the tunnel. On a normal television screen the enlargement is about twenty times. So a median grain with a diameter of 0.21 mm is about half a centimetre at the television screen. A grain travelling with a speed of 1 m/s will shift about 4 cm each frame at the screen.

The tapes were analyzed by hand which was subject to error, moreover only the velocities near the wall could be obtained with this video technique (see for a discussion about velocities near the wall appendix D). A more detailed description of the used techniques is given in appendix A. Velocities were measured around six different phases during the wave cycle, three of them during negative velocities and three of them during positive velocities (equally spaced over the negative and the positive part). Velocities were obtained by following several grains (6-16) and averaging between them. It was tried to select grains which were not trapped in the wave-boundary layer. It is expected that in general too low velocities were obtained, because the faster grains are the most difficult to follow on the screen. Net time averaged velocity profiles could not be determined because of a too low accuracy. Besides these velocities also the phases of the zero crossings were determined, just by looking when the grains at a specified elevation stopped and started to move in opposite horizontal direction.

Results of the analyses can be found in Figure 4.3.4 and in Figure 4.3.5. In Figure 4.3.4 time dependent velocities at different elevations are plotted combined with the free stream velocity (at  $z = 20$  cm). In the plot of E3 also the velocity at  $z = 1.7$  cm measured with the EMF is plotted, to give an impression of the difference with the HSV result. In the negative part of the wave cycle velocities are comparable; in the positive part velocities are generally much too low. This difference of about 30 % can be explained by the fact that near the wall the velocities are smaller than in the middle of the tunnel; this holds especially for the net velocity (see appendix D and Ribberink, 1994). Thus in the positive part the velocities measured in HSV-analysis are too small and in the negative part the velocities measured in HSV-analysis are too large. As in the analysis the velocities are generally underestimated, this will lead to the observed differences between the positive and the negative part.

Neglecting the error which is made by i) measuring near the wall and ii) underestimating of velocities because fast particles are more difficult to determine, the errors made are about 10 %. This error consists of an error of about 5 % in the

measured distance ( $\pm 20$  cm at the television screen with an error of about 0.5 cm) and an error of about 5 % in the measuring time (particles were followed for  $\pm 0.020$  seconds = 10 frames, the made error is 0.001 second).

In Figure 4.3.5 velocity profiles obtained with HSV are plotted. Two different velocity regimes are visible. In a layer very near the bed and in the bed the velocity increases linear with the height. Outside this layer the velocity increases less rapidly. Although the present results are not very accurate, these trends were also reported by other researchers.

Sawamoto and Yamashita (1986) performed tests in a small-scale oscillating water tunnel. A 16 mm movie camera was used as measuring device. They do not report how they have analyzed the recordings. In stead of sand they used imitation pearl ( $\rho_s = 1600$  kg/m<sup>3</sup>,  $D_{50} = 5.0$  mm), the wave period was 3.8 seconds and the velocity amplitude was 0.9 m/s. Very detailed measurements in the sheetflow layer were performed, as well as vertical and horizontal velocities were reported. The horizontal velocity at different phases during the wave cycle was linearly increasing with the height (similar to the present experiments). Vertical velocities tend to be positive in case of accelerating flow. Also during the present study vertical velocities were determined but because of the chaotic pattern which was found results are not reported. To obtain reliable information about vertical velocities a longer measuring period seems to be necessary so that averaging can take place over a larger number of particles.

Another qualitative result reported by Sawamoto and Yamashita was the fact that particles move only once during a half wave cycle. If a particle settles on the bed, it will not move again during the same half wave period. This statement could not be confirmed during the present tests. It was observed that particles were lifted up from the bed and at the same time other particles settled on the bed. Particles soon disappeared in the bulk of grains present, thus it was impossible to check if particles move only one step.

Dick and Sleath (1991,1992) used a laser-doppler anemometer in backscatter mode to measure velocities inside the sheetflow layer. (See for a detailed description of this laser technique Dick and Sleath, 1991, chapter 3.) Measurements were made through the side-wall,  $\pm 3$  mm inside the wave tunnel. In their case this was outside the wave-boundary layer from the side-wall. Tests concerning sheetflow were done with perspex grains of density 1141 kg/m<sup>3</sup>, the velocity amplitude varied between 0.3 and 0.9 m/s. They also found that inside the wave-boundary layer the velocity is linearly increasing with the height. Horikawa et al. (1982) found comparable results.

Measuring with a laser in backscatter mode seems a more effective way to measure velocities than high speed video analysis. Of course measuring near the wall will give the same problems as with the high speed video but the method is more precise and less time-consuming (HSV-analysis of one condition lasted six days). The value of the present HSV-recordings is that an impression of the movement of individual grains is obtained, which can be helpful to gain a better understanding of the processes in the sheetflow layer.

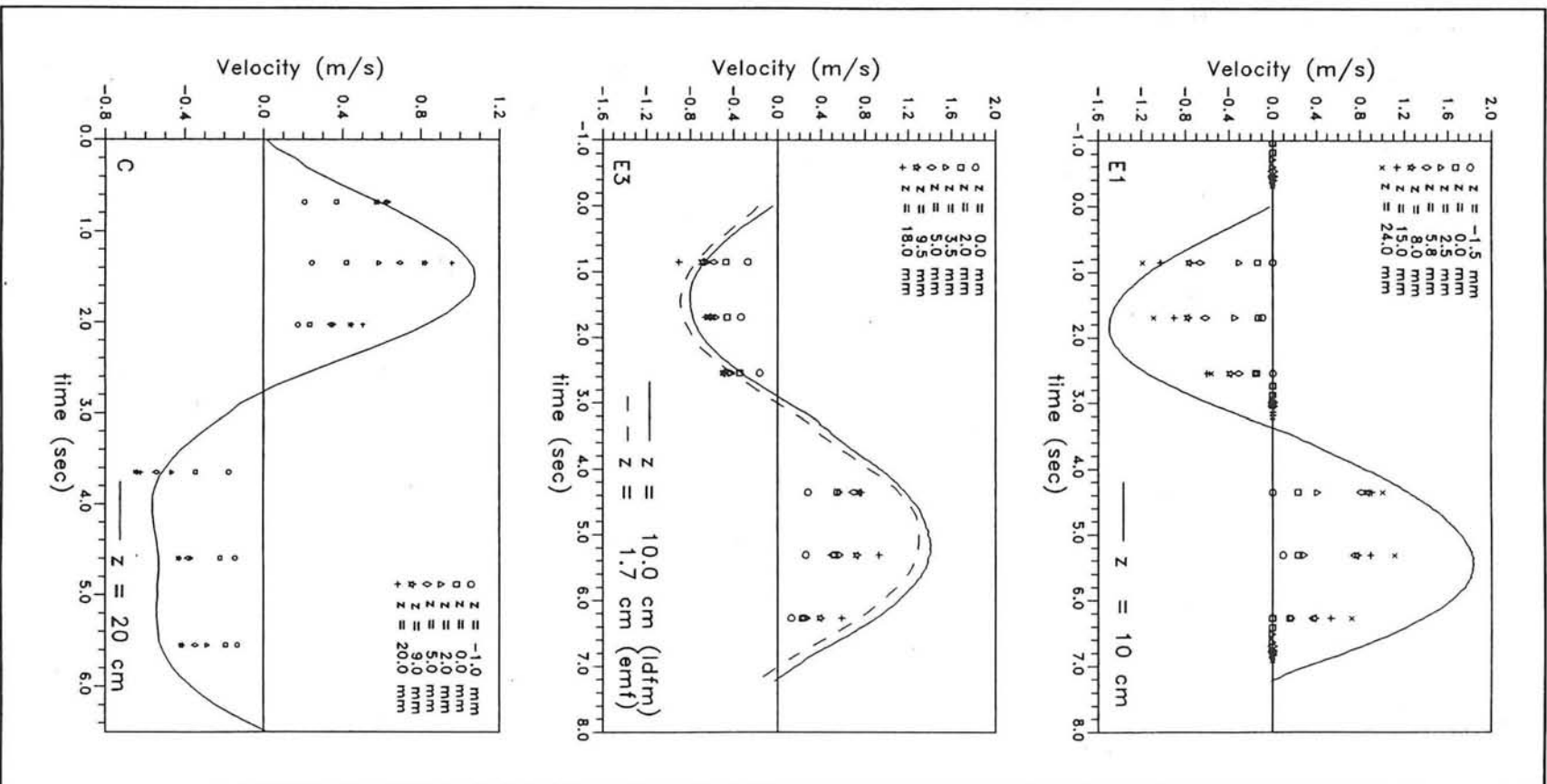


Figure 4.3.4 Horizontal grain velocity profiles in the sheaf flow layer (E1, E3 & C)

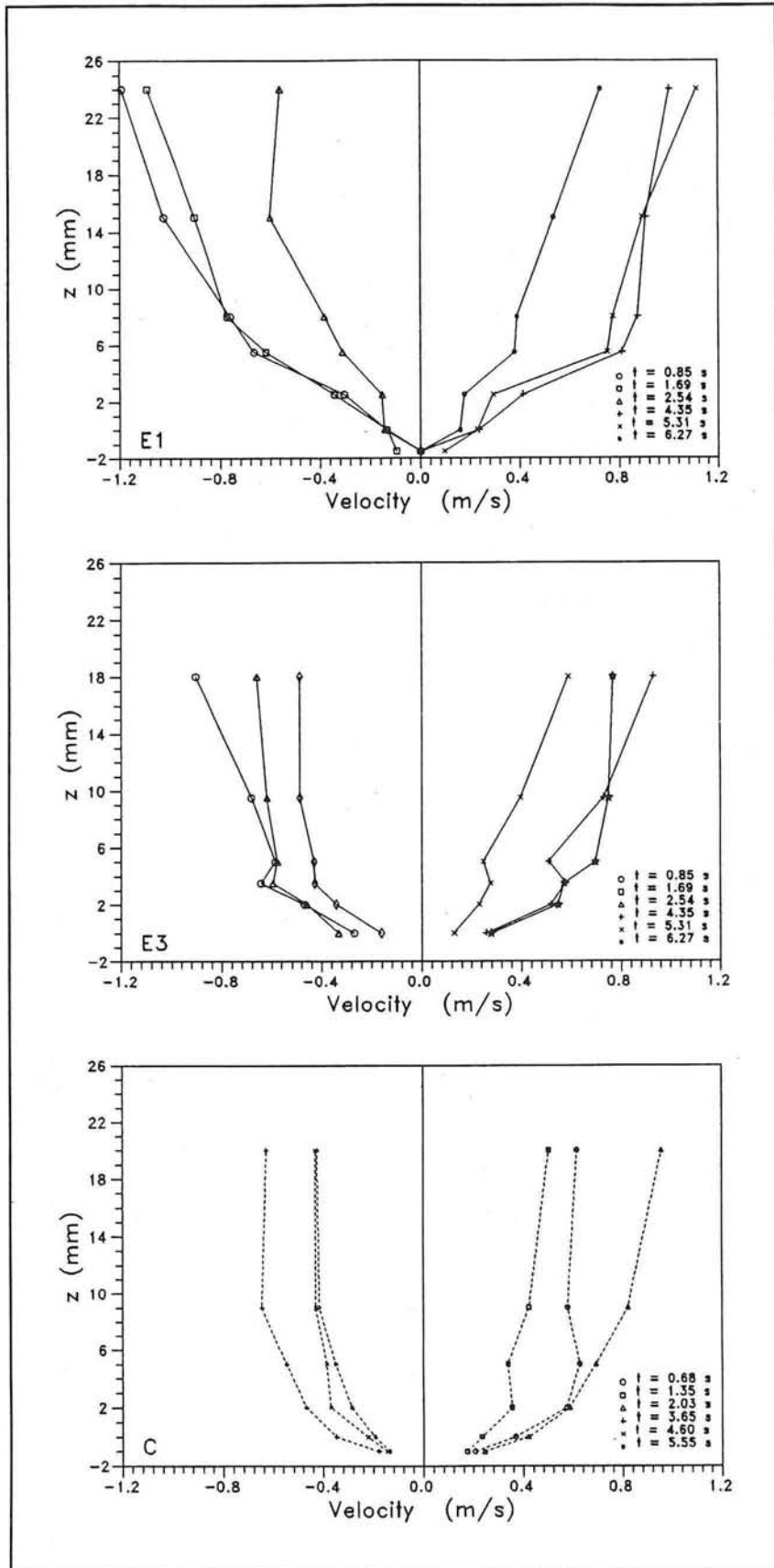


Figure 4.3.5 Horizontal grain velocity profiles in the sheetflow layer (E1, E3 & C)

## 4.4 Sediment fluxes

### 4.4.1 General

The total net sediment transport rates were determined during the first series of experiments (Ei-01..04); the test E1-01 was skipped because of too much erosion. The transport was calculated with the mass-conservation technique (see appendix A6). In Figure 4.4.1 the average bed level change during the tests is plotted. It can be observed that in the middle of the test section the bed stays fairly stable. The calculated sediment transport rates are plotted in Figure 4.4.2. The gap in the lines in the middle of the section arises because of an inaccuracy in the measured bed levels, measured sand weights etc. The measured transport rates as obtained from the average value of  $x = 0$  can be found in table 4.3 (without correction for influence side wall).

For each condition the following statistical parameters were calculated:

- The averaged transport over all the tests:  $\langle q \rangle_{\text{avg}}$
- The standard deviation of the individual tests:

$$\sigma = \sqrt{\frac{1}{N} \sum_{i=1}^{i=N} [\langle q \rangle_i - \langle q \rangle_{\text{avg}}]^2} \quad (4.3)$$

In which:  $\langle q \rangle_i$  = measured transport rate for individual tests  
 $N$  = total number of tests for one condition

- The relative error, defined as:  $r = \frac{\sigma}{\langle q \rangle_{\text{avg}}} * 100\%$  (4.4)
- The relative error of the averaged transport rate, estimated with:

$$r_{\text{avg}} = \frac{r}{\sqrt{N}} \quad (4.5)$$

(this factor indicates the reliability of the calculated transport rate)

test	$\langle q \rangle_{\text{avg}}$ ( $10^{-6} \text{ m}^2/\text{s}$ )	$\sigma$ ( $10^{-6} \text{ m}^2/\text{s}$ )	$r$ (%)	$\frac{r}{\sqrt{N}}$ (%)
E1	92.41	6.01	6.5	3.8
E2	96.35	7.26	7.53	3.8
E3	69.06	8.08	11.7	5.8
E4	70.96	6.60	9.3	4.6

Table 4.3 Sediment transport rates, average

Fluxes on different heights were determined by multiplying the ensemble averaged velocities and concentrations. Fluxes in the suspension layer were calculated by using the results of OPCON, EMF and LDFM measurements. If the velocity was not known on the same height as the concentrations then linear interpolation between two ensemble averaged velocities was carried out. (For a complete review of the used measurements in this analysis see the tables in appendix F.) A value for the total suspended transport was calculated by first integrating over time and then over height.

The fluxes in the sheetflow layer were calculated by using the grain velocities from the HSV-analysis and the concentrations from the CCM. Because of the relative large error in the obtained grain velocities ( $\pm 30\%$ ) the computed fluxes also have a relatively low accuracy. (These results are also included in appendix F.)

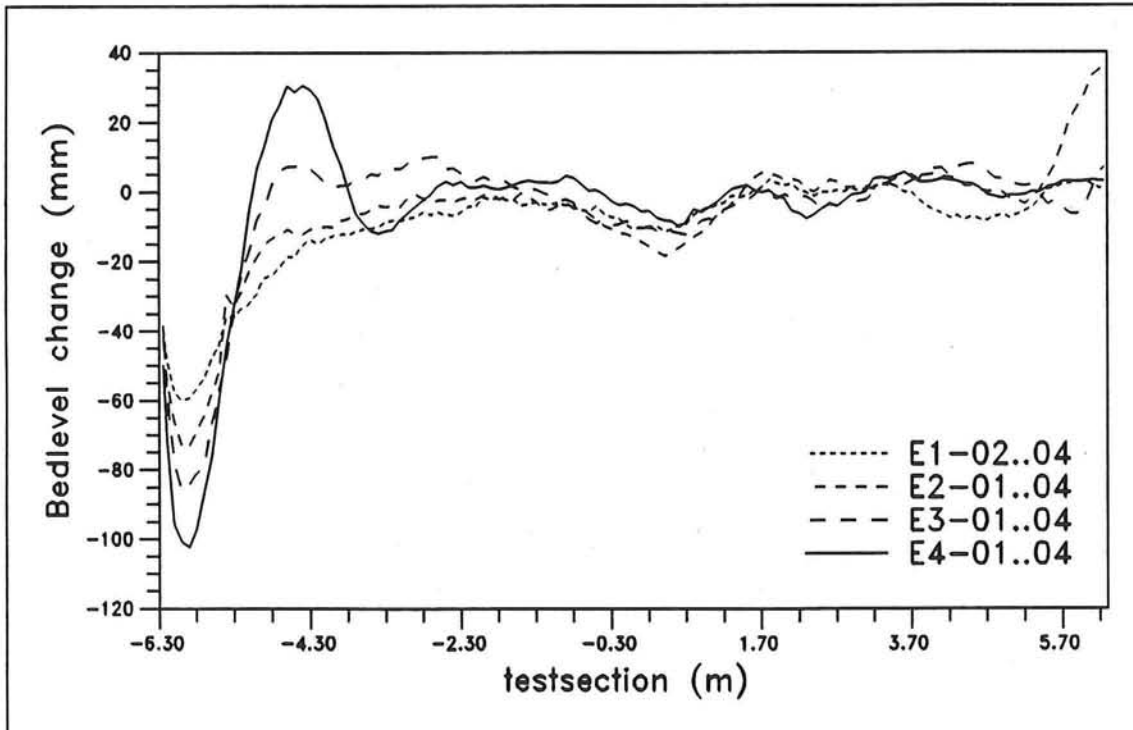


Figure 4.4.1 Averaged erosion of the bed during the experiments

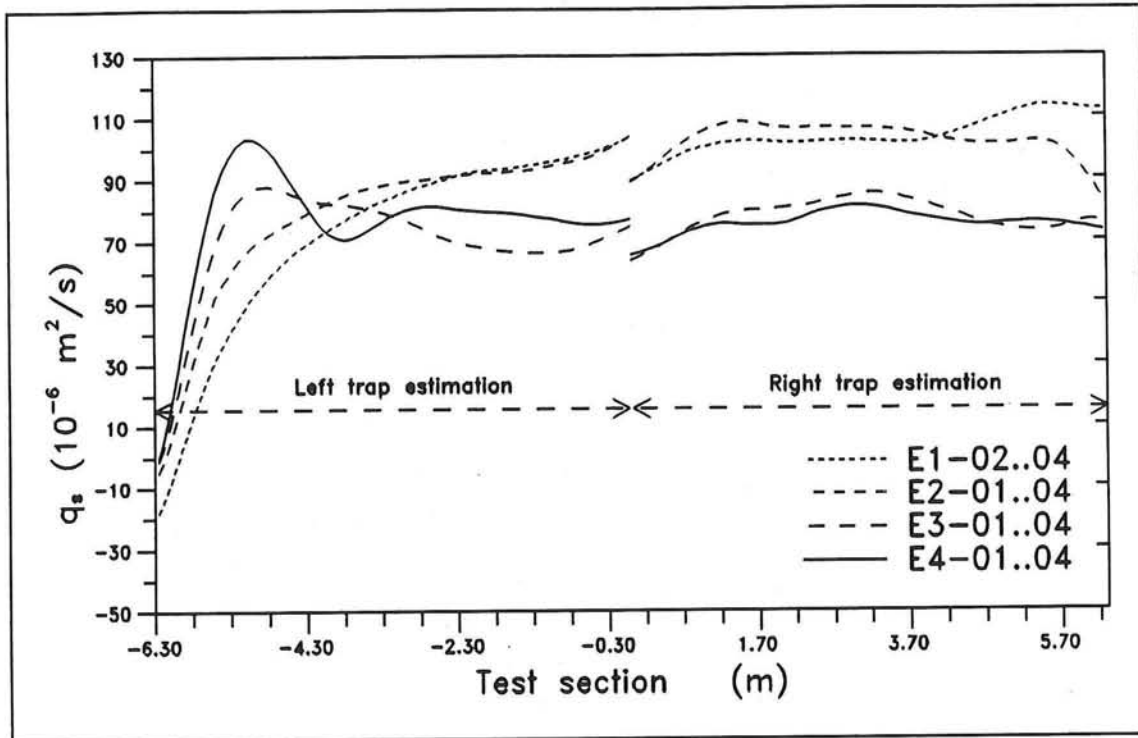


Figure 4.4.2 Measured sediment transport rates over the test section

#### 4.4.2 Flux profiles in the suspension layer

##### Time averaged sediment fluxes

Time averaged flux profiles are plotted in Figure 4.4.3 (for the used instruments see the legends in the lower left corner of the Figures). The total flux is divided in a wave and a current-related part:

$$\langle \phi_s(z) \rangle = \langle u(z,t) * C(z,t) \rangle = \langle u(z) \rangle * \langle C(z) \rangle + \langle \tilde{u}(z) * \tilde{C}(z) \rangle \quad (4.6)$$

Herein:  $\phi$  = flux  
 $C$  = concentration (2650 gram/litre =  $1 \text{ m}^3/\text{m}^3$ )  
 $u$  = velocity  
 $\langle \dots \rangle$  = time averaged  
 $\tilde{\dots}$  = wave-related part

The total fluxes are decreasing from E1  $\rightarrow$  E4, the decrease in wave height is dominating over the increase in net velocity. The Figure is indicating that (if the lines are extrapolated in the direction of the bed) the transport is dominated by the transport

near the bed. In the upper layers the total transport is negative. This negative portion arises because of a negative wave-related transport in these upper layers. Near the bed the wave-related transport is in the direction of the current. The negative transport in the upper layers can be explained by the delayed behaviour of the suspended sediment. Sediment which is brought into suspension during the positive part of the wave cycle is still in suspension when the flow reverses and will be carried in negative direction.

Further it can be concluded that the wave-related part increases faster than the current-related part with decreasing distance to the bed. So it can be assumed that in the sheetflow layer the transport mechanism is dominated by the waves.

In Figure 4.4.4 the total net fluxes are recombined. In the first graph the total flux of the different tests is compared. Increasing wave gives in general an increasing flux, both in negative direction (upper layer) and in positive direction. In the middle Figure the wave-related fluxes are compared, they show the same trend as the total fluxes. With increasing wave height the thickness of the layer above the bed, where the wave-related transport is positive, is increasing. The last graph gives the comparison of the current-related fluxes; they are also increasing with increasing wave height (from E1 → E4). Thus the decrease in the mean velocity (from E4 → E1) is more than compensated by an increase in the mean concentration (caused by the higher turbulence due to the increasing height of the wave).

#### *Time dependent sediment fluxes*

Time dependent fluxes can be found in Figure 4.4.5. An overview of the used measurements, instruments etc. can be found in appendix F. In the four different graphs (one for each condition) the fluxes are plotted together with the free stream velocity. In general near the bed the asymmetry in the fluxes is larger than the asymmetry in the velocity. The degree of asymmetry is defined as the maximum positive velocity divided by the sum of the maximum positive and negative velocity:

$$R = \frac{u_c}{u_c + u_t} \quad (4.7)$$

Herein: R = asymmetry (= 0.5 in case of sinusoidal waves)

$u_c$  = maximum horizontal velocity in the direction of wave propagation

$u_t$  = maximum horizontal velocity opposite to the direction of wave propagation

Peaks in the flux occur just after maximum and minimum flow velocity, a secondary peak occurs after flow reversal. The peak which occurs after the zero-down crossing increases in importance with decreasing wave. For condition E4 this peak is even more important than the peak occurring just after minimum velocity. The peaks found in the fluxes can be explained by the peaks found in the concentration measurements.

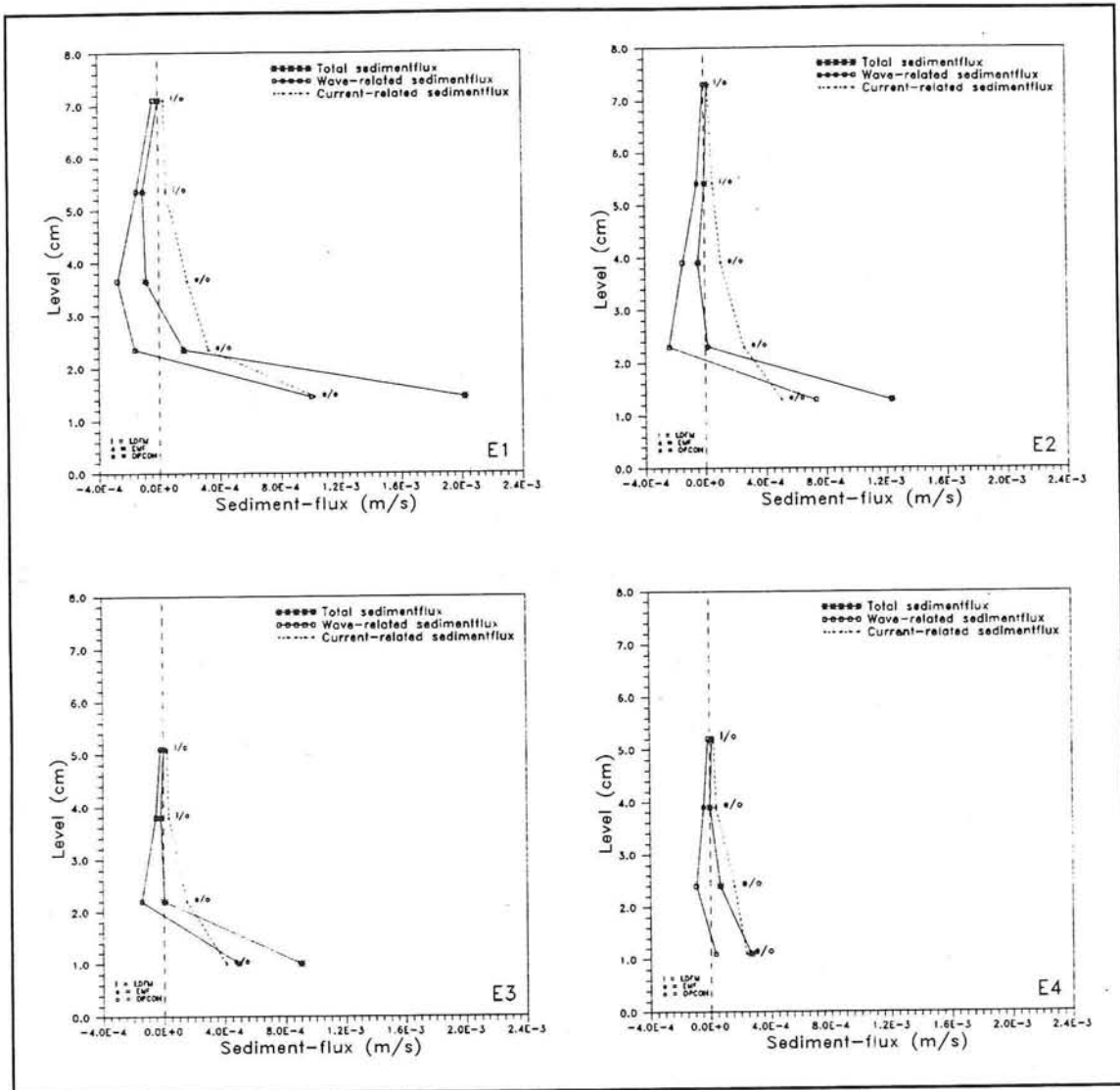


Figure 4.4.3 Averaged sediment fluxes, total, wave- and current-related (E1-E4)

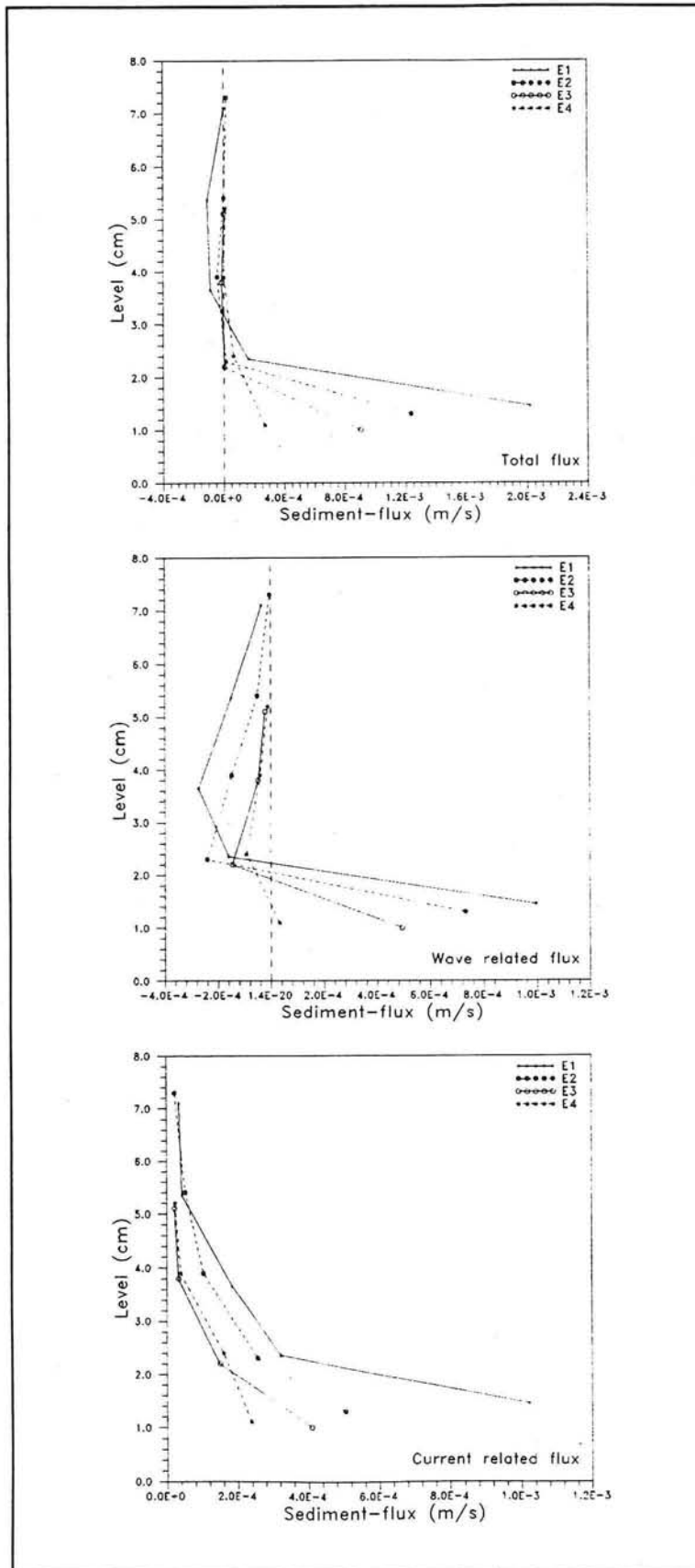


Figure 4.4.4 Combined plot of sediment fluxes in the suspension layer (total, wave and current-related)

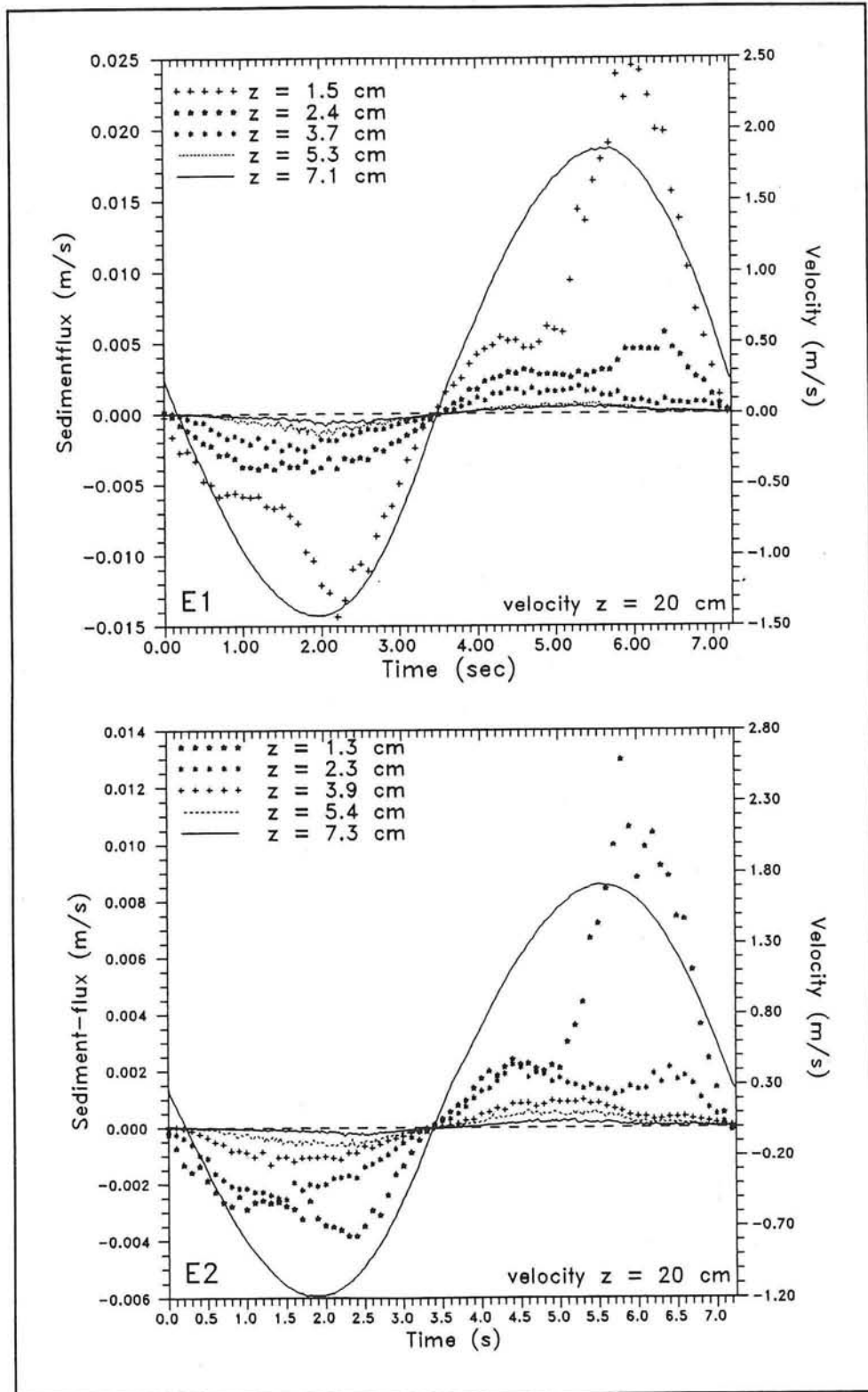


Figure 4.4.5a Ensemble averaged sediment fluxes in the suspension layer (E1-E2)

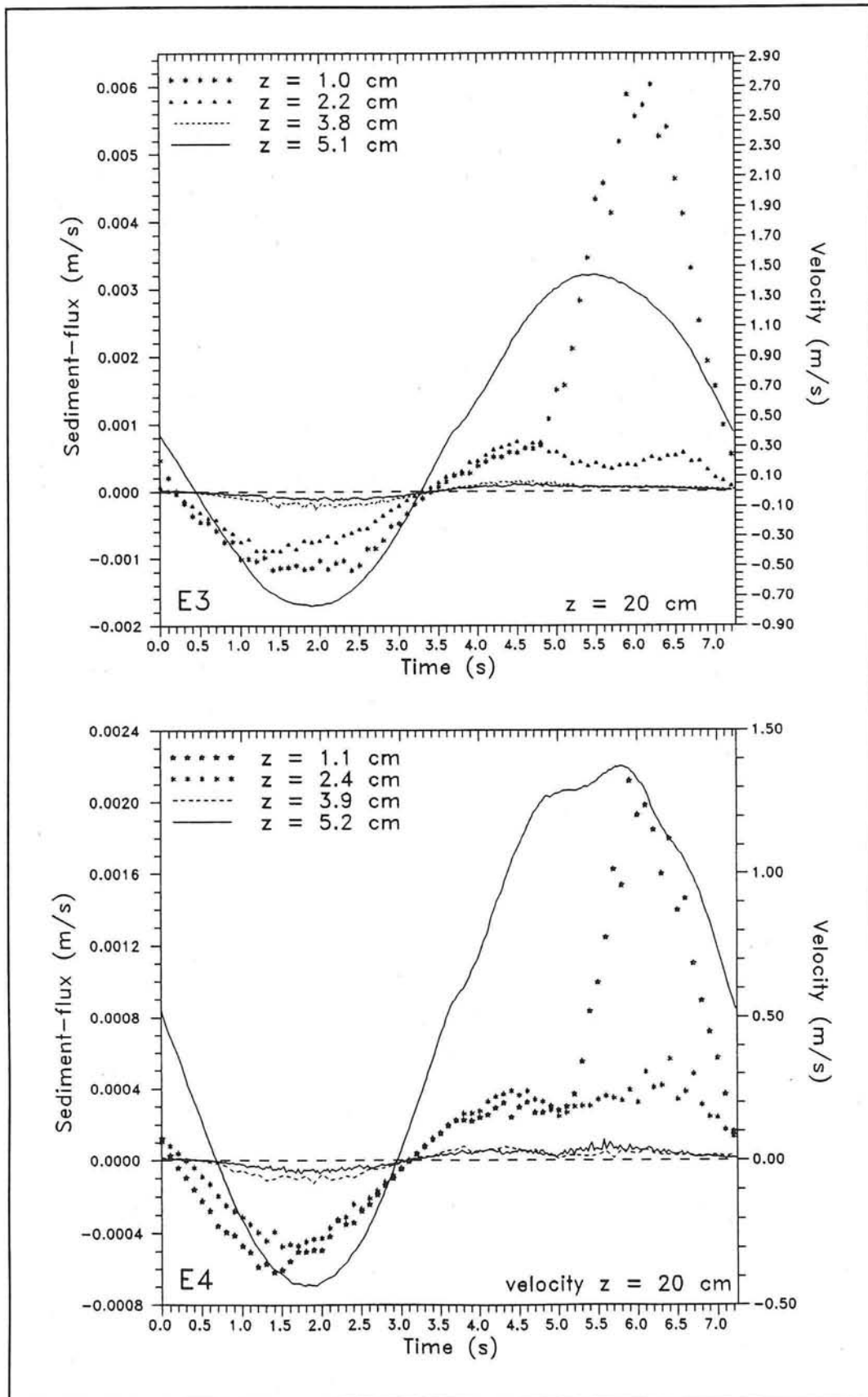


Figure 4.4.5b Ensemble averaged sediment fluxes in the suspension layer (E3-E4)

### 4.4.3 Total flux profiles

By combining the grain velocities obtained from the HSV-analysis with the concentration measurements of the CCM and the OPCON, sediment fluxes near the bed can be obtained. Also net fluxes were calculated by integrating over time and height (see the tables in the appendix F). These net fluxes are combined with the fluxes in the suspension layer and are plotted in Figure 4.4.6. Comparing Figure 4.4.6 with Figure 4.4.3 (with only the fluxes in the suspension layer) shows that a much larger scale had to be chosen in order to be able to plot the fluxes in the sheetflow layer.

The obtained results are not very reliable, because of the observed difference of 30 % between EMF and HSV-analysis (see Figure 4.3.4). Errors in the velocity give errors in the calculated fluxes of the same order (errors in CCM and OPCON measurements are much smaller). After integrating over time theoretically the error becomes more than 100 %<sup>1</sup>, assuming that velocities measured at lower elevations have also an error of the same order. In spite of these reservations the calculated fluxes do not seem completely wrong, most transport takes place in the lower layers, as was expected. Perhaps this result can be explained by the fact that very near to the bed the error is less than 30%. As analyzed in section 4.3.3 an error of about 10 % is reliable for this layers (neglecting the influence of the wall). Assuming an error of 5 % in the CCM measurements a total error of 15 % is obtained for the flux and an error of approximately 60 % in the time integrated flux<sup>2</sup>. These observations match well with the observed behaviour in Figure 4.4.6.

Furthermore it has to be stressed that an unknown error is made by combining velocities near the wall with concentrations measured in the middle of cross-section of the tunnel. Expected is that concentrations do not vary much over the cross-section, because the concentration is dominated by the waves, which have also only a minor variation over the cross-section (see section 4.2 and appendix D). This assumption was not checked by measurements.

Of more interest are the time dependent plots in Figure 4.4.7 and the horizontal flux profiles in Figure 4.4.8, in these plots the maximum errors are between 15 and 30 %. Following the argumentation above, the error in the fluxes decreases nearer to the bed. Only the asymmetry is not reproduced correctly, because of the influence of the boundary layer caused by the side-wall.

---

<sup>1</sup> For example for E1 at 0 mm calculated fluxes were: -55, -42, -43, 102, 72 and 49 (in  $10^{-3}$  m/s), assumed is a relative error in the fluxes of 30 %. Neglecting differences in the period between the measuring points time integrated flux can be estimated with the average of the fluxes:  $((102 \pm 31 + 72 \pm 22 + 49 \pm 15) - (55 \pm 16 + 42 \pm 13 + 43 \pm 31))/6 = (83 \pm 128)/6 = 14 \pm 21 * 10^{-3}$  m/s, which means a relative error of more than 100 %.

<sup>2</sup> Applying the same analysis as above but now with a relative error of 15 % gives for the time integrated flux:  $((102 \pm 15 + 72 \pm 11 + 49 \pm 7) - (55 \pm 8 + 42 \pm 6 + 43 \pm 6)) * 10^{-3}/6 = (83 \pm 53)/6 = 14 \pm 8 * 10^{-3}$  m/s, which means a relative error of about 60 %. The correctness of this analysis is confirmed by the spacing of the lower points in the first graph of figure 4.4.6.

In Figure 4.4.8 flux profiles are plotted on a log-linear scale. To make a quantitative comparison possible the three graphs have the same scale. In all cases the transport is concentrated in the sheetflow layer, although this increase in transport in the lowest layer is more important for E3 and C than for E1. For all tests the fluxes in the sheetflow layer are of the same order of magnitude and not varying much over the height. The difference in transport between the tests is mainly caused by the difference

in sheetflow layer thickness: 
$$q_b(t) = \int_0^{\delta_b} \phi(z,t) dz \approx \delta_b \phi(t) \quad (4.8)$$

Herein:  $\phi$  = flux  
 $\delta_b$  = thickness of sheetflow layer  
 $q_b$  = bed load transport

The difference in the relatively small flux above the sheetflow layer is not so important.

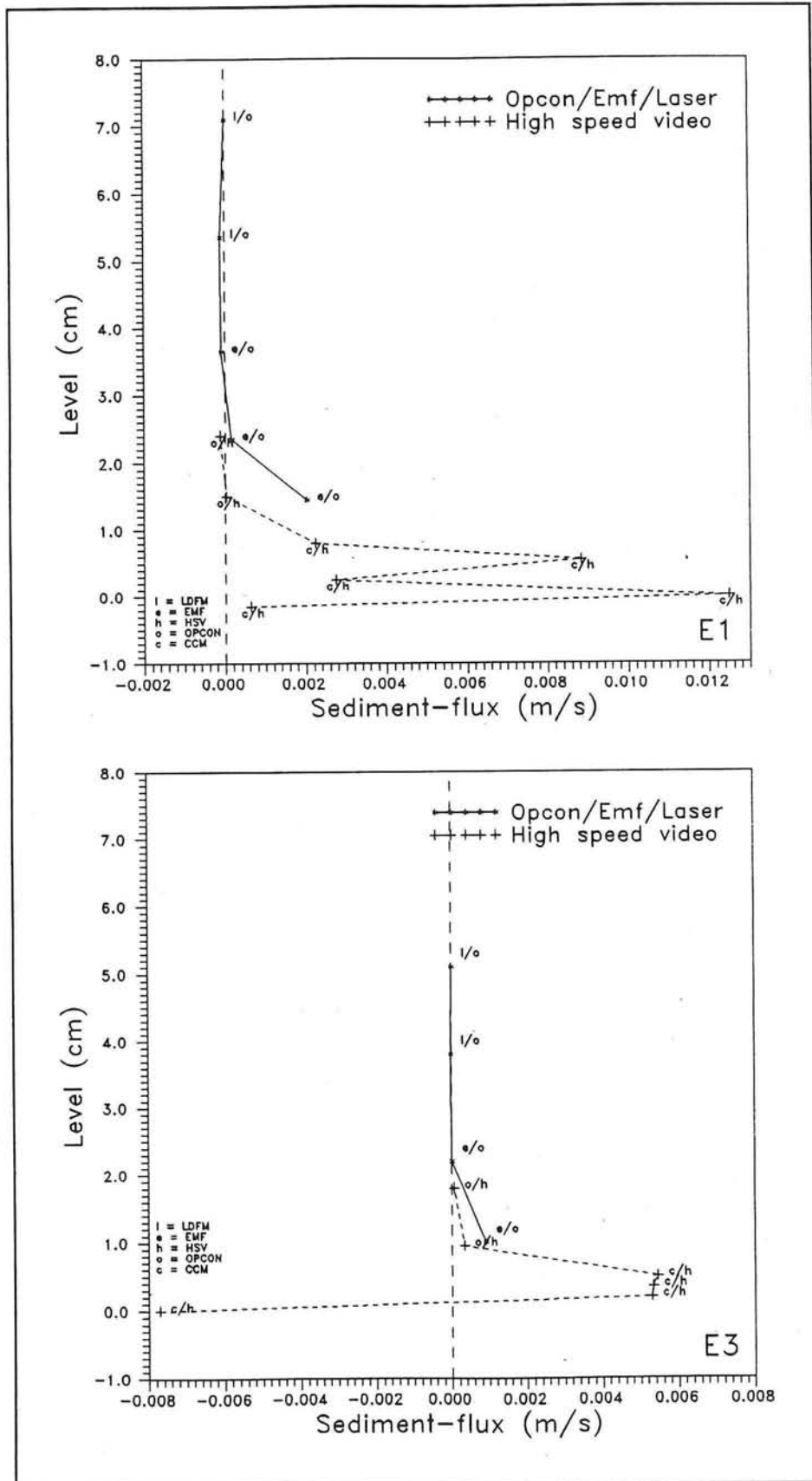


Figure 4.4.6 Combined net flux profiles in sheetflow and suspension layer (E1 & E3)

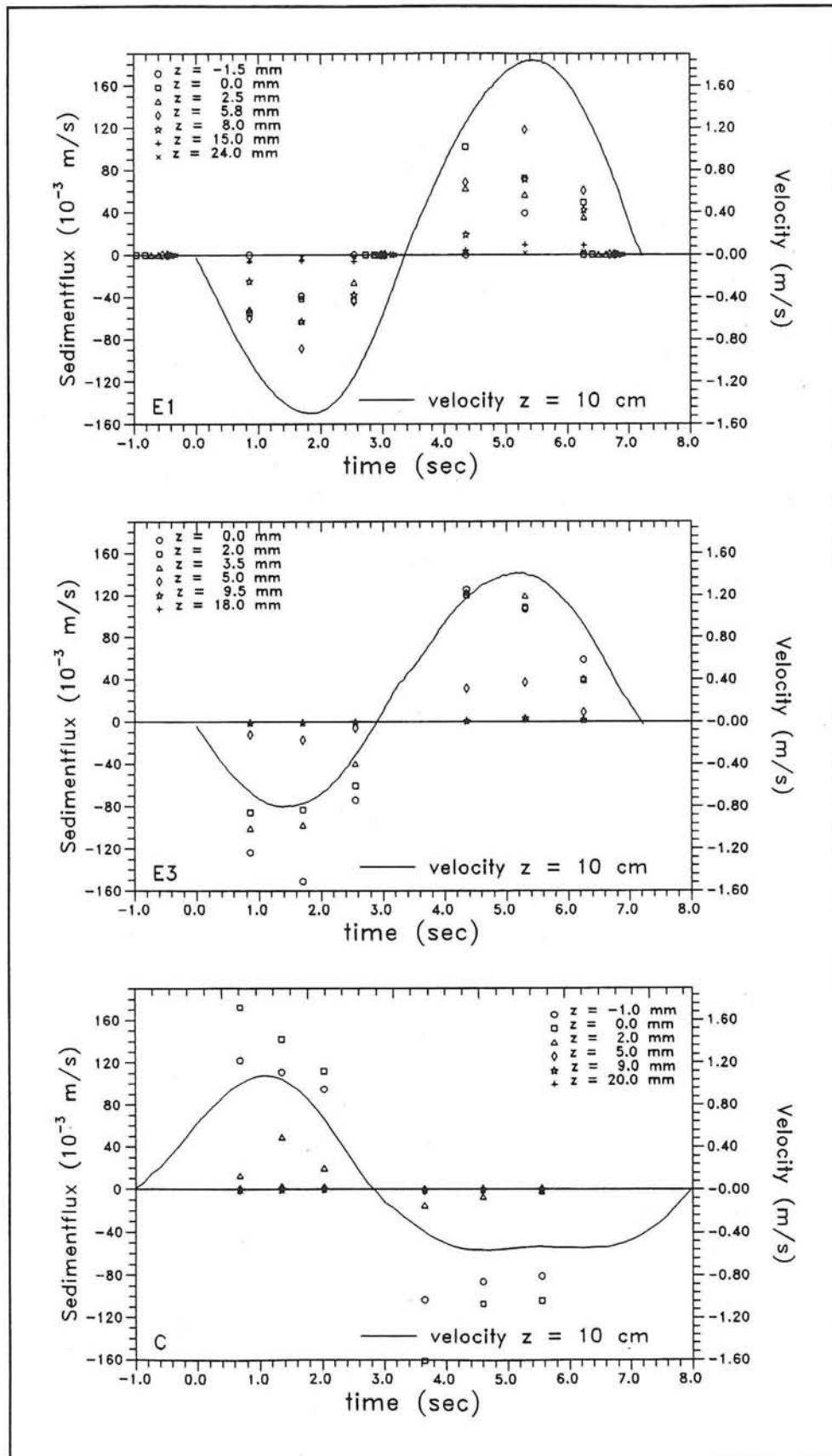


Figure 4.4.7 Time dependent fluxes at various elevations in the sheetflow layer (E1, E3 & C)

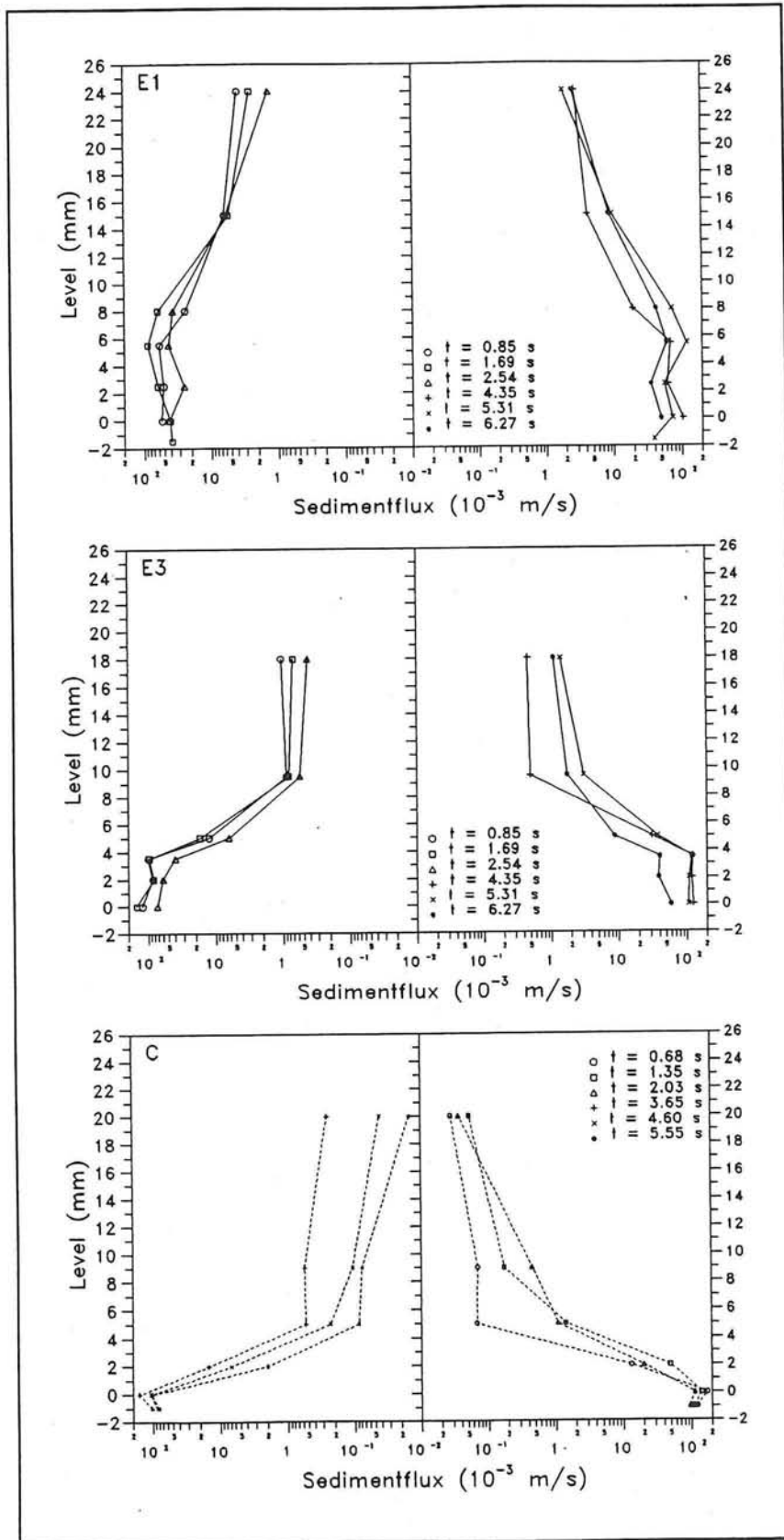


Figure 4.4.8 Horizontal flux profiles in the sheetflow layer (E1, E3 & C)

#### 4.4.4 Discussion about sediment fluxes

Fluxes were determined by combining concentration (OPCON) and velocity (EMF and LDFM) measurements as described in section 4.4.2. The obtained fluxes were integrated over height and time to get the transports.

It was tried to distinguish the transport in bed load and suspended load transport:

- Bed load ( $q_b$ ):  
Sediment transported in a layer just above the bed, which reacts almost instantaneously on changes in the velocity. Phase-lags between concentration and velocity are not important.
- Suspended load ( $q_s$ ):  
Sediment transported higher in the vertical, which is not influenced anymore by the friction of the bed, only the friction of the grains with water plays a role. Phase-lags between velocity and concentration are very important.

According to these definitions the transport in the sheetflow layer is bed load, and transport above this layer is suspended load. Quantifying the bed and suspended load for the present tests had some difficulties.

Reliable time integrated fluxes could be calculated only at the heights where velocities were measured with EMF and LDFM, the velocities calculated with HSV were not used because of the problems with the accuracy (see section 4.4.3). (The exact choices for velocity and concentrations measurements are given in appendix F.1.) The suspended flux is known up to about one centimetre above the bed (E1 → E4: 1.5, 1.3, 1.0 and 1.1 cm). Furthermore the lowest measuring points of the OPCON were combined with velocity measurements a few millimetre higher in the vertical (velocity measurements at a lower elevation were not available). Thus in the lowest points the transport is overestimated. The suspension layer extends till 14 to 5 mm above the bed. A gap arises where the suspended flux is unknown.

The vertical integration of the time averaged fluxes was done by linear interpolating between the measuring points. To calculate the flux in the lower suspension layer a linear extrapolation was carried out.

The values which were finally calculated are listed in the table 4.4. The first column of this table gives the test condition, the second the total transport in the middle of the tunnel calculated with the mass-conservation technique (corrected for influence of the side-wall, as described in appendix D). The third column gives the estimation for the bed load (calculated by  $q_b = q_{\text{total}} - q_s$ ) and the fourth column the bed load calculated from the HSV-analysis (only for E1 and E3). The fourth column gives the suspended load. The last two columns indicate for which heights the suspended and bed loads were calculated.

In a formula the transport can be described with:

$$q_{\text{total}} = q_b + q_s = q_b + \int_b^h \langle u \rangle \cdot \langle c \rangle dz + \int_b^h \tilde{u} \cdot \tilde{c} dz \quad (4.10)$$

herein:  $b$  = boundary between bed load and suspended load (here: the sheetflow layer is assumed to be the layer where bed load transport takes place)

$h$  = water depth or height where transport becomes negligible

Test	$q_{\text{total}}$ ( $10^{-6} \text{ m}^2/\text{s}$ )	bed load ( $q_{\text{total}} - q_s$ ) ( $10^{-6} \text{ m}^2/\text{s}$ )	bed load from HSV- analysis	suspended load ( $10^{-6} \text{ m}^2/\text{s}$ )	Level for suspended load calculation (cm)	Level for bed load calculation (mm)
E1	107.20	97.35	68	9.85	1.4 - 7.1	-1.5 - 14.0
E2	111.77	101.48	---	10.29	1.0 - 7.3	... - 10.0
E3	80.80	73.64	16	7.16	0.6 - 5.1	0.0 - 5.5
E4	84.44	79.86	---	4.58	0.5 - 5.2	... - 5.0

Table 4.4 Sediment fluxes, total, wave- and current-related and bed/suspension load

The bed load transport is approximately 90 % of the total transport for all four conditions. From this results and the HSV-analysis (see section 4.4.3) it can be concluded that the bed load mechanism is dominating over the suspended load mechanism although it is not possible to quantify the importance of the bed load mechanism exactly.

The flux calculated for the HSV-analysis mentioned in table 4.4 is a flux near the wall. The formulas in appendix D were used to correct this transport to a transport in the middle of the tunnel. Assumed is that with the HSV particles were measured at a distance of 2 cm from the side-wall. To obtain a transport in the middle of the tunnel the values in table 4.4 have to be multiplied by  $\pm 1.6$ . This gives a bed load transport rate for E1 of  $108 \cdot 10^{-6} \text{ m}^2/\text{s}$  and for E3 of  $26 \cdot 10^{-6} \text{ m}^2/\text{s}$ . The flux calculated with the HSV-analysis for E1 is of the right order of magnitude. The flux for E3 is too small. This too small flux is partly caused by the high negative flux very near to the bed (see Figure 4.4.6).



## 5 Verification of sediment transport models

### 5.1 Introduction

In this chapter different sediment transport formulas are verified with the experimental data from the present series E tests and the series C tests. Series C concerned regular asymmetric waves (second order Stokes) and series E sinusoidal waves.

The main characteristics of the tests are listed in the Table 5.1 at the end of this section. For a more detailed review see the reports of DELFT HYDRAULICS about conditions with currents and waves part I, II and III (Ramadan, 1993, Ribberink, 1994 and Katapodi et al, 1994). The velocity characteristics in this table are the imposed conditions, not the measured velocity.

- $\langle u \rangle$  = velocity of the current
- $\bar{u}_{rms}$  = the root mean square velocity of the waves (without mean current)
- R = degree of asymmetry of the horizontal flow
- $u_c$  = maximum horizontal velocity in wave direction
- $u_t$  = maximum horizontal velocity opposite to the wave direction
- $\phi$  = angle between current and wave, 0 degrees means a current in the direction of the wave, 180 degrees a current opposite to the direction of the waves
- $\langle q \rangle$  = time averaged sediment transport in real volume per unit width

The mentioned transport in Table 5.1 is the time averaged transport in the middle of the tunnel (thus the measured transport corrected for influence of the side-wall). The transport was measured over the whole cross-section, a correction factor was necessary to obtain the transport in the middle of the tunnel (see appendix D).

The five different sediment transport models as discussed in Chapter 2 have been tested with different choices for the bed-roughness height and the bed shear stress theory. A comparison of the different transport models can be found in section 5.2.

The influence of bed-roughness height (section 5.3) and bed shear stress models (section 5.4.1) on the computed transport model was investigated more in detail. To do this the transport model of Ribberink was chosen, because this model gave the most interesting results. The proposed model for the bed shear stress (model Ribberink/ Van Rijn) was not totally satisfactory. In general the computed transports were too high, so also an adaption for the bed shear stress model is discussed (section 5.4.2).

To test these models a computer program was made using the programming language Turbo Pascal. A listing of the calculation modules can be found in appendix G. The possibilities of the calculation module are shown in Figure 5.1.1. An outline of the total program with input and output modules is given in Figure 5.1.2.

The program needs as input information about the sediment ( $D_{50}$ ,  $\rho_s$  etc.), the liquid ( $\rho$ , viscosity) and a time dependent horizontal velocity at a prescribed level above the bed.

The program gives three possibilities to define this velocity:

- sinusoidal wave (defined by  $u_{rms}$ ) and a net velocity (used for the E series)
- 2<sup>nd</sup> order Stokes wave (defined by  $u_1$  and  $u_2$ :  $u(t) = u_1 \cdot \cos(\omega t) + u_2 \cdot \cos(2\omega t)$  and a net velocity (used for C9)
- time series (used for the rest of the C series)

The velocity was defined at 10 or 20 cm above the bed depending on the available data. As output the calculated transport rate(s) of the desired transport model(s) is/are given and some characteristics of the velocity and the bed shear stress. A total review of the used input and an example of the output of the model is given in appendix E.

Series	Test	$\langle \bar{u} \rangle$ (m/s)	$\bar{u}_{rms}$ (m/s)	R $\bar{u}_c / (\bar{u}_c + \bar{u}_1)$	$\phi$ (degree)	$\langle q \rangle$ ( $10^{-6} \text{ m}^2/\text{s}$ )
C-I	C1	0.00	0.56	0.63	-	19
	C2	0.05	0.56	0.65	0	26
	C3	0.30	0.55	0.81	0	55
	C4	0.15	0.56	0.74	0	36
	C5	0.40	0.55	0.86	0	78
C-II	C9	0.00	0.56	0.63	-	21
	C10	0.40	0.80	0.63	180	55
	C11	0.00	0.80	0.63	-	53
	C12	0.10	0.80	0.63	180	8
	C13	0.40	0.80	0.63	0	176
E	E1	0.15	1.13	0.55	0	107
	E2	0.20	0.95	0.57	0	112
	E3	0.30	0.78	0.64	0	81
	E4	0.40	0.64	0.72	0	84

*Table 5.1 Conditions of tests involved in testing of models*

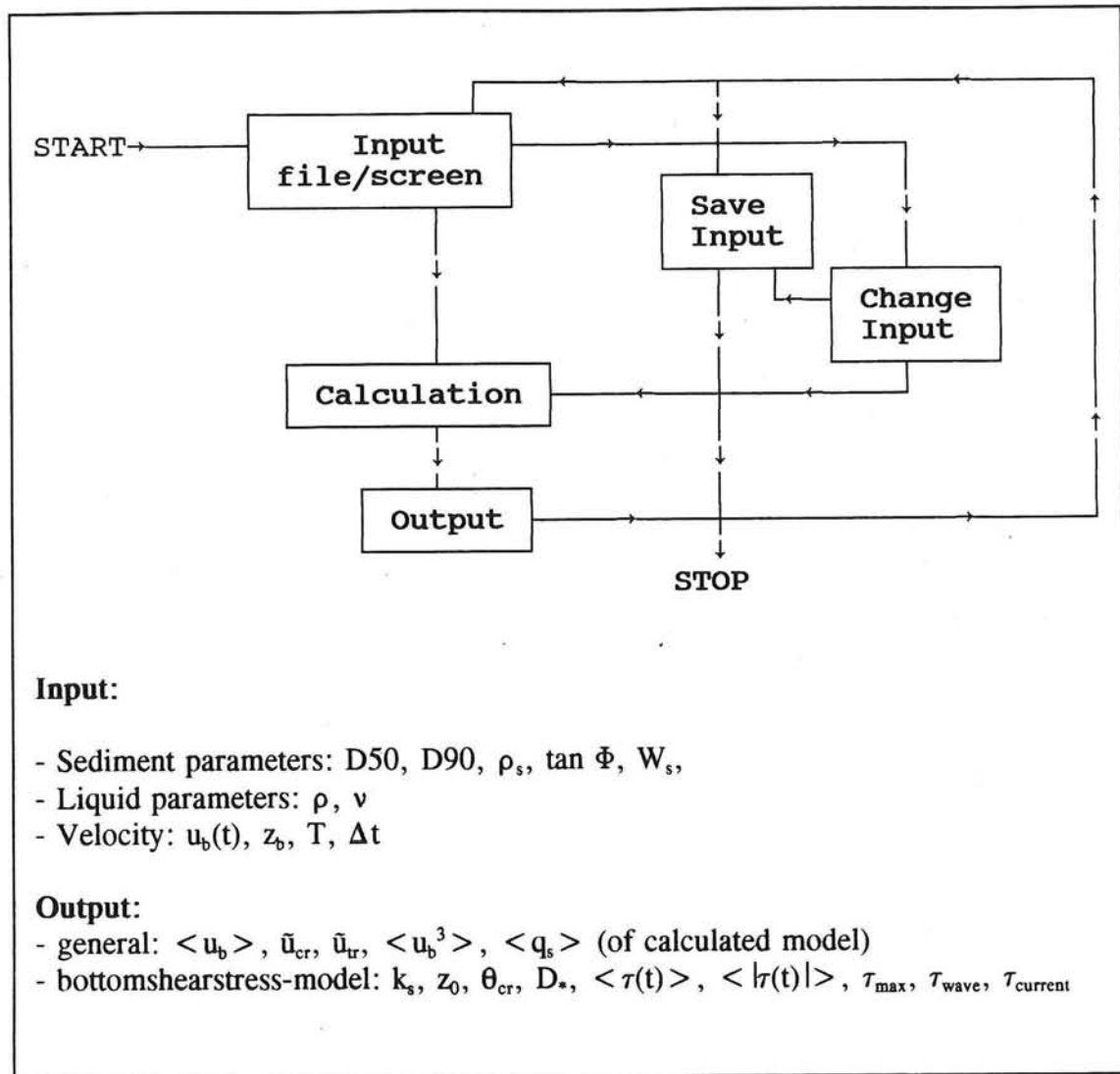


Figure 5.1.1 Schedule of sand transport program

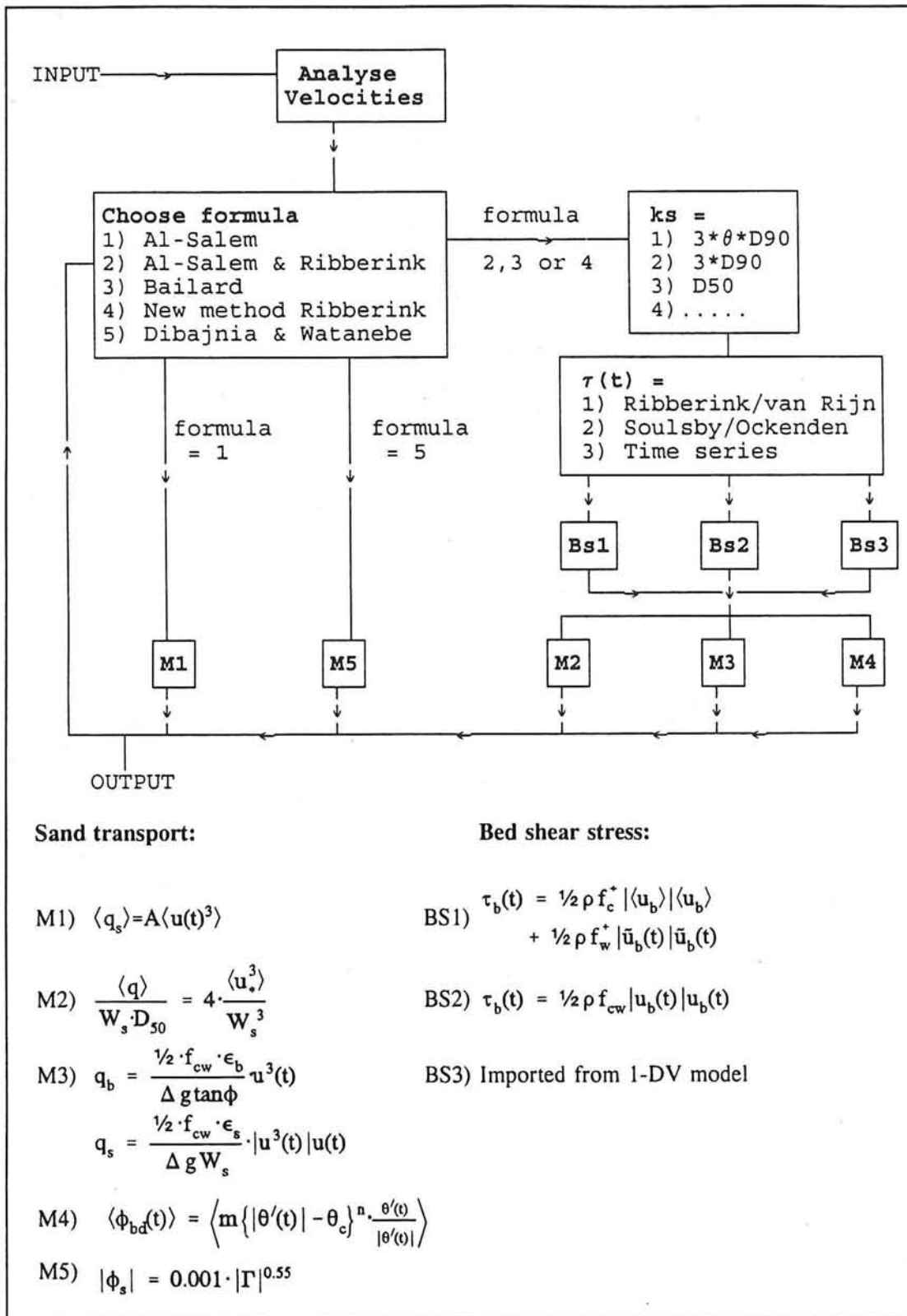


Figure 5.1.2 Calculation module of sand transport program

## 5.2 Comparison of transport models

The different transport models were compared for three possible combinations of the roughness height  $k_s$  and the bed shear stress theory, see the following table:

Model:	Figure 5.2.1	Figure 5.2.2	Figure 5.2.3
Al-Salem (1993)	Input of $k_s$ and bed shear stress not necessary		
Dibajnia & Watanabe			
Ribberink, Al-Salem (1994)	$k_s = D_{50}$	$k_s = 3D_{90}$	$k_s = 3D_{90}$
Bailard	Bed shear stress acc. to Ribberink/ Van Rijn	Bed shear stress acc. to Ribberink/ Van Rijn	Bed shear stress acc. to Soulsby/Ockenden
Ribberink (new)			

Table 5.2 Sandtransport models with choices for  $k_s$  and bed shear stress model

The models of Al-Salem en Dibajnia & Watanabe directly use the velocity as input, so  $k_s$  and a bed shear stress model is not necessary. Dibajnia does not prescribe the level where the velocity should be given. For the present study 10 or 20 cm above the bed was chosen. Bailard does not use bed shear stress as input, but only a friction coefficient. He does not prescribe how this coefficient should be calculated. In this report the maximum bed shear stress is used to determine the value of this coefficient (see section 2.3.3):

$$f_{cw} = \frac{|\tau_{b,max}|}{\frac{1}{2}\rho u_{b,max}^2} \quad (2.41)$$

The new transport model of Ribberink is developed for bed load transport. In the present study the bed load transport is dominating (see section 4.4.4) so it was decided to use this formula without an additional formula for the suspended load transport.

In the Figures 5.2.1 to 5.2.3 the results of the comparisons are shown the measured transport is plotted on the x-axis, the calculated transport on the y-axis. The dotted line is the ideal case (measured transport = calculated transport). The solid lines represent a predicted transport two times too large or two times too small. The model of Al-Salem and Dibajnia and Watanabe is represented in all plots to make the comparison easier, of course they are not changing because they do not depend on the bed shear stress.

The model of Al-Salem (1993) gives quite good results despite the simplicity of the formulation. So it proves again to be a good tool to predict transport in the water tunnel. Dibajnia's model shows a systematical overestimation, calculated transport rates are approximately 1.5 times too large.

The choice of  $k_s = D_{50}$  seems right for the models of Bailard and Ribberink/Al-Salem. Both show an overprediction, but this overprediction increases with the choice  $k_s = 3 \cdot D_{90}$ . The new model of Ribberink underestimates the transport if  $k_s = D_{50}$  is chosen but overestimates in the case of  $k_s = 3 \cdot D_{90}$ .

The bed shear stress model of Soulsby (Figure 5.2.3) gives an increase of the scatter, especially in combination with the transport models of Ribberink and Al-Salem and Ribberink. The model of Bailard is less influenced by the bed shear stress models, because the transport rate is only a linear function of the friction factor.

Especially C12 gives completely wrong results if the model of Soulsby/ Ockenden is used. To check if the computed results are correct the bed shear stress as predicted by the two models is plotted in Figure 5.2.4 for some of the experiments, namely for tests C2, C9 and C12. (C2: asymmetric waves combined with a following net current, C9: asymmetric waves without current and C12: asymmetric waves combined with an opposing current, for C2 and C12 the net velocity was in the positive direction.) During the positive part of the wave cycle the method of Soulsby gives the lowest bed shear stress, during the negative part of the wave cycle the method of Ribberink gives the lowest values. During C12 the transport was in negative direction so the overestimation of the calculated transport with the method of Soulsby/ Ockenden is caused by the higher bed shear stress in the negative part of the wave cycle. To understand why the observed difference between the two methods occur it is useful to repeat the formulations as given in chapter 2. Respectively the formulations of Ribberink/ Van Rijn and Soulsby/ Ockenden:

$$\tau_b(t) = \frac{1}{2} \rho f_{cw} |u_b(t)| u_b(t) = \frac{1}{2} \rho f_{cw} |\tilde{u}_b(t) + \langle u \rangle| (\tilde{u}_b(t) + \langle u \rangle) \quad (2.23)$$

$$\tau_b(t) = \tau_c^+ + \tau_w^+(t) = \frac{1}{2} \rho f_c^+ |\langle u_b \rangle| \langle u_b \rangle + \frac{1}{2} \rho f_w^+ |\tilde{u}_b(t)| \tilde{u}_b(t) \quad (2.26)$$

The coefficient  $f_{cw}$  (from Ribberink/ Van Rijn) is a weighed average of  $f_c$  and  $f_w$ . The coefficients  $f_w^+$  and  $f_c^+$  (from Soulsby/ Ockenden) are respectively the enhanced wave and current friction factors. In Soulsby/ Ockenden the oscillating component is more enhanced than in Ribberink/ Van Rijn ( $f_{cw} < f_w^+$ ), for the mean bed shear stress the opposite is valid ( $f_{cw} > f_c^+$ ). This led to the observed difference in Figure 5.2.4.

Except the fact that during C12 opposing waves in stead of following waves were present the test conditions did not vary considerable from other tests. Also C10 was a test with opposing waves and this test did not show strange results. Probably an explanation can be found in the strong side-wall influence, which caused a transport in the middle of the tunnel with a magnitude of only one third of the averaged transport over the whole tunnel (see also appendix D, Figure D.2). In this range of conditions a small deviation in velocity conditions leads to a large difference in side-wall correction. Based on this analysis it is also estimated that for experiment C12 the transport near the wall takes place in opposite direction as the net transport.

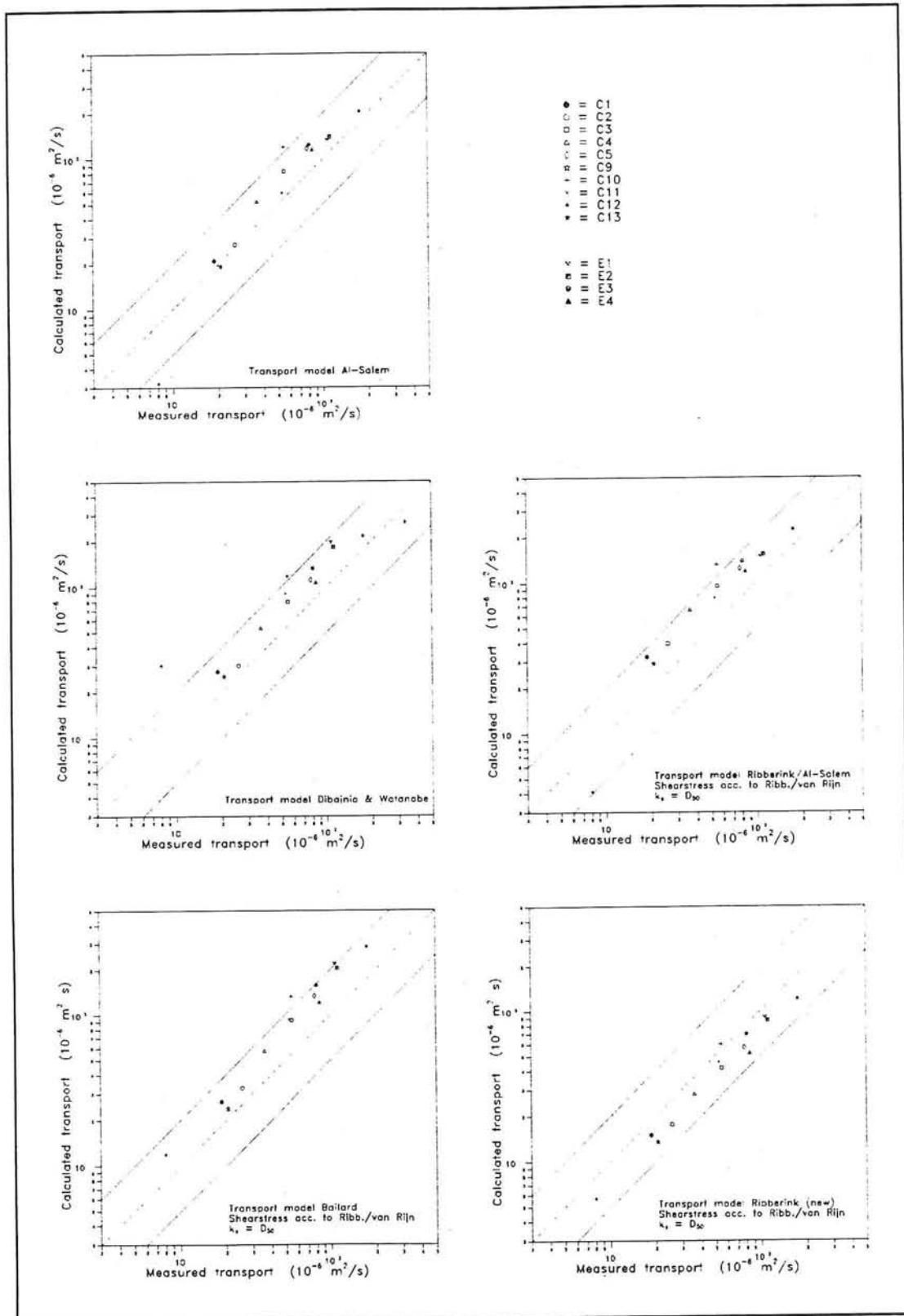


Figure 5.2.1: Comparison sandtransport models,  $k_s = D_{50}$ . Bed shear stress acc. to Ribberink/van Rijn

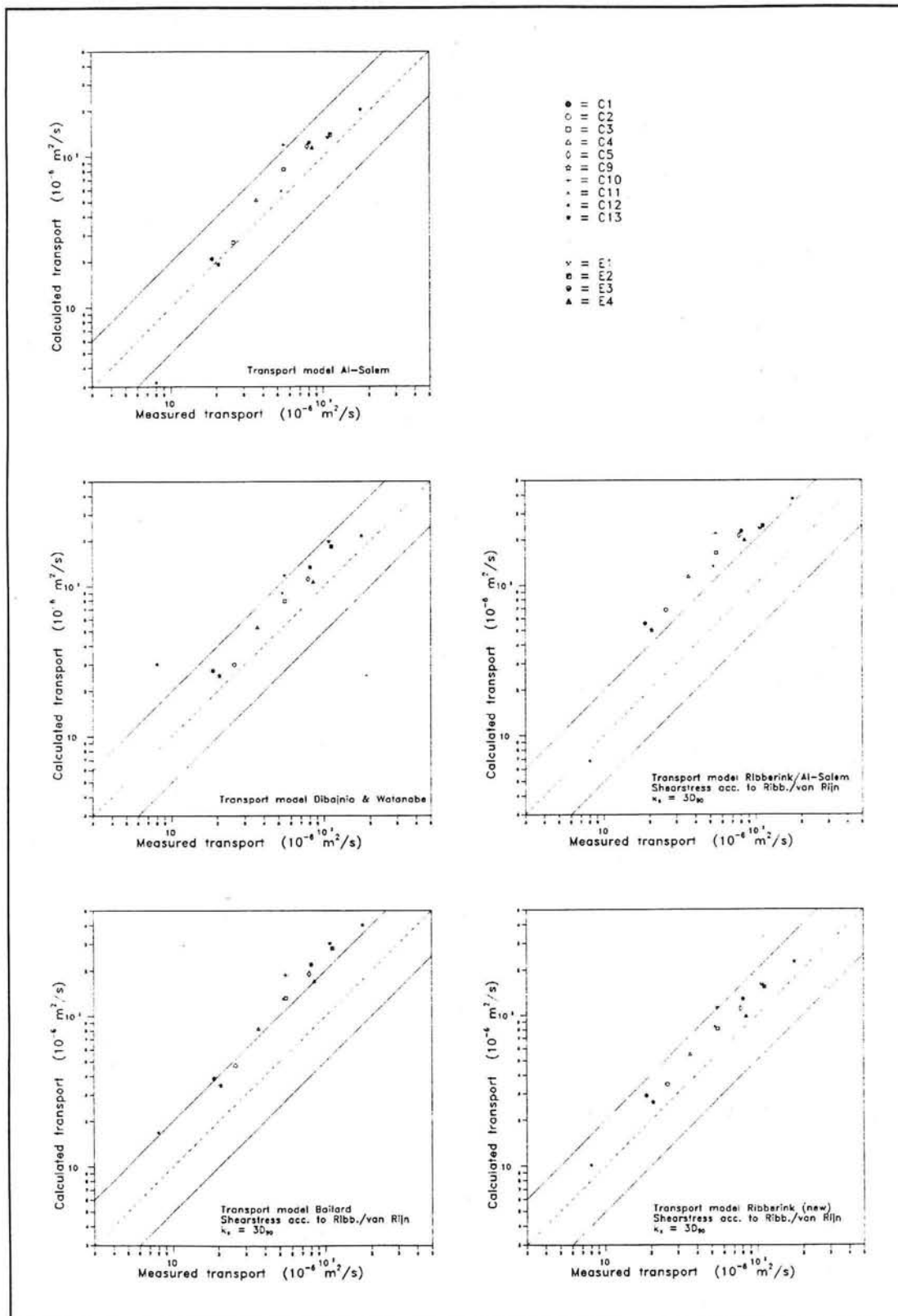


Figure 5.2.2 Comparison sandtransport models,  $k_s = 3 * D_{90}$ . Bed shear stress acc. to Ribberink/van Rijn

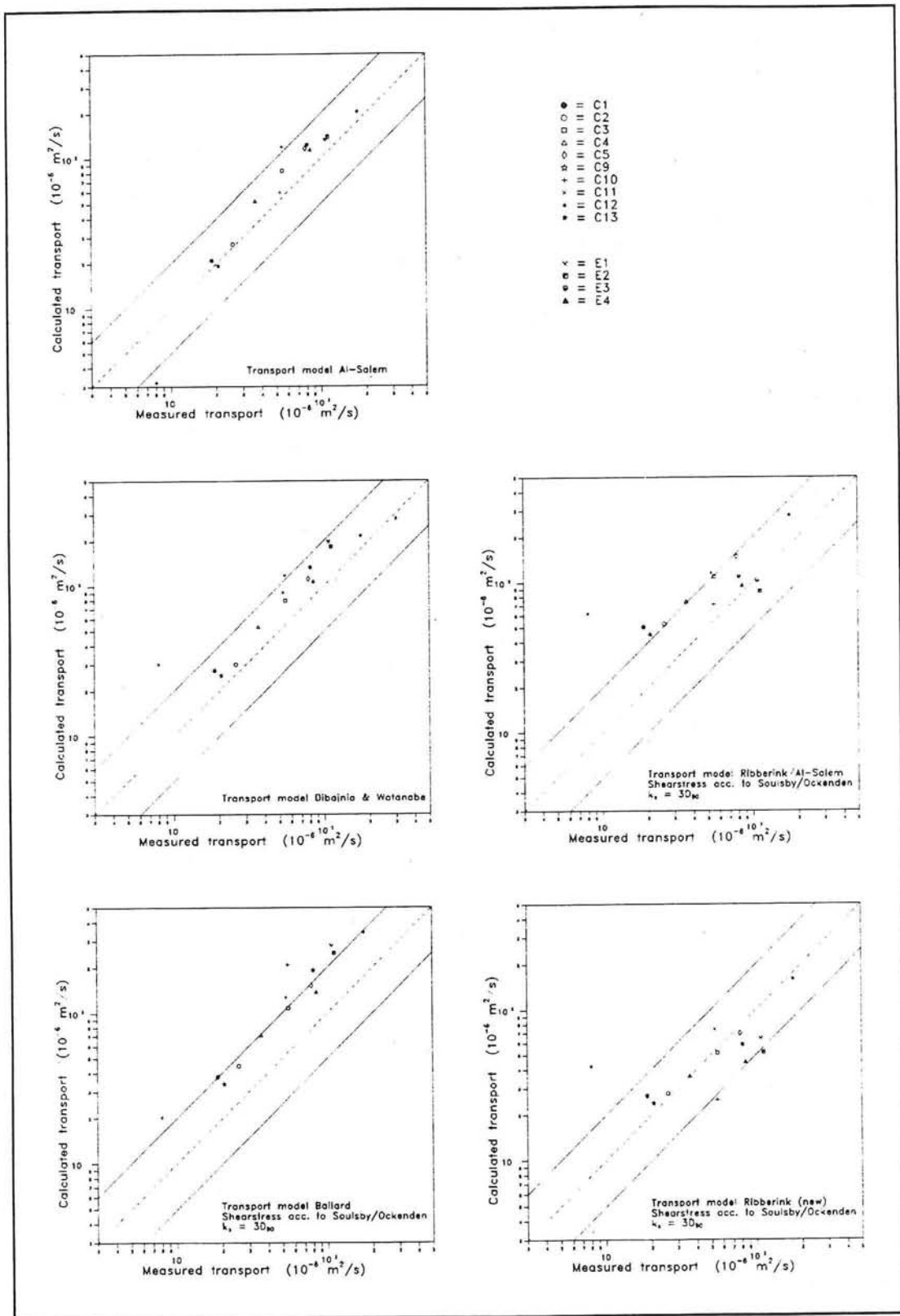


Figure 5.2.3 Comparison sandtransport models,  $k_s = 3 * D_{90}$ . Bed shear stress acc. to Soulsby/Ockenden

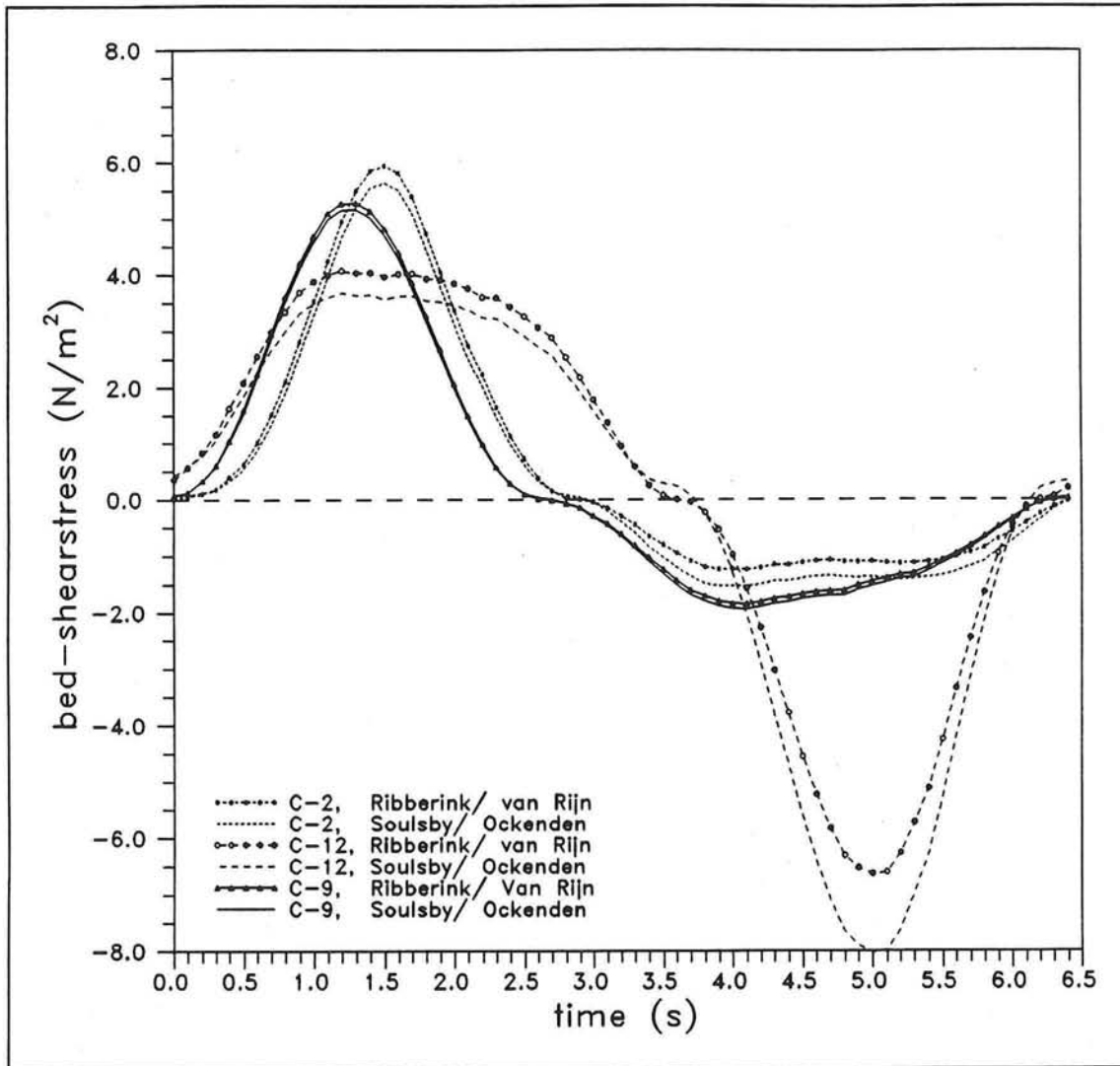


Figure 5.2.4 Time dependent bed shear stress for some tests

### 5.3 Influence of the bed-roughness height on transport models

Three different choices were made for the bed-roughness height:

- for  $\theta \geq 1$ :  $k_s = 3\theta D_{90}$ , for  $\theta < 1$ :  $k_s = 3D_{90}$
- $k_s = 3D_{90}$  ( $k_s = 0.96$  mm, during the present tests)
- $k_s = D_{50}$  ( $k_s = 0.21$  mm, during the present tests)

To calculate the bed-roughness height with the first method, an average value was calculated for  $\theta$  during the wave cycle. The next calculation schema was used:

- 1) Estimate  $k_s$  with  $3D_{90}$
- 2) Calculate an average value for the bed shear stress:  $\tau_b = \frac{1}{4}\rho f_w \hat{u}^2 + \frac{1}{2}\rho f_c \langle u \rangle^2$
- 3) Calculate the Shields parameter:  $\theta = \tau_b / ((\rho_s - \rho)gD_{50})$
- 4) Calculate  $k_s$ :  $k_s = 3\theta D_{90}$
- 5) Repeat step 2, 3 and 4 until  $k_s$  is not changing anymore (difference less than 0.1 %)

The three different bed-roughness heights were combined with the new transport model of Ribberink and the bed shear stress formulation of Ribberink/ Van Rijn. The results can be found in Figure 5.3.1

Ribberink suggested to choose  $k_s = 3\theta D_{90}$  for  $\theta \geq 1$  (sheetflow conditions), in situations with only waves or only a current this choice lead to good results for his model.

For the present tests with combined waves and currents the difference between  $k_s = 3\theta D_{90}$  and  $3D_{90}$  is rather small. Only for the E-series with rather large velocities the calculated transport rates are affected by this parameters. A straight line seems to match the points best if  $k_s = 3\theta D_{90}$  is used.

An increased bed-roughness height gives an increased bed shear stress and thus an increased transport, but the effect is rather small. The difference between the transports calculated with  $k_s = D_{50}$  and  $k_s = 3D_{90}$  is approximately a factor two, whereas  $k_s$  was increased with a factor five.

Regarding the results there is no reason to take another bed-roughness height than is suggested by Ribberink ( $k_s = 3\theta D_{90}$ ).

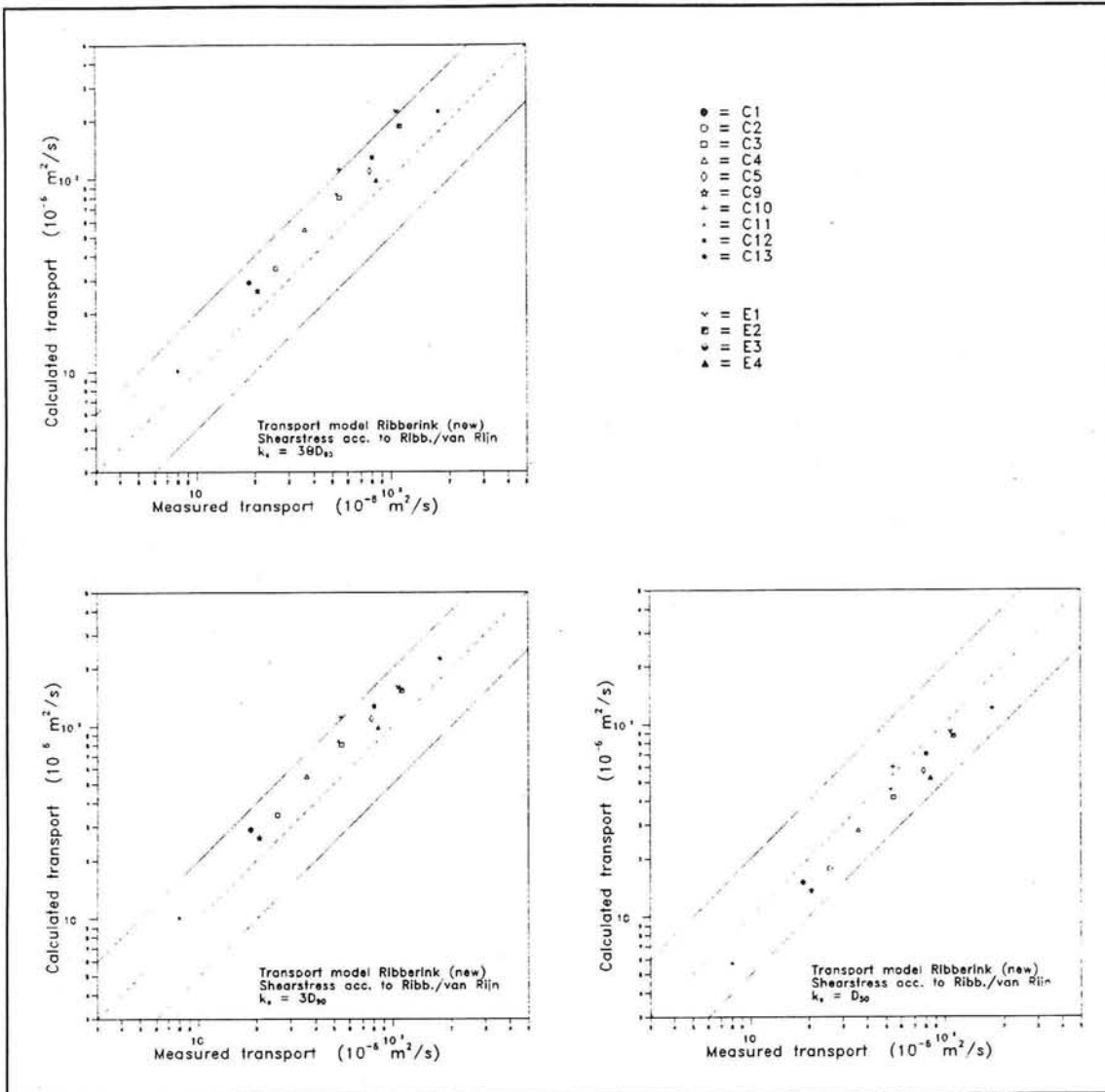


Figure 5.3.1 Influence of bed-roughness height on transport model of Ribberink

### 5.4 Influence of the bed shear stress model

#### 5.4.1 Existing models

The following three models mentioned in Chapter 2 are used as input for the sediment transport formulas (see Figure 5.4.1):

- 1) Ribberink/ Van Rijn
- 2) Soulsby/ Ockenden
- 3) 1-DV model of Al-Salem

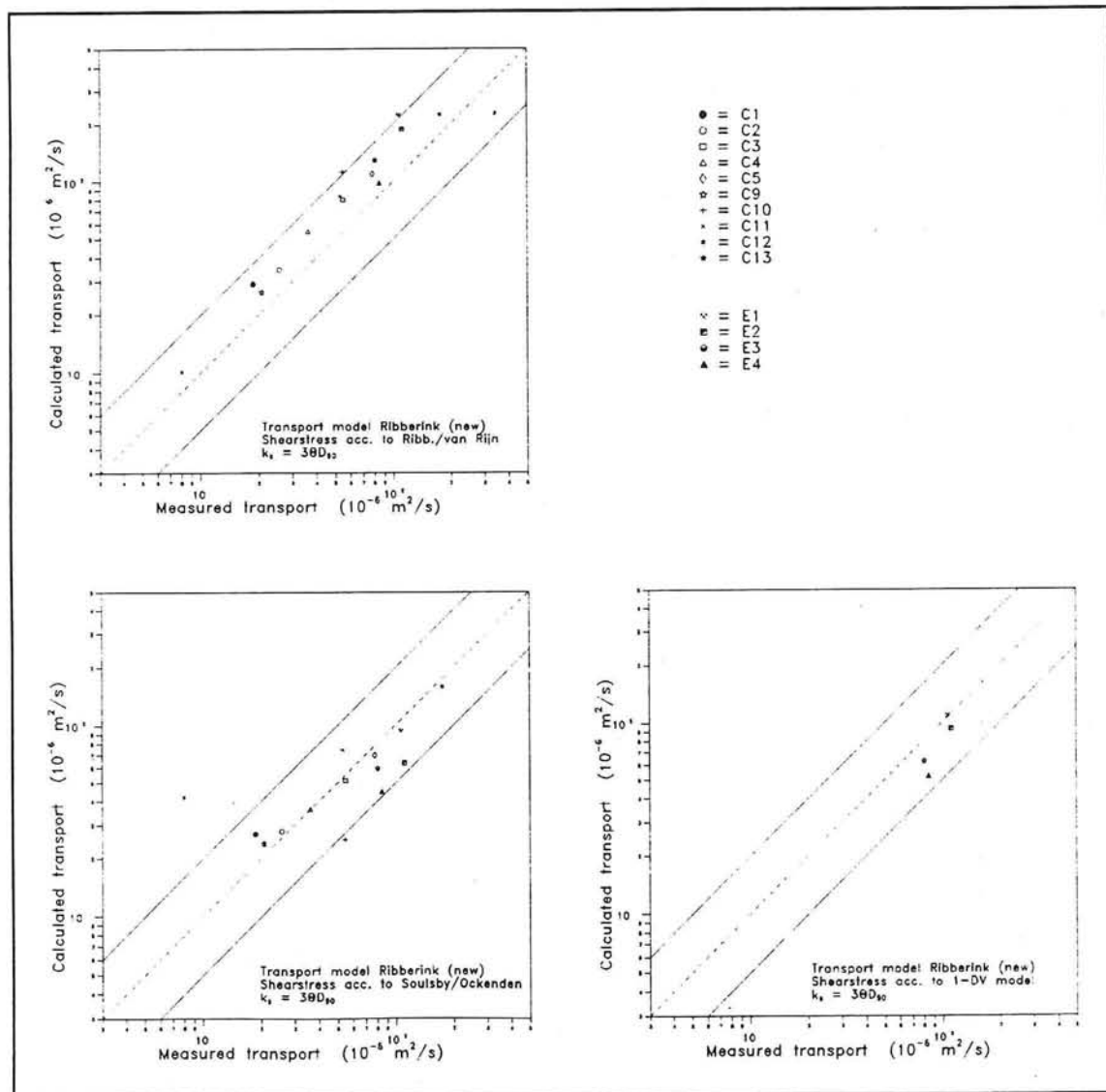


Figure 5.4.1 Influence of bed shear stress model on transport model of Ribberink

The 1-DV model cannot use time series for the velocity as input, it needs a parametrization of the velocity as a sine or a 2<sup>nd</sup> or 3<sup>rd</sup> order Stokes wave. This restriction does not apply to the sandtransport model. Since for the series C experiments (except for C11) velocity time series were used as input only the E series were calculated with the 1-DV model.

The choice of a bed shear stress model strongly influences the computed transport rate. In general the model of Ribberink/ Van Rijn gives the highest transport, followed by the 1-DV model and the model of Soulsby/ Ockenden. The model of Soulsby/ Ockenden shows an increased scatter compared to the other two models.

The time dependent bed shear stresses calculated by the three models are compared in Figure 5.4.2 (for test condition E3). In the Figure the time dependent velocity is plotted also to make phase differences between velocity and bed shear stress visible. Only the bed shear stress calculated with the boundary layer flow model of Al-Salem shows a phase difference as could be expected. The model of Soulsby/ Ockenden gives during the positive part of the wave cycle lower values as Ribberink/ Van Rijn and during the negative part higher (absolute) values.

Conclusions from the analysis are that the model of Ribberink/ Van Rijn is to prefer above the model of Soulsby/ Ockenden (because of the decrease in scatter for the model of Soulsby). The results of the 1-DV model are promising but it is difficult to judge based on only four tests.

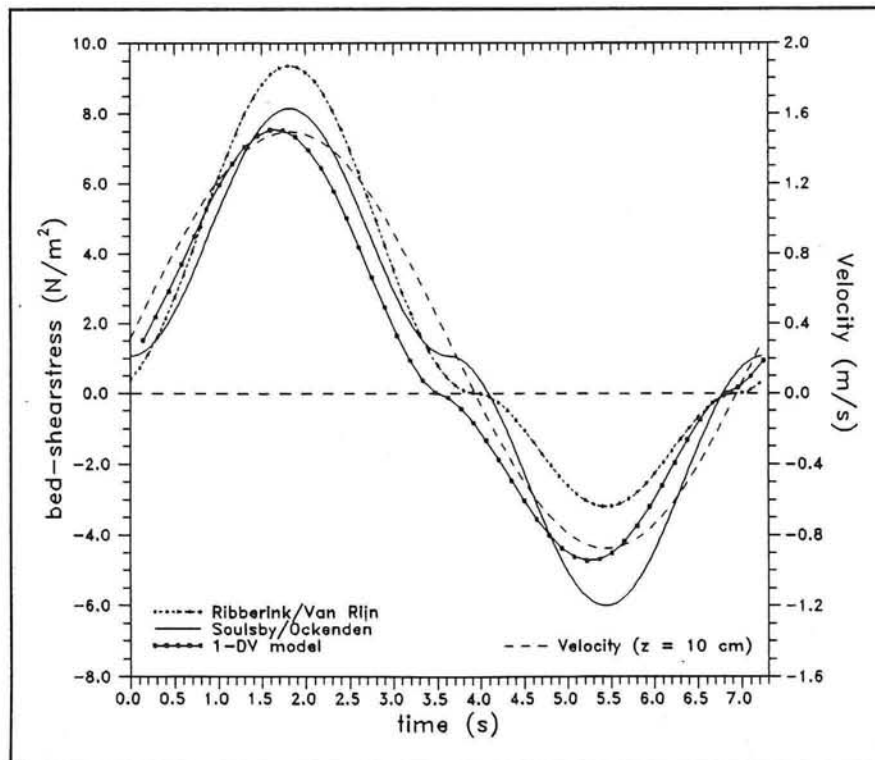


Figure 5.4.2 Time dependent bed shear stress for test E3

### 5.4.2 Alternative formulations

The verification in the preceding section showed that the transport model of Ribberink in combination with the bed shear stress model of Ribberink/ Van Rijn still overpredicts the sediment transport in case of combined wave-current flow. The model functions well in case of only waves or only currents, so an adaption of the model in the only specific wave-current interaction parameter, i.e. the friction factor for combined wave-current flow, would be desirable.

In the present model this factor is defined as a linear relation between the friction factors for waves and for a current:

$$f_{cw} = \alpha f_c + (1-\alpha)f_w \quad \text{with:} \quad \alpha = \frac{|\langle u_b \rangle|}{|\langle u_b \rangle| + \hat{u}_b} \quad (2.24)$$

This factor can be changed by changing the definition of  $\alpha$  or by changing the linear relationship into something else. First was tried to find a more logical definition of  $\alpha$  namely a ratio between the bed shear stresses:

$$\alpha = \frac{\tau_c}{\tau_c + \tau_w} \quad (5.1)$$

This leads to mean and maximum bed shear stresses as plotted in the first graph in Figure 5.4.3. As a comparison also the values for the original model and for the model of Soulsby/ Ockenden are plotted. This attempt leads to even higher values of the bed shear stress, and thus to higher values of the transport rate also (which was already overestimated).

A change in the linear relationship led to the following formula for the wave friction factor:

$$f_{cw} = \sqrt{\alpha} f_c + (1 - \sqrt{\alpha}) f_w \quad (5.2)$$

For  $\alpha$  the original definition (formula 2.24) is used. This gives the results as plotted in the second graph in Figure 5.4.3. Now the results are between the results of Ribberink-Van Rijn and Soulsby/ Ockenden.

The last model (formula 5.2) is applied to the sandtransport formula, the results can be found in Figure 5.4.4. A reduction of the calculated transport rate is realized now and the model predicts the measured transport rates quite well.

In Figure 5.4.5 the results are compared in another way, the non-dimensional measured transport rate is plotted against the representative Shields parameter minus the critical Shields parameter (see also section 2.3.3). The solid line represent the formula, the symbols represent the dimensionless measured transport rate and  $\theta_{repr} - \theta_c$ . As bed-

roughness height  $3\theta D_{90}$  ( $\theta > 1$  else  $k_s = 3D_{90}$ ) is used in both formulas. The stars represents the formula of Ribberink with the bed shear stress according to Ribberink/Van Rijn, the circles represent the results of the adapted formulation. Again it can be seen that the new suggested formula is superior to the original one.

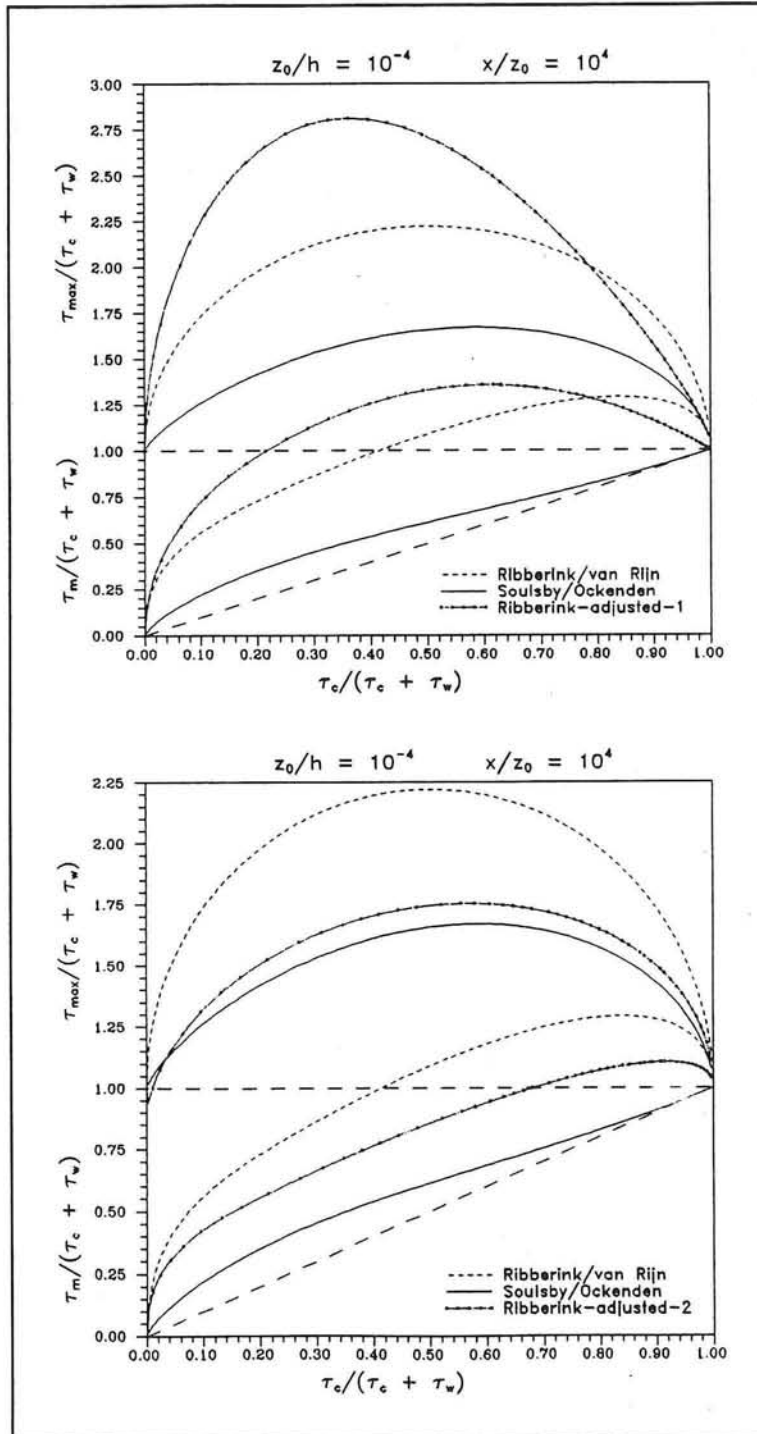


Figure 5.4.3 Alternative formulations for bed shear stress

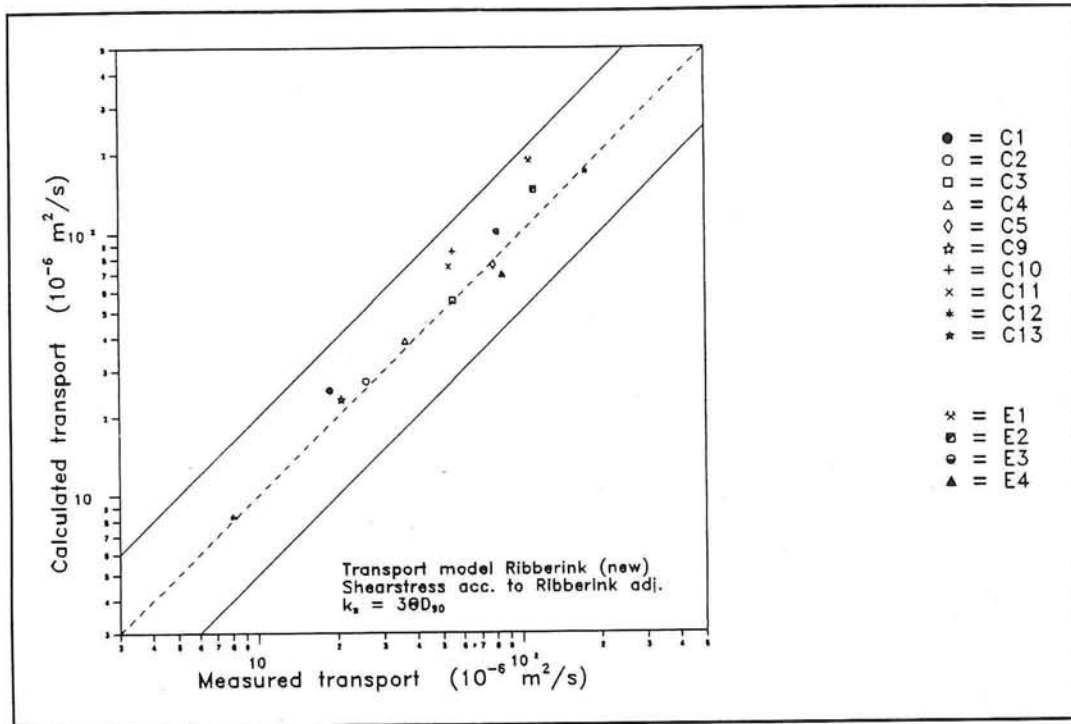


Figure 5.4.4 Alternative model for bed shear stress applied to Ribberink's transport model

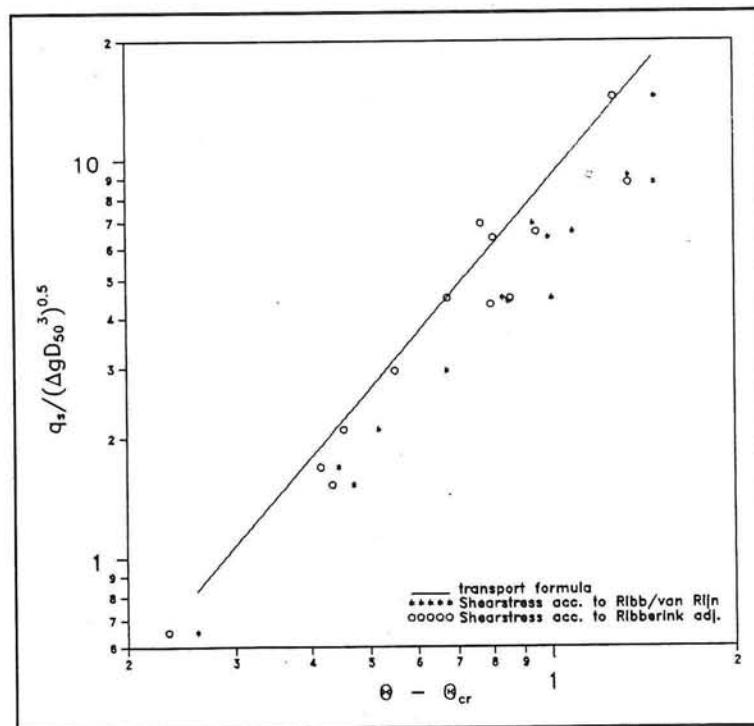


Figure 5.4.5 Ribberink's transport model



## 6 Summary of conclusions and recommendations for future research

### 6.1 Experimental research

The present oscillating water tunnel experiments were carried out in the framework of the Large Installations Programme of the European Community. The main scope of the present experiments (series E) was to obtain a dataset concerning sheetflow conditions. Measurements were focused on a detailed time dependent description of the processes in the sheetflow and suspension layer. For this purpose time dependent concentrations and velocities were measured with several measuring devices. The four different test conditions concerned sinusoidal waves combined with different net currents, all with approximately the same third-order velocity moment ( $\langle u^3 \rangle$ ).

The present report was focused on obtaining time dependent and net fluxes in the sheetflow and suspension layer. It was tried to prescribe the net transport with different sand transport formulations. Attention was paid to the division between suspended load and transport in the sheetflow layer (bed load transport).

#### *Concentrations*

In the sheetflow layer time dependent concentrations were measured with a conductivity concentration meter (CCM). An optical concentration meter (OPCON) was used to measure time dependent concentrations in the suspension layer (upto  $\pm 10$  cm). A transverse suction system was used to measure time averaged concentrations and to obtain a  $D_{50}$  distribution in the vertical. The measurements led to the conclusion that three different zones in the vertical can be distinguished. From top to bottom:

- Suspension layer:  
Averaged concentrations can be described with the formula:

$$\langle C \rangle = C_a \left( \frac{z_a}{z} \right)^\alpha \quad (4.1)$$

Time dependent concentrations show a phase-lag compared with the velocities. Major peaks are present just after maximum and minimum velocity and minor peaks just after flow-reversal.

- Upper sheetflow layer:  
Averaged concentrations can be described with the formula:

$$\langle C \rangle = C_0 \exp\left(\frac{-z}{l}\right) \quad (4.2)$$

Time dependent concentrations show only a minor phase-lag with the velocity. Peaks are present just after maximum and minimum flow velocity. The peaks at flow-reversal are for E1 and E2 more important than the peaks at maximum and minimum velocity. Probably the peaks at flow-reversal can be explained by the increased turbulence caused by phase differences in the velocity at different heights above the bed.

- Pick-up layer (lower sheetflow layer):  
Time averaged concentrations are almost constant over the height, time dependent concentrations show a behaviour opposite to the concentrations in the sheetflow layer.

The sheetflow layer is defined as the layer where time averaged concentrations are larger than 1 volume percent. The thickness of the sheetflow layer increases with increasing wave height (For E1 the sheetflow layer extends till 14 mm and for E4 only 5 mm). The division in the three layers is given in Table 6.1.

Test	Sheetflow layer ((C) > 1 %)		Suspension layer
	Pick-up layer	Upper sheetflow layer	((C) < 1 %)
E1	-3.0 - 1.0 mm	1.0 - 14.0 mm	14.0 mm →
E2	-2.0 - 2.0 mm	2.0 - 10.0 mm	10.0 mm →
E3	-1.0 - 2.5 mm	2.5 - 5.0 mm	5.0 mm →
E4	-0.5 - 2.5 mm	2.5 - 5.5 mm	5.5 mm →

*Table 6.1 Division in concentration layers*

### *Velocities*

Velocities were measured with an electro-magnetic flow meter (EMF) and a laser-doppler flow meter (LDFM) in the suspension layer. Measurements with EMF reached until a lowest level of  $\pm 1$  cm above the bed, measurements with LDFM until  $\pm 4$  cm (depending on the concentrations). The measurements of the EMF and the LDFM deviated from each other, the found differences are still not fully explained. Further research should be done to compare and recalibrate the EMF.

Time dependent velocities for EMF and LDFM are (until now) only available for E1 and E3, time averaged velocities are available for all tests.

In the sheetflow layer velocities were estimated with help of high speed video recordings (HSV) for E1, E3 and one C test of Al-Salem. Comparison with EMF results showed that velocity estimates from the HSV-recordings were too low. The current was not reproduced correctly because of the influence of the wall boundary layer (recordings were made trough the side-wall). Another disadvantage of the technique was the time-consuming analysis. The technique is useful to gain qualitative information about the processes in the sheetflow layer, the quantitative information has a low accuracy. And also the qualitative information obtained with this technique has to be used with care because it is not known if the side-walls influence the observed behaviour.

### *Fluxes*

Time dependent fluxes were calculated by multiplying velocities (measured by EMF, LDFM, HSV) and concentrations (measured by OPCON and CCM). In the suspension layer reliable fluxes were obtained. In the sheetflow layer the errors in the obtained fluxes were between 15 and 30 % because of the uncertainty in the velocities obtained in HSV-analysis.

In the suspension layer the current-related and wave-related part of the flux are equally important. Peaks in the time dependent fluxes (suspension layer) correspond with peaks into the concentration. Extrapolation of the time averaged fluxes measured in the suspension layer justify the assumption that the flux in the sheetflow layer is dominated by the wave-related part. The peaks at flow-reversal in the layer near the bed were not represented in the fluxes. This is caused by i) the HSV-analysis was only carried out for a limited number of phases within the wave cycle and ii) the low flow velocity near flow-reversal.

From the HSV-analysis and from extrapolating of the fluxes in the suspension layer it is concluded that most transport takes place in the layer near the bed. The thickness of the sheetflow layer is important for the transport rate. A value for suspended load was calculated by extrapolating the measurements in the suspension layer to the boundary between suspension and sheetflow layer. A bed load transport rate was calculated by i) subtracting the suspended load transport from the total transport rate and ii) linear integration of fluxes obtained from the HSV-analysis. For test E1 both bed load transport rates were of the same order of magnitude, for test E3 the bed load calculated from the HSV-analysis was much smaller than the bed load calculated with the first method.

## **6.2 Transport modelling**

The present experiments justify the assumption that in case of sheetflow most transport takes place near the bed, thus the modelling can be focused on quasi-steady bed load formulations.

Different quasi-steady transport models were tested with help of a computer program in Pascal:

- Two models based on velocity moments: the model of Al-Salem (which was specially developed for the oscillating water tunnel) and the Bailard model.
- Two models based on bed shear stress formulations: the model of Al-Salem and Ribberink and the new model of Ribberink. The last model which tries to give one concept usable for as well as currents, waves as combinations for both is still under development. In this report it was tested for the first time with a series of combined wave-current flows.
- The model of Dibajnia and Watanabe: this model takes the delayed behaviour of the suspended sediment into account.

In the analysis oscillating water tunnel tests with a wide range of conditions were used (series C-I, C-11 and E). Series C concerned tests with asymmetric waves (second order Stokes) combined with a following or an opposing current. Series E (the present tests) concerned sinusoidal waves combined with a net current.

Transport models were combined with different bed shear stress formulations (Ribberink/ Van Rijn, Soulsby/ Ockenden and the boundary layer flow model of Al-Salem) and different bed-roughness heights ( $k_s = D_{50}$ ,  $3D_{90}$  or  $3\theta D_{90}$ ).

Measurements executed by Ramadan (see Ribberink, 1994) showed that in case of waves combined with a current the transport over the *whole* cross-section of the tunnel should not be correlated to the velocity in the *middle* of the tunnel. Analysis of his measurements showed that correction of the measured transport rate was necessary. A correction procedure was developed starting from the assumption that the net velocity distributions in the cross-section have a shape similarity. The profile shape was based on one measurement of Ramadan (1993).

The simple formulation of Al-Salem (1993) shows good agreement with the measured transport rates. It confirms the assumption that transport is in proportion to the third-order velocity moments. The model of Ribberink/ Al-Salem ( $k_s = D_{50}$ ) shows over the whole range of conditions an overprediction approximately with a factor 1.5.

The model of Bailard shows an overestimation especially at high transport rates. This overestimation can be explained with the knowledge that a dominating part of the calculated transport is in proportion to the fourth order velocity moment. The model should be used with a bed-roughness height equal to  $D_{50}$ . The new model of Ribberink ( $k_s = 3\theta D_{90}$  and bed shear stress according to Ribberink/ Van Rijn) gives systematically a too large calculated transport rate.

The model of Dibajnia and Watanabe does not need the bed shear stress as input but uses directly the velocity signal. The model shows an overprediction of about a factor 1.5. The delayed behaviour of the suspended sediment, which is taken into account in this model, did not play an important role in the present experiments.

#### *Influence of bed-roughness height*

The bed-roughness height appeared to be not a very sensitive parameter. It can be used to calibrate a model (an increase in  $k_s$  gives an increase in the calculated transport). The best value of  $k_s$  depends on the used transport model, it is not possible to make one choice. For the transport model of Ribberink/Al Salem and the transport model of Bailard  $k_s = D_{50}$  can be advised and for the new transport model of Ribberink  $k_s = 3\theta D_{90}$ .

#### *Influence of method for bed shear stress*

The application of the model of Soulsby/ Ockenden for the bed shear stress for combined waves and currents increased the scatter of the computed sediment transport

rates, compared with the model of Ribberink/ Van Rijn. This is most likely caused by the fact that the model is developed for sinusoidal waves; The model does not deal correctly with the wave-asymmetry. At the present state of art it is better to use the formulation of Ribberink/ Van Rijn as input for sediment transport models. No opinion is given about the calculated bed shear stress itself, because no bed shear stress was measured during the present experiments. Input in the transport model of bed shear stress obtained from the 1-DV model of Al-Salem (1993) shows promising results. A disadvantage of the model is that it needs a parameterization of the velocity, it is not possible to use time series directly.

To improve the transport model of Ribberink the formulation for the wave-current friction coefficient was slightly adapted. A good prediction for the measured transport was obtained with this adapted coefficient.

### **6.3 Recommendations for further research**

- To obtain a better understanding of the processes in the sheetflow layer it is necessary to measure instantaneous velocities. The HSV is not (very) suitable for this purpose. The desired measuring device should be able to measure in the centre of the flow, without disturbance of this flow and it should not be hindered by large sediment concentrations. Ideally velocities should be measured very near to the bed, where concentrations can be 100-1400 g/l. Then time dependent fluxes over the whole vertical can be measured accurately and thus a better insight in the division between bed load and suspended load can be obtained.
- To obtain a better insight in the velocity distribution in the cross-section more velocity profiles should be measured at different levels above the bed. The assumption of uniform shaped velocity distributions should be tested for a wide range of conditions.
- The new formulation of Ribberink should be tested with sediment with another grain-size distribution (for combined waves and currents as well as for only waves). This is necessary to test whether the influence of the grain-size is reproduced correctly. Furthermore it is possible that quasi-steady modelling is not correct for sediment with a smaller  $D_{50}$ . Moreover research should be done after the usefulness of this bed load transport formula in conditions with relatively more suspended transport (e.g. transport over ripples).
- The 1-DV boundary flow model should be extended with the possibility to use time series directly as input.



## **Appendices**



## **A Measuring techniques - General information and calibration**

### **A1 Laser-doppler flow meter (LDFM)**

A laser-doppler system, developed by DELFT HYDRAULICS, for 2-dimensional local flow velocity measurement with a 'forward scatter reference beam method'. The doppler-frequency shift of scattered laser light (by small particles) with respect to the frequency of the incident laser light is directly proportional to the velocity. A lens with 502 mm focal length is used for focusing of incident and reference laser-beams (beam thickness 0.8 mm, wave length laser light 632.8 nm). In the sensing volume the angle between incident and reference beam is approximately 4 degrees. The thickness of the sensing volume (vertical direction) is approximately 0.3 mm, the length of the sensing volume (horizontal, perpendicular to the flow) is approximately 13 mm. The standard range of bi-directional velocities is 0.001 - 2 m/s.

The output of a two-channel tracker-counter electronic signal processor (measuring the Doppler signal) is directly proportional to the velocity with the following calibration factor, 1 Volt = 0.1786 m/s.

See Figure 3.7 for the laser-beam configuration in the test section.

### **A2 Electro-magnetic flow meter (EMF)**

An electro-magnetic liquid velocity meter (developed by DELFT HYDRAULICS) based on the principles of Faraday's Induction Law for the measurement of the velocity of a conductive liquid moving across a magnetic field. An ellipsoidal sensor (disk type) is used with two pairs of diametrically opposed platinum electrodes in the disk bottom. The probe senses the voltages produced by the flow along the plane of the electrodes. The sensor has been designed in such a way that two voltages proportional to two components of the velocity vector are measured. In the tunnel application the measuring plane is horizontal, the sensing volume is positioned approximately 2 mm below the disk and the two horizontal x and y velocity components are measured. The dimensions of the sensing volume are 3-5 mm thick and 20-25 mm in diameter. The velocity range is 0-5 m/s, the specified accuracy of the system is  $\pm 1\%$  of the measured value.

The following linear calibration is used based on two towing tank calibrations: 1 Volt = 0.4875 m/s ( $\pm 0.5\%$ ). Deviations from the linear calibration lead to errors with maximum magnitudes of  $\pm 1.7$  cm/s in the velocity range 0-2.5 m/s.

See Figure 3.6 for the used EMF configuration.

**A3 Optical concentration meter (OPCON)***General*

An instrument, developed by DELFT HYDRAULICS, for the measurement of (sand) volume concentration based on the extinction of infrared light.

The range of concentrations is approximately 0.005 - 2 volume percent (sand: 0.1 - 50 gr/lit). Figure 3.5 shows the OPCON configuration in the test section of the tunnel. The light beam has a thickness of 2.6 mm (= height of sensing volume). The distance between the optical transmitter and the receiver is 3 cm (= length of the sensing volume). Bosman (1982, 1984) developed the OPCON probe and calibrated it extensively for different unsorted and sorted sand types (in a calibration vessel). Figure A3.1 shows the calibration results for sand type SU (unsorted dune sand with  $D_{50} = 0.21$  mm, as used for the present experiments). The (linear) calibration relation for the OPCON can be written as:

$$C_{op} \text{ (gr/lit)} = K_1 \cdot W_v \text{ (Volts)} \quad (\text{A.1})$$

with calibration factor  $K_1$ :

- $K_1 = \rho_s / (a_g \cdot a_c \cdot \gamma)$  = sediment density
- $a_g$  = amplification factor of electronic amplifier (factor 1 or 10)
- $a_c$  = electronic conversion factor for the log-amplifier (=  $3 \cdot \log_e = 1.303$  for the applied OPCON)
- $\gamma$  = calibration factor of the OPCON probe (grain-size dependent)

Bosman (1984) found  $\gamma = 147$  for sand SU, which coincides with  $K_1 = 13.8$  for the electronics of the used (TUD) OPCON ( $a_g = 1$ , see calibration line Figure A3.1). The OPCON is strongly grain-size dependent. Figure A3.2 shows the increasing  $K_1$  value for increasing  $D_{50}$  (Bosman, 1984). Chen (1991) calibrated the same (TUD) OPCON probe, as used for the present experiments, for two sand types ( $D_{50} = 0.18$  and  $0.20$  mm) and with concentrations in the range 0-3 gr/lit. The obtained  $K_1$  values are also plotted in Figure A3.2 and coincide well with Bosman's results. The  $D_{50}$  dependence of the calibration factor  $K_1$  was used for the present experiments in order to cope with vertical sorting effects of the suspended sediment (range  $D_{50}$ : 0.14–0.21 mm).

*Correction of OPCON voltages for variations in  $D_{50}$* 

The relation between  $D_{50}$  and calibration factor  $K_1$  (g/lit/Volt) of the OPCON probe is shown in Figure A3.2 (for OPCON amplification factor  $a_g = 10$ ). The relation can be written as:

$$K_1 = 8.41 (D_{50} - 0.05325) \quad \text{for } a_g = 10 \quad (\text{A.2})$$

$$K_1 = 84.1 (D_{50} - 0.05325) \quad \text{for } a_g = 1 \quad (\text{A.3})$$

with:  $D_{50}$  in mm  
 $K_1$  in g/l/Volt

This means that an increase in  $D_{50}$  gives an increase in calibration factor  $K_1$ . With this relation the measured  $D_{50}$  profiles (of suction samples) were transformed to  $K_1$ -profiles, see Figure A3.3 ( $a_g = 1$  has been used !).

The maximum variation of  $K_1$  occurs in the upper layer ( $z > 3$  cm):

$$K_1 = 10.7 \pm 0.85 \text{ g/l/Volt} = 10.7 \pm 8\% \text{ g/l/Volt} \quad (\text{A.4})$$

The E1 and E3 results vary more or less randomly within this range. The E2 and E4 results show a systematic shift (E2 app. 3% lower, E4 app. 4.5% higher than  $K_1 = 10.7$ ). Considering these rather small variations of the calibration factor (the variations in concentrations are the same), and considering other possible error sources (e.g. time-dependency of  $K_1$  is not accounted for !), the choice has been made to use *one*  $K_1 - z$  distribution for all four experiments. Figure A3.4 shows the data points of all 4 experiments and a fitted polynomial curve of the 4th degree; the curve can be written as:

$$K_1(z) = 15.3 - 2.39 \cdot 10^2 z + 4.46 \cdot 10^3 z^2 - 3.53 \cdot 10^4 z^3 + 9.73 \cdot 10^3 z^4 \quad (\text{A.5})$$

with:  $K_1$  in g/l/Volt (for  $a_g=1$ )  
 $z$  in m

and (elevation) range of validity:  $0 < z < 0.1$  m

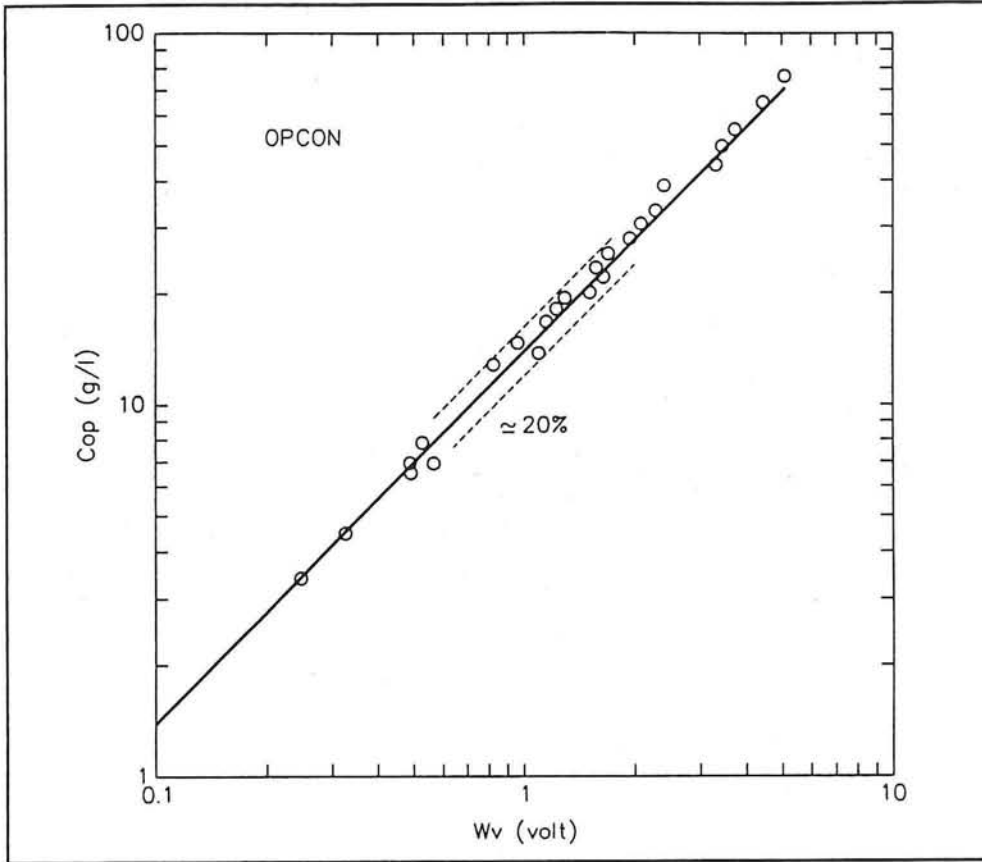


Figure A3.1 Calibration OPGON - concentration

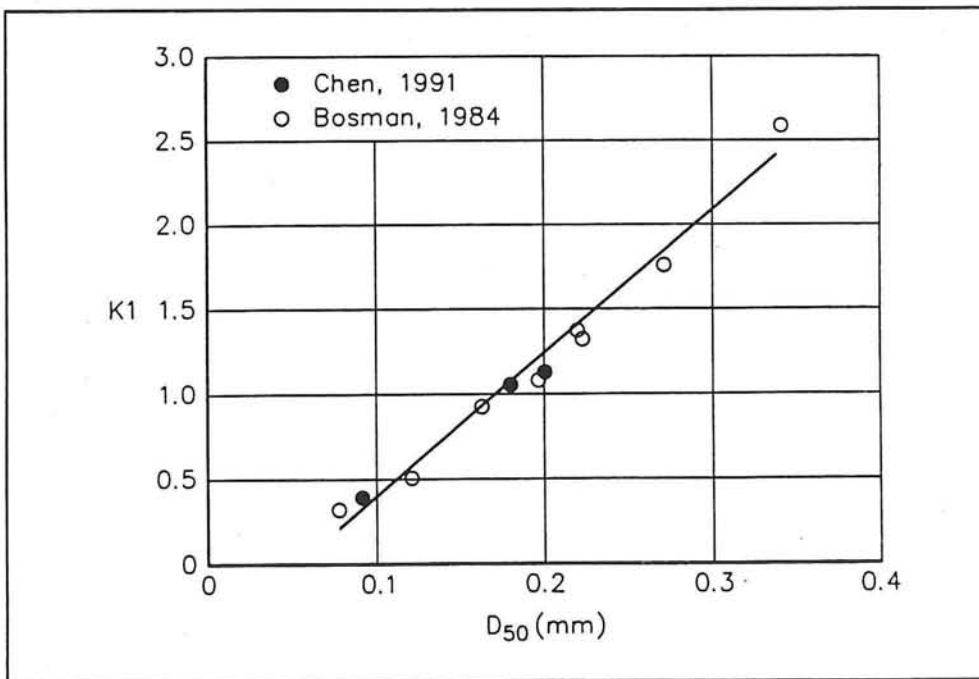


Figure A3.2 Influence of  $D_{50}$  on OPGON calibration

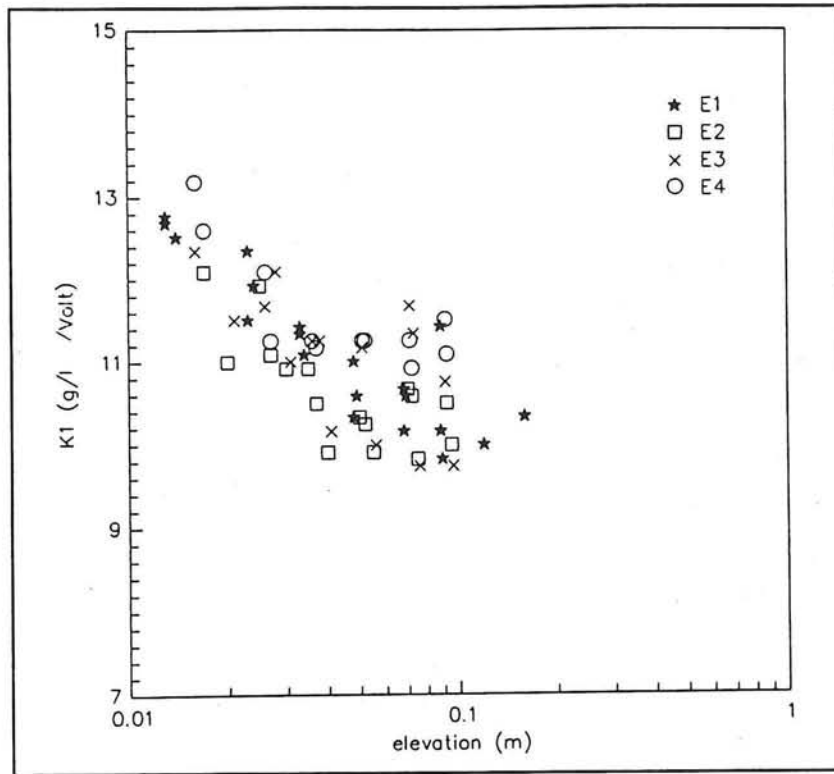


Figure A3.3 Calibration OPCON as a function of elevation

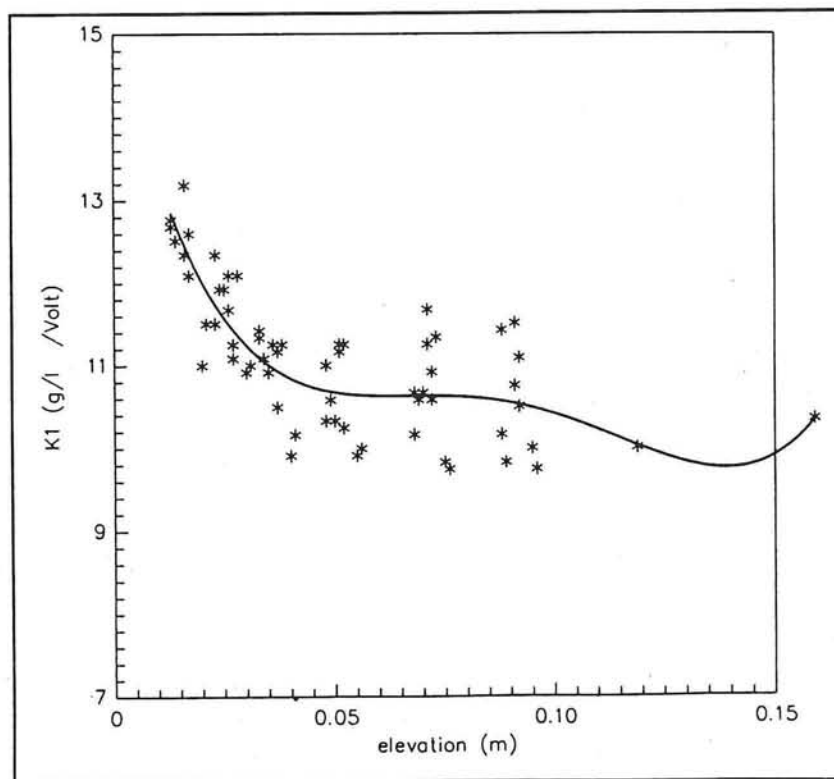


Figure A3.4 Calibration constant OPCON fitted polynomial curve

#### A4 Conductivity concentration meter (CCM)

The CCM is an instrument developed by DELFT HYDRAULICS for the measurement of large sand concentrations ( 5 - 50 volume percent, 100 - 1500 gr/lt) with a four-point electro-resistance method. See Figure 3.8 for the CCM configuration in the tunnel.

A constant electrical (AC) current is generated between two outer electrodes and the voltage between two inner electrodes is measured. The measured voltage is proportional to the electro-resistance of the sand-water mixture in a small sensing volume directly above the electrodes. The electro-resistance increases (or the conductivity decreases) for increasing sand concentrations.

The CCM was calibrated before by Ribberink and Al-Salem (1992). In order to check whether the probe was working correctly it was decided to do a new calibration. The calibration took place in a vessel (inner diameter 19 cm) with different sand-water mixtures which were brought into suspension with a propeller (diameter 7.4 cm). The propeller is positioned at the bottom of the vessel and is driven by an electric drilling machine (350 rotations/min). The vessel was provided with four vertical strips (height 2 cm) in order to obtain a relatively homogeneous sand-water mixture. The calibration was carried out with the same unsorted dunesand as used for the tunnel experiments.

The conductivity of water can vary considerably, a relative conductivity  $Gr$  is used for the calibration, defined as:

$$Gr = \left( 1 - \frac{U_o}{U_m} \right) * 100 \% \quad (A.6)$$

with:  $U_o$  = output voltage of the probe for 'clear water'  
 $U_m$  = output voltage of the probe for the sand-water mixture

Measurements were done by the CCM and the (transverse) suction system. Comparison of these measurements was difficult because for these circumstances the trapping efficiency of the suction technique was not known. To solve this problem it was decided to do a CCM measurement along vertical lines every centimetre. In this way it was possible to calculate a mean  $Gr$ -value and combine this with the mean concentration in the vessel (which is known by measuring sand weight and watervolume before starting the test). This method holds only if along each vertical in the vessel the same amount of sediment is present, this assumption was proven by measuring at different locations in the vessel.

Figure A4.1 shows the calibration results. In the vessel a maximum suspended concentration of 40 volume percent could be realized. The upper points were obtained from a non moving sand bed with a known porosity. The following linear calibration relation was obtained and used for the present experiments:

$$C \text{ (Volume \%)} = 1.1 \text{ Gr \%} \tag{A.7}$$

The suction measurements were not used for the calibration, but with the measurements of the CCM a trapping efficiency of 1.1 was found for these conditions.

The distance between the electrodes is 0.6 mm and the electrodes have a thickness of 0.3 mm. The length of the sensing volume (along the ends of the 4 electrodes) is approximately 2 mm. According to Ribberink and Al-Salem (1992) the height of the sensing volume (above the ends of the electrodes) is approximately 1 mm. Two additional measurements were carried out to check the height of the sensing volume. The CCM was positioned some millimetres above a sand-water interface ( $z = 0$ ) and was moved down with steps of 0.5 millimetre until  $z = -6$  mm. The probe output (Gr) is shown in Figure A4.2 as a function of the vertical CCM position relative to the interface. Position equal to zero means that the ends of the electrodes are positioned at level  $z = 0$ . The steepest part of the measured transition in concentration indicates again a sensing volume height of approximately 1 mm.

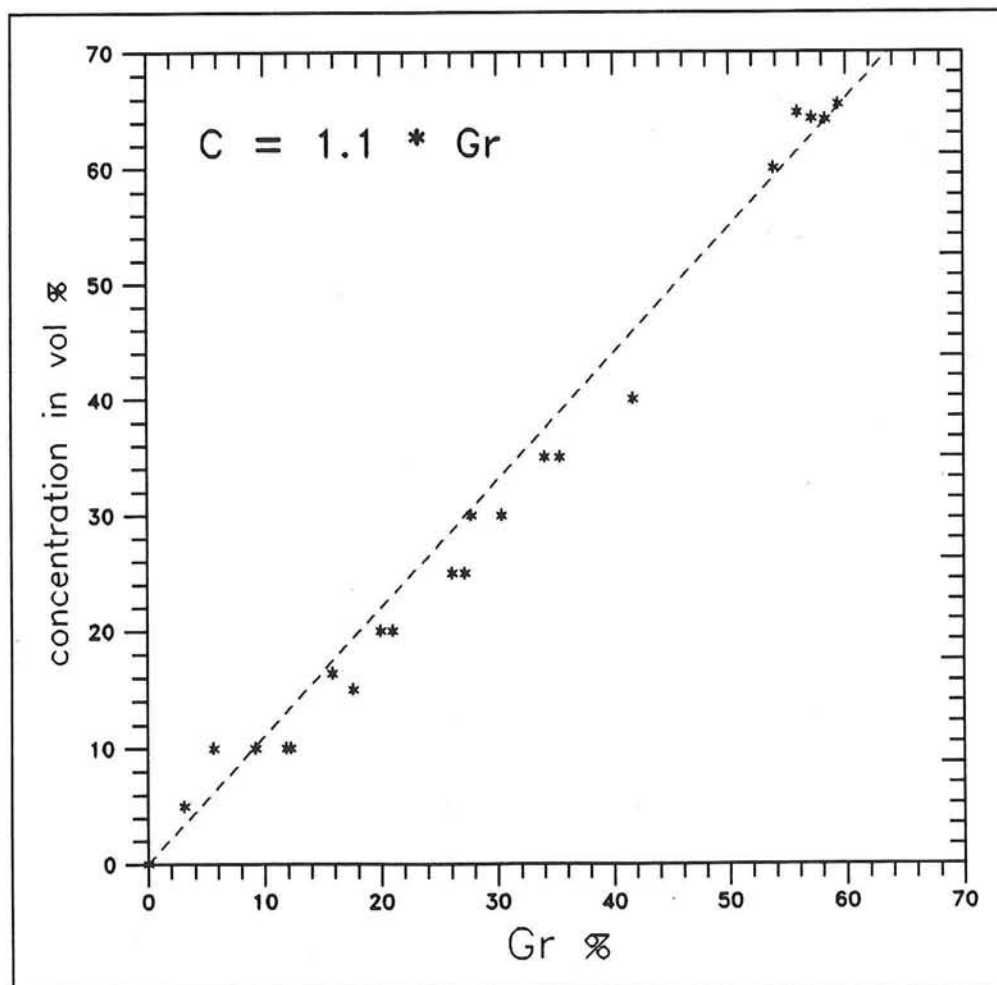


Figure A4.1 CCM calibration

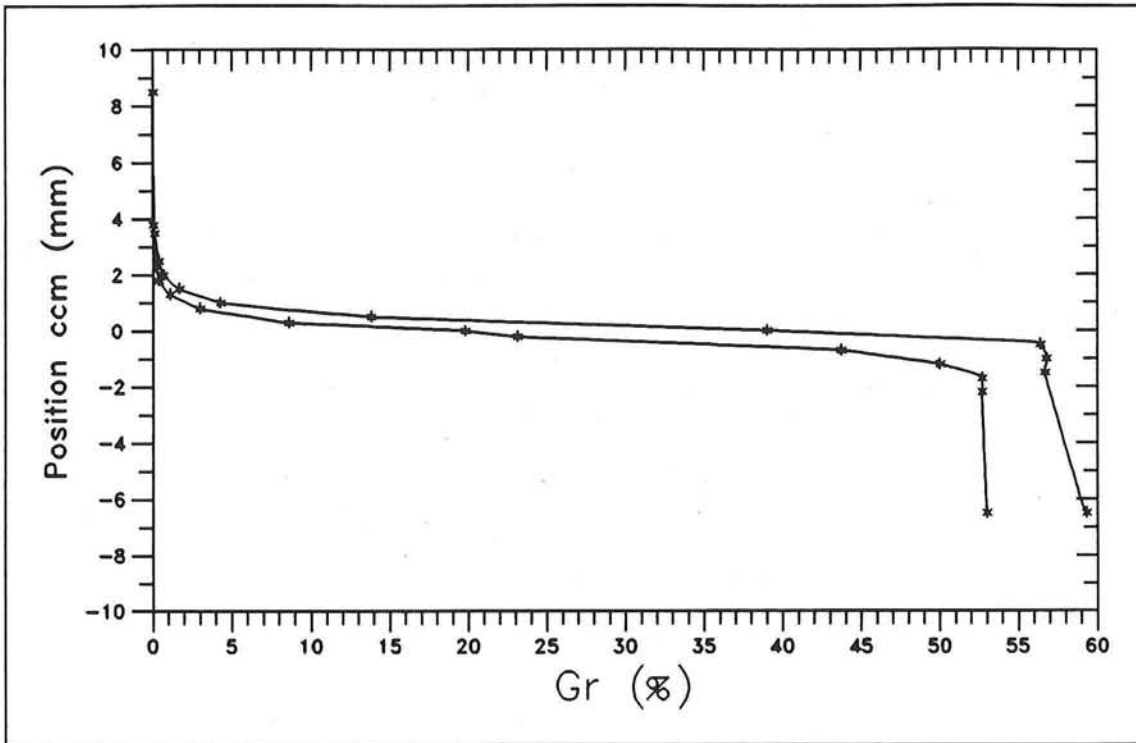


Figure A4.2 Sensing volume of CCM

### **A5 High speed video (HSV)**

A high speed video system (NAC HSV-1000 colour) was used for the recording of the oscillatory sand (grain) motions along the inner side of one of the glass side-walls of the test section.

The following specifications can be given:

- video image dimensions: approximately 15.5 x 21.5 mm,
- 500 frames per second,
- exposure time: 1/5000 sec,
- focus plane : about 2 cm inside the test section.

A time counter on the video image could be started and stopped with an electronic switch which simultaneously started and stopped a constant voltage produced by a battery (on: 9.5 Volts, off: 0 Volts). The latter signal was recorded together with the other analogue measuring signals (piston position, piston velocity etc.) assuring the synchronization of the video recording time and the piston motion.

The frames were used for the measurement of particle velocities in and above the sheetflow layer. The following method was used:

The frames were displayed on a television screen provided with a grid using a video system with variable speed (including image freezing). For each phase during the wave cycle and each level above the bed the speed of 7-13 particles was obtained by measuring the horizontal and vertical displacement during 0.01-0.07 s. Seven elevations (between -1.5 mm and 24 mm) and three phases per half cycle were analyzed. The phases of (velocity) zero crossings were separately measured. Based on the measured variation of particle speeds (same level and phase) the error of the final average particle speed is estimated as 5-10%.

The video recordings were also analyzed by bit-mapping the frames and detect the centre of the particles with a mouse. See fore a more detailed description the data report.

### **A6 Mass-conservation technique**

A mass-conservation technique was used for calculating the net sediment transport for the experiments series C. The bottom of the cylindrical risers and the recirculating pipe are provided with valves which enable the removal of trapped sand from the test section and can be applied for the measurement of the sand transport at both ends of the test section.

Because sediment traps are used on either side of the tunnel test section, the sediment continuity equation can be integrated from the left side and also from the right side. Consequently, during each test two estimates can be obtained of the transport rate in

the middle of the test section under the condition that the porosity of the sand bed in the test section is known. The porosity of the sand in the tunnel, i.e. the average porosity of all eroded and deposited sand during the experiment can be determined from the collected sand weights in the traps (volume without pores) and the total eroded volume (including pores) from the tunnel test section.

In principle the following equations are used in the analysis:

*Measured porosity:*

$$1 - \epsilon_0 = \frac{G}{\rho_s} \frac{1}{\Delta V_{ip}} \quad (\text{A.8})$$

Transport rate in the middle of the tunnel test section:

*Left trap estimation:*

$$q_{sL} = \frac{\Delta V_{lip}(1 - \epsilon_0)}{\Delta t \cdot W} - \frac{G_l}{\rho_s} \frac{1}{\Delta t \cdot W} \quad (\text{A.9})$$

*Right trap estimation:*

$$q_{sR} = \frac{\Delta V_{rip}(1 - \epsilon_0)}{\Delta t \cdot W} - \frac{G_r}{\rho_s} \frac{1}{\Delta t \cdot W} \quad (\text{A.10})$$

in which:  $\Delta V_{ip}$  =  $\Delta V_{lip} + \Delta V_{rip}$  = total eroded volume including pores from the tunnel test section during one test ( $\text{m}^3$ )  
 $\Delta V_{lip}$  = total eroded volume including pores from the left half of the tunnel test section during one test ( $\text{m}^3$ )  
 $\Delta V_{rip}$  = total eroded volume including pores from the right half of the tunnel test section during one test ( $\text{m}^3$ )  
 $G$  =  $G_l + G_r$  = total (dry) mass of the sand collected in the both sand traps (kg)  
 $G_l$  = total (dry) mass of the sand collected in the left trap (kg)  
 $G_r$  = total (dry) mass of the sand collected in the right trap (kg)  
 $\rho_s$  = density of sand =  $2650 \text{ kg/m}^3$   
 $\epsilon_0$  = sand porosity (-)  
 $W$  = width of the tunnel test section  
 $q_s$  = measured net transport rate in real sand volume (without pores) per unit width and time during one test in the middle of the tunnel test section ( $\text{m}^2/\text{s}$ )  
 $\Delta t$  = duration of one test (s)

Both formulas A.9 and A.10 give the same answer for the measured transport rate for a certain test, as long as the measured porosity during the same test is substituted. However, variations were found of the measured porosity ( $\varepsilon_o$ ) during different tests. The maximum possible extremes of  $1 - \varepsilon_o$  are 0.54 (loosely packed) and 0.67 (fully packed). The measured variation is mainly caused by errors made during the bed level measurements. The measurements were carried out by hand and with visual observations through the glass side windows of the test section. Another error source is the measurement of the mass of the sand as collected from the traps. Both errors have a random character and decrease when more sand is eroded from the tunnel during one test. This eroded volume increased for increasing test duration. The test duration is limited because bed level disturbances, generated at the boundaries, propagate into the tunnel and will ultimately reach and disturb the central part of the test section where the actual transport measurement takes place. For this reason a number of tests with a limited duration were carried out for each experiment. Between the separate tests the observed boundary effects are removed.

For the present study the measured transport rates are obtained by using equations A.9, A.10 in combination with the averaged measured porosity of all previous experiments of Ribberink and Al-Salem (1992) ( $1 - \varepsilon_o = 0.62$ ). The averaged value was considered as the measured transport rate.



## B Important non-dimensional parameters

Most of the semi-empirical models use non-dimensional parameters to prescribe the sediment transport. A review of the most important parameters is given in this appendix.

*Non-dimensional transport rate:*

The ratio of bed load transport rate  $q_b$  and a settling flux parameter  $W_s D_{50}$ :

$$\Phi_{bw} = \frac{q_b}{W_s D_{50}} \quad (\text{B.1})$$

The ratio of bed load transport rate  $q_b$  and a the square-root of a parameter representing the specific under-water mass of sand grains:

$$\Phi_{bd} = \frac{q_b}{\sqrt{\Delta g D_{50}^3}} \quad (\text{B.2})$$

*Non-dimensional sediment forcing:*

The Shields parameter, representing the ratio of the flow drag-force on the grains and the under-water mass of the grains.

$$\theta = \frac{\tau_b}{(\rho_s - \rho)g D_{50}} \quad (\text{B.3})$$

The ratio of friction velocity  $u_*$  and settling velocity  $W_s$  of sand.

$$\frac{u_*}{W_s} \quad (\text{B.4})$$

The ratio of horizontal near bed velocity  $u_b$  and the settling velocity

$$\frac{u_b}{W_s} \quad (\text{B.5})$$

*Critical Shields parameter:*

The critical Shields parameter indicates the beginning of the movement of sediment. (If the Shields parameter is larger than the critical Shields parameter sediment movement will take place.)

The parameter depends on the non-dimensional grain-size:  $\theta_{cr} = f(D_*)$  (B.6)

Herein:  $D_*$  is the non-dimensional grain-size:  $D_* = D_{50} \left[ \frac{g\Delta}{v^2} \right]^{1/3}$  (B.7)

The relationship was described by van Rijn (1993), see also Figure B.1:

$$\begin{aligned}
 1 < D_* \leq 4 & \Rightarrow \theta_{cr} = 0.24 D_*^{-1} \\
 4 < D_* \leq 10 & \Rightarrow \theta_{cr} = 0.14 D_*^{-0.64} \\
 10 < D_* \leq 20 & \Rightarrow \theta_{cr} = 0.04 D_*^{-0.1} \\
 20 < D_* \leq 150 & \Rightarrow \theta_{cr} = 0.013 D_*^{0.29} \\
 D_* > 150 & \Rightarrow \theta_{cr} = 0.055
 \end{aligned}$$

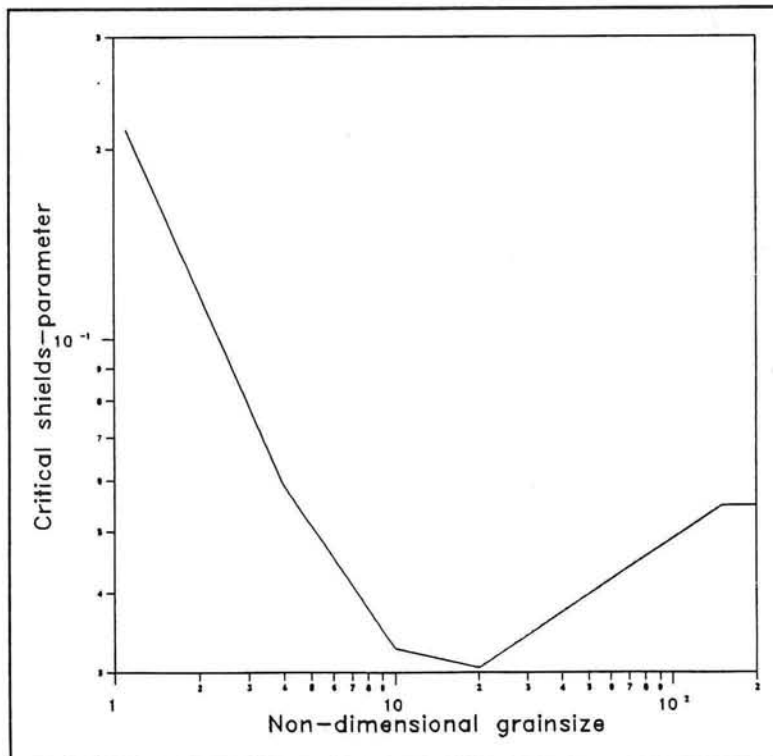


Figure B.1 Critical Shields parameter

## C Method of Soulsby/Ockenden to calculate bed shear stress

The mean and maximum bed shear stress are calculated by using a parametrization of boundary layer models as developed within MAST (Soulsby et al, 1993). This maximum and mean bed shear stress are used to calculate enhanced friction factors for the current and the waves, as described by Soulsby and Ockenden (1994). A disadvantage of the method is that phase shifts between velocity and bed shear stress are ignored.

Used parameters:

$C_D$	= current drag coefficient
$f_c$	= current friction factor
$f_c^+$	= current friction factor enhanced by waves
$f_w$	= wave-related bed shear stress
$f_w^+$	= wave friction factor enhanced by the current
$\tau_{b,max}$	= maximum bed shear stress
$\langle \tau_b \rangle$	= time averaged bed shear stress
$\tau_c^+$	= current-related bed shear stress enhanced by waves
$\tau_w^+$	= wave-related bed shear stress enhanced by the current
$\tilde{u}_b(t)$	= oscillatory component of the near bed velocity
$\langle u_b \rangle$	= net (wave averaged) near bed velocity
$z$	= height above bed where velocity is defined
$z_0$	= zero level velocity

The total time dependent bed shear stress can be expressed in the following formula:

$$\tau_b(t) = \tau_c^+ + \tau_w^+(t) = \frac{1}{2}\rho f_c^+ |\langle u_b \rangle| \langle u_b \rangle + \frac{1}{2}\rho f_w^+ \tilde{u}_b(t) |\tilde{u}_b(t)| \quad (2.26)$$

*The following procedure is followed:*

- 1) First the current- ( $\tau_c$ ) and wave- ( $\tau_w$ ) related bed shear stress are calculated (without interaction).

$$\tau_w = \frac{1}{2}\rho f_w W^2 \quad (C.1)$$

$$f_w = \exp\left\{-6 + 5.2\left(\frac{A}{k_s}\right)^{-0.19}\right\} \quad (C.2)$$

$$f_{w,max} = 0.3$$

Herein:  $A$  = wave excursion amplitude =  $\sqrt{2} \cdot \tilde{u}_{rms} \cdot T / 2\pi$   
 $W$  = maximum orbital velocity =  $\sqrt{2} \cdot \tilde{u}_{rms}$

These definitions are chosen in such a way that they apply to each wave spectrum, like non-sinusoidal waves or irregular wave spectra.

$$\tau_c = \rho \left\{ \frac{\kappa}{\ln(z/z_0)} \right\}^2 |\langle u_b \rangle| \langle u_b \rangle = \frac{1}{2} \rho f_c |\langle u_b \rangle| \langle u_b \rangle \quad (C.3)$$

$$C_D = \left[ \frac{\kappa}{\ln(z/z_0) - 1} \right]^2 \quad (C.4)$$

2) A non-dimensional parameter  $x$  is calculated:

$$x = \frac{|\tau_c|}{|\tau_c| + \tau_w} \quad (0 \leq x \leq 1) \quad (C.5)$$

3) The non-dimensional coefficients  $a$ ,  $b$ ,  $m$ ,  $n$ ,  $p$  and  $q$  are calculated with as input the values from Table C.1; In this report the coefficients based on the model of Fredsoe are used:

$$i = (i_1 + i_2) + (i_3 + i_4) \cdot {}^{10}\log(f_w/C_D) \quad i = a, b, m, n, p, q \quad (C.6)$$

	a	b	m	n	p	q
$i_1$	-0.06	0.29	0.67	0.75	-0.77	0.91
$i_2$	1.70	0.55	-0.29	-0.27	0.10	0.25
$i_3$	-0.29	-0.10	0.09	0.11	0.27	0.50
$i_4$	0.29	-0.14	0.42	-0.22	0.14	0.45

Table C.1 Coefficients used to calculate bed shear stress

Example:  $a = (-0.06 + 1.70) + (-0.29 + 0.29) {}^{10}\log(f_w/C_D)$

4) Calculate the non-dimensional coefficients  $Y$  and  $y$ :

$$Y = 1 + ax^m(1-x)^n \quad (C.7)$$

$$y = x[1 + bx^p(1-x)^q] \quad (c.8)$$

5) Use the coefficients  $Y$  and  $y$  to calculate the maximum and the mean bed shear stress:

$$\tau_{b,max} = Y(\tau_c + \tau_w) \quad (C.9)$$

$$\langle \tau_b \rangle = y(\tau_c + \tau_w) \quad (C.10)$$

- 6) Use the mean and maximum bed shear stress to calculate the enhanced coefficients  $f_c^+$  and  $f_w^+$ .

$$\langle \tau_b(t) \rangle = \frac{1}{2} \rho f_c^+ |\langle \mathbf{u}_b \rangle| \langle \mathbf{u}_b \rangle \quad \Leftrightarrow \quad f_c^+ = \frac{\langle \tau_b \rangle}{\frac{1}{2} \rho |\langle \mathbf{u}_b \rangle| \langle \mathbf{u}_b \rangle} \quad (\text{C.11})$$

$$\tau_{b,\max} = |\langle \tau_b \rangle| + \frac{1}{2} \rho f_w^+ W^2 \quad \Leftrightarrow \quad f_w^+ = \frac{\tau_{b,\max} - \langle \tau_b \rangle}{\frac{1}{2} \rho W^2} \quad (\text{C.12})$$



## D Influence of the side-walls on the velocity moment

In many of the sediment transport formulas it is supposed that the sand transport depends on the third-order velocity moment. Also in former wave tunnel tests this relationship was obtained, as well as for only waves (see Al-Salem, 1993) as for situations with waves and a current (see Ribberink, 1994).

During the present tests velocities were measured in the middle of the tunnel but the total transport rates (across the whole section) were measured. Ramadan (1994) measured also a velocity profile across the tunnel. He concluded that the oscillating component of the velocity was almost constant over the cross-section, but the mean velocity was varying too much to justify the assumption of a constant velocity in the cross-section. Below it is discussed which impact this has on the third-order velocity moment and its relation with the measured transport.

Used parameters:

$\langle \dots \rangle$	= averaged over wave cycle
$u_0$	= time averaged horizontal velocity
$u_{0,max}$	= $u_0$ in the middle of the cross-section
$\tilde{u}$	= periodic component of the horizontal velocity
$\tilde{u}_{rms}$	= the root mean square value of the horizontal periodic velocity
$u^3$	= third-order velocity moment
$b$	= width of wave tunnel (0.30 m)

Ramadan measured in a situation with a sinusoidal wave and a net current (see fig D.1). The third-order velocity moment can be expressed in the mean velocity and the amplitude of the periodic velocity:

$$u^3 = (u_0 + \tilde{u})^3 = u_0^3 + 3u_0^2\tilde{u} + 3u_0\tilde{u}^2 + \tilde{u}^3 \quad (D.1)$$

Averaging over the wave cycle gives:

$$\langle u^3 \rangle = u_0^3 + 3u_0^2\langle \tilde{u} \rangle + 3u_0\langle \tilde{u}^2 \rangle + \langle \tilde{u}^3 \rangle \quad (D.2)$$

The second term of the right-hand side of equation 2 is zero, in case of sinusoidal waves this holds also for the last term:

$$\langle u^3 \rangle = u_0^3 + 3u_0\tilde{u}_{rms}^2 \quad (D.3)$$

The maximum velocity moment in the middle of the cross-section (at  $y=0$ ) is:

$$\langle u^3 \rangle_{max} = u_{0,max}^3 + 3u_{0,max}\tilde{u}_{rms}^2 \quad (D.4)$$

The next step is to average the third-order velocity moment over the cross-section:

$$\overline{\langle u^3 \rangle} = \overline{u_0^3} + \overline{3u_0 \tilde{u}_{rms}^2} = \overline{u_0^3} + 3\overline{u_0} \tilde{u}_{rms}^2 \quad (D.5)$$

To make this calculation the distribution of  $u(y)$  over the cross-section has to be known. The profile measured by Ramadan is schematized with a polynomial distribution:

$$u_0 = \left( 1 - \left\{ \frac{y}{1/2 \cdot b} \right\}^n \right) * u_{0,max} \quad n = 2, 4, 6, \dots \quad (D.6)$$

$$\overline{u_0^3} = \frac{u_{0,max}^3}{b} \int_{-1/2b}^{1/2b} \left( 1 - \left\{ \frac{y}{1/2 \cdot b} \right\}^n \right)^3 dy \quad (D.7)$$

$$\overline{u_0} = \frac{u_{0,max}}{b} \int_{-1/2b}^{1/2b} \left( 1 - \left\{ \frac{y}{1/2 \cdot b} \right\}^n \right) dy \quad (D.8)$$

Finally the following expression can be obtained:  $\overline{\langle u^3 \rangle} = C_1 u_{0,max}^3 + 3C_2 u_{0,max} \tilde{u}_{rms}^2$  (9)

with the following numeric values for  $C_1$  and  $C_2$ :

n	$C_1$	$C_2$
2	0.457	0.667
4	0.656	0.800
6	0.750	0.857

Table D.1 Values of  $C_1$  and  $C_2$

None of the polynomial distributions gives a very good fit. To improve the fit a parabola is combined with a logarithmic profile (see fig D.1), this gives:

$$\begin{aligned} u_0 &= [0.147 \cdot \ln(0.15 + x) + 1.19] u_{0,max} & y < -0.10 \text{ m} \\ u_0 &= [1 - 16.136 \cdot y^2] u_{0,max} & -0.10 \text{ m} < y < 0.10 \text{ m} \\ u_0 &= [0.147 \cdot \ln(0.15 - x) + 1.19] u_{0,max} & y > 0.10 \text{ m} \end{aligned} \quad (D.10)$$

Again values for  $C_1$  and  $C_2$  are obtained:  $C_1 = 0.698$  and  $C_2 = 0.865$ .

It is assumed that all tests in the tunnel have a net velocity distribution with the same shape as measured by Ramadan. The transport in the middle of the tunnel can then be

calculated with the help of the calculated correction factors  $C_1$  and  $C_2$ . The following relationship is obtained. In the Table below C is calculated using equation C.10.

$$\langle q_s \rangle_{\max} = \frac{\langle u^3 \rangle_{\max}}{\langle u^3 \rangle} \cdot \langle \overline{q_{s,\text{measured}}} \rangle = C \langle \overline{q_{s,\text{measured}}} \rangle \quad (\text{D.11})$$

Test	$u_{0,\max}$	$u_{\text{rms}}$	$\langle \overline{u^3} \rangle$ (n = 6)	$\langle \overline{u^3} \rangle$ (eq 10)	$\langle u^3 \rangle_{\max}$	C
E1	0.19	1.17	0.674	0.679	0.787	1.16
E2	0.24	1.03	0.665	0.670	0.778	1.16
E3	0.31	0.79	0.520	0.523	0.610	1.17
E4	0.44	0.64	0.527	0.527	0.626	1.19

*Table D.2 Correction factors for measured transport series E*

This approach can also be used when the velocity is not a parabola, but a second order Stokes wave:

$$u(t) = u_0 + u_1 \cos(\omega \cdot t) + u_2 \cos(2\omega \cdot t) \quad (\text{D.12})$$

The third-order velocity moment expressed in  $u_0$ ,  $u_1$  and  $u_2$ :

$$\langle u^3 \rangle = u_0^3 + \frac{3}{2}u_0(u_1^2 + u_2^2) + \frac{3}{4}u_1^2 u_2 \quad (\text{D.13})$$

Again this is averaged over the cross-section assuming that  $u_1$  and  $u_2$  are constant:

$$\langle \overline{u^3} \rangle = C_1 u_{0,\max}^3 + \frac{3}{2}C_2 u_{0,\max}(u_1^2 + u_2^2) + \frac{3}{4}u_1^2 u_2 \quad (\text{D.14})$$

The correction factor C is a function of  $u_0/u_1$  (current/wave parameter) and  $u_2/u_1$  (wave-asymmetry parameter). In Figure D.2 correction factors are plotted against these parameters.

Test	$u_{0,\max}$	$u_1$	$u_2$	$\langle \overline{u^3} \rangle$ (eq 10)	$\langle u^3 \rangle_{\max}$	C
C1	0.0152	0.819	0.239	0.135	0.137	1.02
C2	0.0552	0.824	0.227	0.168	0.176	1.05
C3	0.357	0.828	0.217	0.486	0.549	1.14
C4	0.203	0.813	0.220	0.302	0.333	1.11
C5	0.470	0.840	0.200	0.633	0.735	1.16

Test	$u_{0,max}$	$u_1$	$u_2$	$\overline{\langle u^3 \rangle}$ (eq 10)	$\langle u^3 \rangle_{max}$	C
C9	0.0214	0.855	0.176	0.118	0.121	1.03
C10	-0.460	1.200	0.250	-0.695	-0.864	1.24
C11	0.0290	1.138	0.277	0.321	0.329	1.03
C12	-0.105	1.120	0.235	0.042	0.014	0.33
C13	0.556	1.270	0.184	1.531	1.768	1.16

Table D.3 Correction factors for measured transport series C

Test C12 gives at first sight surprising results, transport in the middle of the test section is only one third of the transport averaged over the cross-section. This can be explained by a transport in opposite direction near the side-walls of the tunnel.

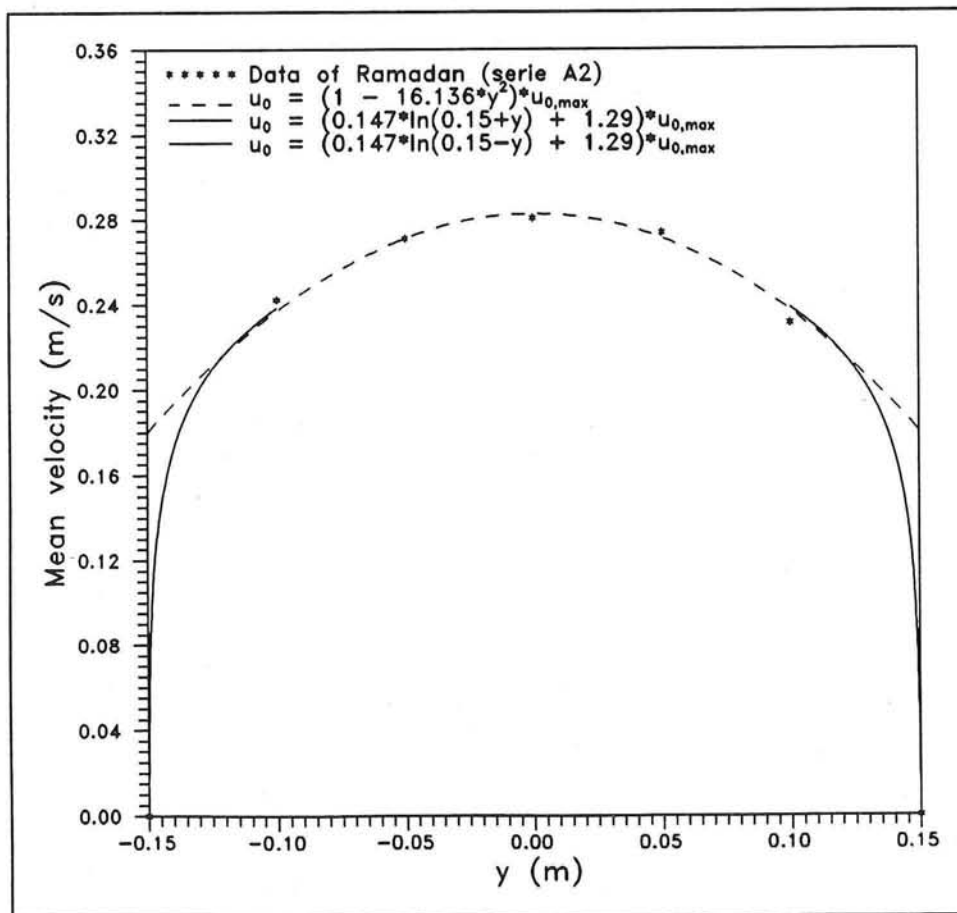


Figure D.1 Measured velocity profile over cross-section

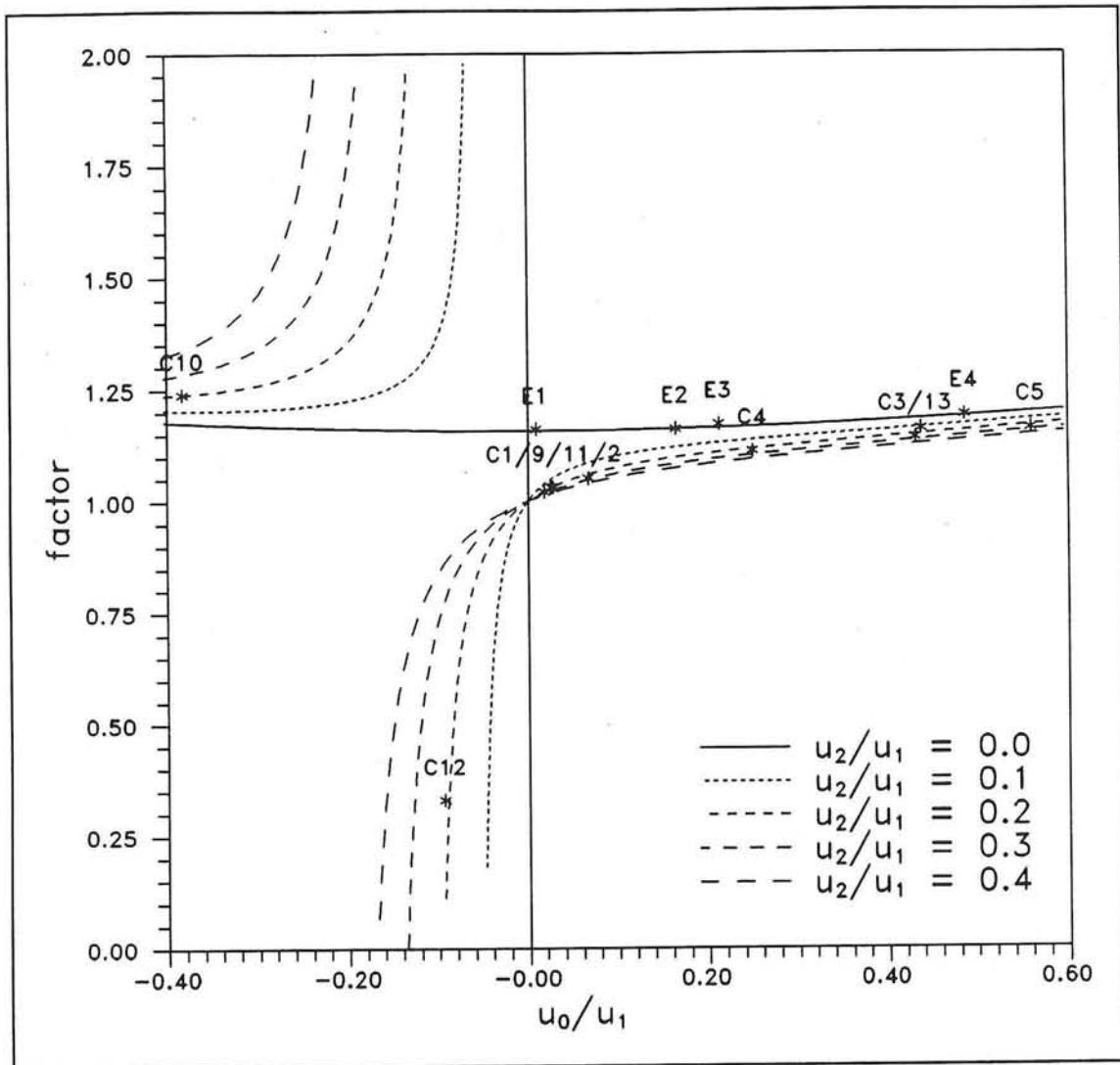


Figure D.2 Correction factors for measured sediment transport



## E Input and output of the sediment transport program

### E.1 Input

A computer program was made to calculate the sediment transport rates with the formulas treated in Chapter 2. The computer program needs three different groups of information, namely characteristics of the used sediment and liquid and information about the free stream velocity. During all tests the same sediment and liquid (water) were used, so these data are equal for all tests, only the viscosity changes with the temperature.

Used parameters:

- $D_{50}$  = median grain diameter
- $D_{90}$  = grain-size for which 90 % of the sediment (by weight) is finer
- $W_s$  = fall velocity
- $\rho_s$  = density of sediment
- $\rho$  = density of water
- $\nu$  = viscosity
- $\phi$  = angle of internal friction
- $\langle u \rangle$  = mean velocity
- $u_{\text{rms}}$  = root mean square of the velocity
- $u_1, u_2$  = coefficients in the definition of a 2<sup>nd</sup> order Stokes wave

#### *Data sediment*

- $D_{50}$  = 0.21 mm
- $D_{90}$  = 0.32 mm
- $W_s$  = 2.6 cm/s
- $\rho_s$  = 2650 kg/m<sup>3</sup>
- $\tan \phi$  = 0.610

#### *Data water*

- $\rho$  = 1000 kg/m<sup>3</sup>
- $\nu$  =  $1.3 \cdot 10^{-6}$  m<sup>2</sup>/s (series E and C-I)
- =  $1.1 \cdot 10^{-6}$  m<sup>2</sup>/s (series C-II)

Because of the small influence on the transport of a different value for the viscosity this parameter is taken as a constant during each series. For series E and C-I the value of the viscosity which would apply in case of a temperature of 10° C was used, for series C-II (executed during summertime) a value of 16° C was chosen.

The program asks for the temperature of the water also, but this value is not used in the calculation (it is only given in the output file as reference).

### Velocity

The program gives three possibilities to define the velocity:

- sinusoidal wave (defined by  $u_{rms}$ ) and a net velocity
- 2<sup>nd</sup> order Stokes wave (defined by  $u_1$  and  $u_2$ :  $u(t) = u_1 \cdot \cos(\omega t) + u_2 \cdot \cos(2\omega t)$ ) and a net velocity
- time series (the program will ask for a filename and a time step)

For the C series the last possibility was used except for case C11. In this case no time series was available and the velocity was modelled with a second order Stokes wave. Schematizing as a second order Stokes wave was also tried for the other C-tests but had the disadvantage that deformation of waves in the tunnel was present, so the time series and the schematisation gave deviating velocity moments ( $\pm 20\%$ ). During the E-series almost no deformation took place and the velocity could be schematized as a sinusoidal wave with a net current. The advantage of schematizing is that  $u_{rms}$  and  $\langle u \rangle$  can be taken as an average from several tests, a time series represents only one test.

The program needs further the period (T) and the level where the velocity is defined, a review of the given input can be found in Table E.1.

Series	Test	Velocity characteristics (m/s):	Period (s)	$\Delta t$ (s)	level (cm)
E	E1	$\langle u \rangle = 0.176, u_{rms} = 1.180$	7.25	0.025	10
	E2	$\langle u \rangle = 0.239, u_{rms} = 1.031$	7.25	0.025	20
	E3	$\langle u \rangle = 0.311, u_{rms} = 0.839$	7.25	0.025	10
	E4	$\langle u \rangle = 0.443, u_{rms} = 0.643$	7.25	0.025	20
C-I	C1	file: c1-v.dat	6.5	0.1	20
	C2	file: c2-v.dat	6.5	0.1	20
	C3	file: c3-v.dat	6.5	0.1	20
	C4	file: c4-v.dat	6.5	0.1	20
	C5	file: c5-v.dat	6.5	0.1	20
C-II	C9	file: inv9.dat	6.5	0.1	10
	C10	file: inv10.dat	6.5	0.1	10
	C11	$\langle u \rangle = 0.029, u_1 = 1.138, u_2 = 0.277$	6.5	0.025	10
	C12	file: inv12.dat	6.5	0.1	10
	C13	file: inv13e.dat	6.5	0.1	10

Table E.1: Input for Sediment transport program

## E.2 Output

An example of the output of the sediment transport model is given below (for test E3). In the output first a review of the input is given. (The output is directly taken from the program, so the used language is Dutch, an English version of the program is not yet available.)

Next the calculation results are given. First some velocity parameters are listed, the mean velocity, the crest and trough velocity, the third-order velocity moment and  $u_{rms}$ . Further the amplitude of the horizontal oscillatory flow is given.

Next the calculated transport rates are given combined with some other parameters depending on the transport formula used. If a transport formula is used which needs the bed shear stress as input some characteristics of the bed shear stress and the used bed roughness height are given. All values are in the S.I. units metres, seconds or kilograms (or combinations). The calculated transport is the time averaged transport in real volume per unit width.

Testnummer = H1570 E3

Invoer gegevens

Gegevens sediment

D50 = 0.000210 D90 = 0.000320  $\tan \phi = 0.610$   
rho = 2650.00  $W_s = 0.026000$

Gegevens vloeistof

rho = 1000.00 viscositeit = 1.30700000000074E-0006 temperatuur = 10.0

Gegevens snelheid (sinus)

$u_0 = 0.3108$   $u_{rms} = 0.8387$

Hoogte boven de bodem = 0.10  
Tijdstap = 0.02500  
Periode = 7.250

Analyse snelheden:

Gemiddelde snelheid.. = 0.3108 Orb. snelheid = 1.1862  
Ucrest..... = 1.1862 Utrough..... = 1.1862  
derde snelheidsmoment = 0.6858 Xmax..... = 1.3687  
Urms..... = 0.8387

Uitvoer rekenprocedure

Bodemtransport volgens Al-Salem = 1.23452474433689E-0004

Totaaltransport volgens Watanabe = 4.22215773469447E-0005 7.73288962397783E+0000

$\Omega_c = 319.87$   $\Omega_c' = 0.00$   
 $\Omega_t = 115.66$   $\Omega_t' = 0.00$

$D^* = 4.4438$  shields kritiek = 5.38971715672005E-0002

$k_s = 3 \cdot \Theta \cdot D_{90} = 9.84674807877894E-0004$   
 $P_1 = 3.28127500280662E-0004$   $P_2 = 4.17121945287585E+0004$

Bodemschuifspanning volgens Ribberink/van Rijn

fc = 4.97284684166743E-0003 fw = 9.23008369747436E-0003 fcw = 8.34631240948625E-0003

eerst is de absolute waarde gegeven daarna de dimensieloze

TAUgem = 1.9810 0.5828  
TAUgem.abs = 3.3388 0.9822  
TAUmax = 9.3502 2.7507  
TAUwave = 6.4934 1.9103  
TAUcurrent = 0.2401 0.0706  
x = 0.0357 y1 = 0.2942 y2 = 1.3886

Bodemtransport volgens Abdullah & Ribberink = 2.29750701310740E-0004 4.20788830239326E+0001

Totaal transport volgens Bailard = 2.21615146195370E-0004

Bodemtransport = 2.89846967811702E-0005

Suspensietransport = 1.92630449414199E-0004

Bodemtransport volgens nieuw methode Ribberink = 1.28989446720940E-0004 1.05353450011462E+0001

shields-representatief = 1.13965877009832E+0000

-----

## F Tables

In this appendix contains different Tables, as obtained in the framework of this thesis, with additional information the series E experiments, for more information about tests, datafiles etc. reference is made to the data report (Katapodi et al, 1994).

### F.1 Tables with fluxes

In Table F.1.1 - F.1.4 is specified which concentration and velocity measurements were used to calculate the fluxes and which instrument was used to carry out the measurements.

In Table F.1.5 - F.1.8 the calculated fluxes are given. In the first column the level is given, in the second up to the fourth column the sediment flux during *one* wave cycle. In the last three columns time averaged fluxes are given split in a wave-related and a current-related part, according to the formula:

$$\langle \phi_s(z) \rangle = \langle u(z,t) * C(z,t) \rangle = \langle u(z) \rangle * \langle C(z) \rangle + \langle \tilde{u}(z) * \tilde{C}(z) \rangle \quad (4.2)$$

Herein:  $\phi$  = flux  
 $C$  = concentration  
 $u$  = velocity  
 $\langle .. \rangle$  = time averaged  
 $\tilde{..}$  = wave-related part

A summary of all the fluxes can be found in Table F.1.5 - F.1.9.

level (cm)	Concentration			Velocity		
	instrument	test	level (cm)	instrument	test	level (cm)
1.5	OPCON	E1-09-3	1.45	EMF	E1-17-1	1.45
2.4	OPCON	E1-09-2	2.35	EMF	E1-18-1	2.40
3.7	OPCON	E1-05-2	3.65	EMF	E1-17-2 E1-16-2	3.05 5.25
5.3	OPCON	E1-05-3	5.35	LDFM	E1-28-3	5.30
7.1	OPCON	E1-10-2	7.10	LDFM	E1-28-2 E1-23-2	6.45 7.75

Table F.1.1 Velocities and concentration measurements used in calculations of sediment fluxes for E1

Level (cm)	Concentration			Velocity		
	instrument	test	level (cm)	instrument	test	level (cm)
1.3	OPCON	E2-08-3	1.30	EMF	E2-15-3	1.50
2.3	OPCON	E2-06-3	2.30	EMF	E2-16-3 E2-18-1	2.10 2.40
3.9	OPCON	E2-05-2	3.90	EMF	E2-15-2 E2-18-2	3.20 5.15
5.4	OPCON	E2-10-3	5.45	LDFM	E2-23-3 E2-27-3	5.00 5.85
7.3	OPCON	E2-07-2	7.25	LDFM	E2-23-2 E2-25-2	7.00 7.65

*Table F.1.2 Velocities and concentration measurements used in calculations of sediment fluxes for E2*

Level (cm)	Concentration			Velocity		
	instrument	test	level (cm)	instrument	test	level (cm)
1.0	OPCON	E3-12-3	0.95	EMF	E3-15-3	1.65
2.2	OPCON	E3-14-3	2.20	EMF	E3-16-3	2.20
3.8	OPCON	E3-10-3	3.75	LDFM	E3-24-3 E3-24-2	3.50 4.40
5.1	OPCON	E3-10-2	5.10	LDFM	E3-25-3 E3-23-2	5.00 5.70

*Table F.1.3 Velocities and concentration measurements used in calculations of sediment fluxes for E3*

Level (cm)	Concentration			Velocity		
	instrument	test	level (cm)	instrument	test	level (cm)
1.1	OPCON	E4-12-3	1.05	EMF	E4-17-1	1.30
2.4	OPCON	E4-14-3	2.35	EMF	E4-18-1	2.00
					E4-17-2	3.10
3.9	OPCON	E4-13-3	3.90	EMF	E4-15-2	3.65
					E4-18-2	5.05
5.2	OPCON	E4-10-2	5.20	LDFM	E4-24-3	5.05
					E4-26-2	5.50

Table F.1.4 Velocities and concentration measurements used in calculations of sediment fluxes for E4

Level (cm)	Sediment flux during a wave cycle ( $10^{-3}$ m)			Sediment flux averaged over time ( $10^{-6}$ m/s)		
	Negative	Positive	Total	Total	Wave-related	Current-related
1.5	22.95	37.48	14.53	2018	996	1022
2.4	9.16	10.31	1.15	160	-161	321
3.7	4.60	3.96	-0.64	-88.5	-273	184
5.3	2.02	1.24	-0.78	-107	-151	44.4
7.1	1.02	1.01	-0.01	-0.946	-36.8	35.9
Total Sediment flux over height ( $10^{-6}$ m <sup>2</sup> /s)				7.72	-4.15	11.87

Table F.1.5 Sediment fluxes calculated for E1

Level (cm)	Sediment flux during wave cycle ( $10^{-3}$ m)			Sediment flux averaged over time ( $10^{-6}$ m/s)		
	Negative	Positive	Total	Total	Wave-related	Current-related
1.3	8.00	16.9	8.88	1235	730	505
2.3	4.92	5.03	0.098	13.7	-241	255
3.9	2.27	1.94	-0.331	-46.0	-149	103
5.4	1.07	1.07	-0.0002	-0.028	-52.6	52.6
7.3	0.321	0.450	0.129	17.9	-5.3	23.2
Total Sediment flux over height ( $10^{-6}$ m <sup>2</sup> /s)				5.81	-2.74	8.55

Table F.1.6 Sediment fluxes calculated for E2

Level (cm)	Sediment flux during wave cycle ( $10^{-3}$ m)			Sediment flux averaged over time ( $10^{-6}$ m/s)		
	Negative	Positive	Total	Total	Wave-related	Current-related
1.0	2.51	9.00	6.49	901	492	409
2.2	1.68	1.70	0.02	3.44	-146	149
3.8	0.40	0.28	-0.12	-16.7	-50.4	33.7
5.1	0.21	0.21	-0.00	-0.315	-22.5	22.2
Total Sediment flux over height ( $10^{-6}$ m <sup>2</sup> /s)				5.21	0.03	5.17

Table F.1.7 Sediment fluxes calculated for E3

Level (cm)	Sediment flux during wave cycle ( $10^{-3}$ m)			Sediment flux averaged over time ( $10^{-6}$ m/s)		
	Negative	Positive	Total	Total	Wave-related	Current-related
1.1	1.03	2.96	1.93	268	31	237
2.4	0.776	1.24	0.468	65.0	-95	160
3.9	0.176	0.156	-0.0199	-2.76	-42.0	39.2
5.2	0.0914	0.172	0.0809	11.2	-12.6	23.8
Total Sediment flux over height ( $10^{-6}$ m <sup>2</sup> /s)				2.69	-1.79	4.48

Table F.1.8 Sediment fluxes calculated for E4

Test	$q_{total}$ ( $10^{-6}$ m <sup>2</sup> /s)	integrated flux calculated with OPCON, EMF, and LDFM ( $10^{-6}$ m <sup>2</sup> /s)			Levels, where between integrated flux was calculated (cm)
		total	wave-related	current-related	
E1	107.20	7.72	-4.15	11.87	1.5 - 7.1
E2	111.77	5.81	-2.74	8.55	1.3 - 7.3
E3	80.80	5.21	0.03	5.17	1.0 - 5.1
E4	84.88	2.69	-1.79	4.48	1.1 - 5.2

Table F.1.9 Sediment fluxes, total, wave- and current-related

## F.2 Result of High speed video analysis

In Table F.2.1 - F.2.3 the estimated grain velocities can be found. This velocities represent the average value of the measured velocities of 8-16 grains.

In Table F.1.4 - F.1.6 the measured concentrations (used to calculate fluxes) in the sheetflow layer are given.

In Table F.1.7 - F.1.9 the calculated fluxes (velocity \* concentration) can be found. Total fluxes (integrated over time and length) are given in Table F.1.10 and F.1.11 (only for E1 and E3).

level (mm)	Velocity (m/s)					
	0.85s	1.69s	2.54s	4.35s	5.31s	6.27s
-1.5	0.000	-0.096	0.000	0.000	0.096	0.000
0.0	-0.136	-0.135	-0.145	0.234	0.230	0.159
2.5	-0.305	-0.344	-0.154	0.412	0.290	0.176
5.5	-0.667	-0.618	-0.312	0.810	0.750	0.377
8.0	-0.762	-0.775	-0.384	0.874	0.773	0.387
15.0	-1.028	-0.904	-0.601	0.907	0.894	0.535
24.0	-1.193	-1.092	-0.561	1.004	1.113	0.725

Table F.2.1 Grain velocities estimated with HSV-analysis for E1

level (mm)	Velocity (m/s)					
	0.85s	1.69s	2.54s	4.35s	5.31s	6.27s
0.0	-0.271	-0.333	-0.162	0.277	0.258	0.129
2.0	-0.470	-0.461	-0.343	0.546	0.517	0.230
3.5	-0.645	-0.595	-0.428	0.570	0.575	0.274
5.0	-0.585	-0.577	-0.432	0.696	0.507	0.246
9.5	-0.683	-0.620	-0.489	0.749	0.730	0.394
18.0	-0.903	-0.661	-0.489	0.767	0.930	0.588

Table F.2.2 Grain velocities estimated with HSV-analysis for E3

z(mm)	phase-lag (s)	velocity (mm/s)					
		0.68s	1.35s	2.03s	3.65s	4.60s	5.55s
-1.0	-0.3	206	243	173	-179	-146	-135
0.0	-0.3	368	419	234	-348	-222	-194
2.0	-0.3	574	586	354	-469	-370	-288
5.0	-0.2	626	692	338	-548	-387	-351
9.0	-0.2	578	821	422	-647	-431	-417
20.0	-0.1	616	957	502	-627	-431	-425

Table F.2.3 Grain velocities estimated with HSV-analysis for C

level (mm)	Instrument	Concentration (g/l)					
		0.85s	1.69s	2.54s	4.35s	5.31s	6.27s
-1.5	CCM	1205	1085	1065	1215	1085	1007
0.0	CCM	1063	819	792	1154	835	824
2.5	CCM	451	487	452	396	514	525
5.5	CCM	237	383	376	223	417	422
8.0	CCM	87	217	260	57	244	292
15.0	OPCON	16.8	16.4	27.5	12.0	17.6	42.5
24.0	OPCON	9.1	6.5	6.5	7.2	4.2	9.0

Table F.2.4 Concentrations used in calculation of fluxes for E1

level (mm)	Instrument	Concentration (g/l)					
		0.85s	1.69s	2.54s	4.35s	5.31s	6.27s
0.0	CCM	1210	1203	1213	1198	1094	1204
2.0	CCM	485	480	471	580	553	448
3.5	CCM	414	435	248	568	548	391
5.0	CCM	57	80	40	118	193	94
9.5	OPCON	3.4	3.5	3.1	1.7	11.0	11.8
18.0	OPCON	3.1	2.8	2.3	1.6	4.0	5.0

Table F.2.5 Concentrations used in calculations of fluxes for E3

z(mm)	instru- ment	concentration (g/l)					
		0.68s	1.35s	2.03s	3.65s	4.60s	5.55s
-1.0	CCM	1564	1214	1452	1526	1566	1594
0.0	CCM	1237	897	1273	1224	1289	1414
2.0	CCM	59	220	152	83	50	18
5.0	OPCON	0.289	5.443	8.547	2.647	1.580	0.658
9.0	OPCON	0.320	0.561	2.837	2.322	0.665	0.494
20.0	OPCON	0.120	0.146	0.194	1.079	0.260	0.095

Table F.2.6 Concentrations used in calculations of fluxes for C

level (mm)	Sediment flux ( $10^{-3}$ m/s)					
	0.85s	1.69s	2.54s	4.35s	5.31s	6.27s
-1.5	0	-39	0	0	39	0
0.0	-55	-42	-43	102	72	49
2.5	-52	-63	-26	62	56	35
5.5	-60	-89	-44	68	118	60
8.0	-25	-63	-38	19	71	42
15.0	-6.5	-5.6	-6.2	4.1	5.9	8.6
24.0	-4.1	-2.7	-1.4	2.7	1.8	2.5

Table F.2.7 Sediment fluxes in the sheetflow layer for E1

level (mm)	Sediment flux ( $10^{-3}$ m/s)					
	0.85s	1.69s	2.54s	4.35s	5.31s	6.27s
0.0	-124	-151	-74	125	106	59
2.0	-86	-83	-61	120	108	39
3.5	-101	-98	-40	122	119	40
5.0	-13	-17	-6	31	37	9
9.5	-0.9	-0.8	-0.6	0.5	3.0	1.8
18.0	-1.1	-0.7	-0.4	0.5	1.4	1.1

Table F.2.8 Sediment fluxes in the sheetflow layer for E3

z(mm)	instru- ment	sediment flux ( $10^{-3}$ m/s)					
		0.68s	1.35s	2.03s	3.65s	4.60s	5.55s
-1.0	CCM	122	111	95	-103	-86	-81
0.0	CCM	172	142	112	-161	-107	-104
2.0	CCM	13	49	20	-15	-7	-2
5.0	OPCON	0.068	1.421	1.090	-0.547	-0.231	-0.087
9.0	OPCON	0.070	0.174	0.452	-0.567	-0.108	-0.078
20.0	OPCON	0.028	0.053	0.037	-0.255	-0.042	-0.015

Table F.2.9 Sediment fluxes in the sheetflow layer for C

Level (mm)	Negative Sediment flux ( $10^{-3}$ m)	Positive Sediment flux ( $10^{-3}$ m)	Total Sediment flux ( $10^{-3}$ m)	Sediment flux averaged over time ( $10^{-3}$ m/s)
-1.5	33.0	37.4	4.48	0.62
0.0	126.9	217.1	90.20	12.48
2.5	128.1	147.9	19.80	2.74
5.5	168.1	231.9	63.77	8.82
8.0	104.3	120.4	16.14	2.23
15.0	16.1	16.2	0.19	0.03
24.0	7.4	6.5	-0.90	-0.12
Total Sediment flux over height ( $10^{-6}$ m <sup>2</sup> /s)				67.5

Table F.2.10 Total fluxes in the sheetflow layer for E1

Level (mm)	Negative Sediment flux ( $10^{-3}$ m)	Positive Sediment flux ( $10^{-3}$ m)	Total Sediment flux ( $10^{-3}$ m)	Sediment flux averaged over time ( $10^{-3}$ m/s)
0.0	324.8	269.0	-55.8	-7.72
2.0	214.4	252.7	38.2	5.29
3.5	228.0	266.4	38.4	5.32
5.0	33.7	73.0	39.3	5.45
9.5	2.1	4.5	2.4	0.33
18.0	2.1	2.5	0.4	0.06
Total Sediment flux over height ( $10^{-6}$ m <sup>2</sup> /s)				28.27

*Table F.2.11 Total fluxes in the sheetflow layer for E3*

## G Listing of calculation modules of transport program

### G.1 Introduction

Only the calculation modules are listed below, not the whole program. In the total program this modules are arranged in such a way that calculation starts with the analysis of the velocity. Second the user chooses which transport module(s) should be used to calculate the transport. This transport modules are combined if necessary with modules to calculate the critical shields parameter, the bed-roughness height (method chosen by the user) and the bed shear stress (chosen by the user).

### G.2 Analysis of velocities

```
Procedure veloana(var urms,ugem,ucr,utr,xmax,u3,uorb:real);
var help3,xpos,xneg,ttest1,test2,tijd,factor,uoud:real;
    beg:boolean;

begin
  WRITELN(f);
  WRITELN(f, 'Analyze snelheden:');
  case keuzev of
    't': begin
      assign(h,velofile);
      reset(h);
      ugem := 0;
      xmax := 0;
      ucr := 0;
      utr := 0;
      u3 := 0;
      urms := 0;
      teller := 0;
      tijd := 0;
      factor := 1;
      beg := false;
      while not eof(h) do
        begin
          read(h,x,y);
          readln(h,u);
          help3 := sqrt(u)*u;
          u3 := u3 + help3;
          urms := urms + sqrt(u);
          ugem := ugem + u;
          if (u >= ucr) and (u > 0) then ucr := u;
          if (abs(u) >= utr) and (u < 0) then utr := abs(u);
          teller := teller + 1;
        end;
      urms := sqrt(urms/teller);
      u3 := u3/teller;
      ugem := ugem/teller;
      ucr := ucr - ugem;
      utr := utr + ugem;
      uorb := (ucr + utr)/2;
      close(h);
      reset(h);
      while not eof(h) do
        begin
          read(h,x,y);
          readln(h,u);
          if (u-ugem) > 0 then xmax := xmax + deltat*(u-ugem);
        end;
    end;
```

```

xmax := xmax/2;
close(h);
end;
'2': begin
  ugem := u0;
  uorb := abs(u1);
  ucr := u1 + u2;
  utr := u1 - u2;
  urms := sqrt(0.5*(u1*u1 + u2*u2));
  if u0 = 0 then u3 := 0.75*sqrt(u1)*u2
  else u3 := u0*u0*u0 + 1.5 * u0 * (sqrt(u1) + sqrt(u2)) + 0.75*sqrt(u1)*u2;
  xmax := abs(u1*periode/(2*pi));
end;
's': begin
  ugem := u0;
  urms := u1;
  uorb := abs(u1*sqrt(2));
  ucr := abs(u1*sqrt(2));
  utr := u1*sqrt(2);
  u3 := u0*u0*u0 + 3*u0*sqrt(u1);
  xmax := ucr*periode/(2*pi);
end;
end;

WRITELN(f, ' Gemiddelde snelheid.. = ', ugem:6:4, ' Orb. snelheid = ', uorb:6:4);
WRITELN(f, ' Ucrest..... = ', ucr :6:4, ' Utrough..... = ', utr:6:4);
WRITELN(f, ' derde snelheidsmoment = ', u3 :6:4, ' Xmax..... = ', xmax:7:4);
WRITELN(f, ' Urms..... = ', urms:6:4);
end;

```

### G.3 Calculation of critical shields parameter

Procedure shckr;

```

begin
  ds := g*(rho0-rho)/(rho*sqrt(visco));
  ds := macht(ds, 1/3);
  dster := d50*ds;
  WRITELN(f);
  WRITE(f, ' D* = ', dster:7:4);
  if (dster > 1) and (dster <= 4) then shc := 0.24/dster;
  if (dster > 4) and (dster <= 10) then shc := 0.14*macht(dster, -0.64);
  if (dster > 10) and (dster <= 20) then shc := 0.04*macht(dster, -0.1);
  if (dster > 20) and (dster <= 150) then shc := 0.013*macht(dster, 0.29);
  if dster > 150 then shc := 0.055;
  WRITELN(f, ' shields kritiek = ', shc);
  writeln;
end;

```

### G.4 Calculation of bed-roughness height

Procedure berekks(mb:char);

```

begin
  case mb of
    '1' : begin
      hks := 3*D90;
      ks := 3*D90;
      afw := 1;
      while (afw > 0.001) do begin
        z0 := hks/30;
        fc := 2*sqrt(0.4/ln(nivz/z0));
        fw := exp(-6 + 5.2*macht(hxmax/hks, -0.19));
        if fw >= 0.3 then fw := 0.3;
        taub := 0.25*rho*fw*sqrt(huorb) + 0.5*rho*fc*sqrt(hugem);
      end;
    end;
  end;

```

```

shields := taub/((rhos-rho)*g*D50);
if abs(shields) >= 1 then ks := 3*abs(shields)*D90;
afw := (abs(hks-ks))/ks;
hks := ks;
end;
WRITELN(f,' ks = 3* $\Theta$ *D90 = ',ks);
end;
'2': begin
ks := 3*D90;
z0 := ks/30;
WRITELN(f,' ks = 3*D90 = ',ks);
end;
'3': begin
ks := D50;
z0 := ks/30;
WRITELN(f,' ks = D50 = ',ks);
end;
'4': begin
write(' ks = '); readln(ks);
z0 := ks/30;
WRITELN(f,' ks = eigen keuze = ',ks);
end
end; {case}
writeln;
P1 := z0/nivz;
P2 := hxmax/z0;
WRITELN(f,' P1 = ',P1,' P2 = ',P2);
end;

```

## G.5 Modules to calculate bed shear stress

### G.5.1 Bed shear stress according to Ribberink/ van Rijn

```

Procedure Bsl(var taumax:real; var aantst:integer;var taub:ttype; ugem,uorb,xmax:real);

var y1,y2,taumaxw,tauc,taugem,taugemab,u,x,y,t,alpha:real;
i:integer;

begin
WRITELN(f);
WRITELN(f,'Bodemschuifspanning volgens Ribberink/van Rijn');
if keuzev = 't' then begin
assign(h,velofile);
reset(h);
end;
taumax := 0;
z0 := ks/30;
fc := 2*sqr(0.4/ln(nivz/z0));
fw := exp(-6 + 5.2*macht(xmax/ks,-0.19));
if fw > 0.3 then fw := 0.3;
alpha := abs(ugem)/(abs(ugem) + uorb);
fcw := alpha*fc + (1-alpha)*fw;
WRITELN(f,' fc = ',fc,' fw = ',fw,' fcw = ',fcw);
WRITELN(f);
taugem:=0; taugemab:=0;
aantst:= round(periode/deltat);
for i := 1 to aantst do begin
t := (i-1)*deltat;
case keuzev of
't':begin
read(h,x,y);
readln(h,u);
end;
's':u := ugem + uorb*sin((2*pi/periode)*t);
'2':u := u0 + u1*cos((2*pi/periode)*t) + u2*cos(2*(2*pi/periode)*t);
end;

```

```

taub[i] := 0.5*rho*fcw*u*abs(u);
taugem := taugem + taub[i];
taugemab := taugemab + abs(taub[i]);
if abs(taub[i]) >= taumax then taumax := abs(taub[i]);
end;

tauc := 0.5*rho*fc*abs(ugem)*ugem;
taumaxw := 0.5*rho*fw*abs(uorb)*uorb;
taugem := taugem/aantst;
taugemab := taugemab/aantst;

if keuzev = 't' then close(h);
WRITELN(f, ' eerst is de absolute waardegegeven daarna de dimensieloze');
WRITELN(f);
WRITELN(f, ' TAUgem = ',taugem:7:4, ', ',taugem/shfactor:7:4 );
WRITELN(f, ' TAUgem,abs = ',taugemab:7:4, ', ',taugemab/shfactor:7:4 );
WRITELN(f, ' TAUmax = ',taumax:7:4, ', ',taumax/shfactor:7:4 );
WRITELN(f, ' TAUwave = ',taumaxw:7:4, ', ',taumaxw/shfactor:7:4 );
WRITELN(f, ' TAUcurrent = ',tauc:7:4, ', ',tauc/shfactor:7:4 );
x := tauc/(tauc+taumaxw);
y1 := taugem/(tauc+taumaxw);
y2 := taumax/(tauc+taumaxw);
WRITELN(f, ' x = ',x:6:4, ' y1 = ',y1:6:4, ' y2 = ',y2:6:4);
if keuze = '7' then write(qq,x:10:5,y1:10:5,y2:10:5);
end;

```

## G.5.2 Bed shear stress according to Soulsby/ Ockenden

```

Procedure Bs2(var taumax:real;var aantst:integer;var taub:ttype;ugem,uorb,xmax:real);

var Ax,Wx,tauc,taumaxw,cd,tc,tw,a,b,m,n,p,q,x1,taugem,taugemab,fwplus,fcplus,t,x,y,u:real;
y1,y2:double;
i:integer;

begin
Ax := sqrt(2)*urms*periode/(2*pi);
Wx := sqrt(2)*urms;
if keuzev = 't' then begin
assign(h,velofile);
reset(h);
end;
writeln(f);
writeln(f,'Bodemschuifspanning volgens Soulsby');

cd := sqrt(0.4/(ln(30*nivz/ks)-1));
fc := 2*sqrt(0.4/(ln(30*nivz/ks)));
fw := exp(-6 + 5.2*macht(Ax/ks,-0.19));

a := (-0.06 + 1.70) + (-0.29+0.29)*log(fw/cd);
b := (0.29 + 0.55) + (-0.10-0.14)*log(fw/cd);
m := (0.67 - 0.29) + (0.09+0.42)*log(fw/cd);
n := (0.75 - 0.27) + (0.11-0.02)*log(fw/cd);
p := (-0.77 + 0.10) + (0.27+0.14)*log(fw/cd);
q := (0.91 + 0.25) + (0.50+0.45)*log(fw/cd);

tc := 0.5*rho*fc*ugem*ugem;
tw := 0.5*rho*fw*sqrt(Wx);

x1 := tc/(tc+tw);
y1 := macht(1-x1,n);
y1 := y1*a * macht(x1,m) + 1;
y2 := macht(1-x1,q);
y2 := 1 + b*macht(x1,p)* y2;
y2 := y2*x1;
taumax := y1 *(tc + tw);
taugem := y2 *(tc + tw);
fcplus := taugem/(0.5*rho*ugem*ugem);
fwplus := (taumax - taugem)/(0.5*rho*sqrt(wx));

```

```

WRITELN(f, ' fc = ',fc, ' fw = ',fw );
WRITELN(f, ' fc+ = ',fcplus, ' fw+ = ',fwplus );
aantst:= round(periode/deltat);
taugem := 0;
taugemab:=0;
taumax := 0;
for i := 1 to aantst do begin
  t := (i-1)*deltat;
  case keuzev of
    't':begin
      read(h,x,y);
      readln(h,u);
      u := u-ugem;
      end;
    's':u := uorb*sin((2*pi/periode)*t);
    '2':u := u1*cos((2*pi/periode)*t) + u2*cos(2*(2*pi/periode)*t);
  end;
  taub[i] := 0.5*rho*fcplus*ugem*abs(ugem)+0.5*rho*fwplus*abs(u)*u;
  taugem := taugem + taub[i];
  taugemab := taugemab + abs(taub[i]);
  if abs(taub[i]) >= taumax then taumax := abs(taub[i]);
end;
tauc := 0.5*rho*fc*abs(ugem)*ugem;
taumaxw := 0.5*rho*fw*abs(uorb)*uorb;
taugem := taugem/aantst;
taugemab := taugemab/aantst;

if keuzev = 't' then close(h);
WRITELN(f);
WRITELN(f, ' eerst is de absolute waardegegeven daarna de dimensiezoze');
WRITELN(f);
WRITELN(f, ' TAUgem = ',taugem:7:4, ' ',taugem/shfactor:7:4 );
WRITELN(f, ' TAUgem,abs = ',taugemab:7:4, ' ',taugemab/shfactor:7:4 );
WRITELN(f, ' TAUmax = ',taumax :7:4, ' ',taumax/shfactor:7:4 );
WRITELN(f, ' TAUwave = ',taumaxw:7:4, ' ',taumaxw/shfactor:7:4 );
WRITELN(f, ' TAUcurrent = ',tauc :7:4, ' ',tauc/shfactor:7:4 );
x := tauc/(tauc+taumaxw);
y1 := taugem/(tauc+taumaxw);
y2 := taumax/(tauc+taumaxw);
WRITELN(f, ' x = ',x:6:4, ' y1 = ',y1:6:4, ' y2 = ',y2:6:4);
if keuze = '7' then writeln(qq,y1:10:5,y2:10:5);
end;

```

### G.5.3 Bed shear stress imported from 1-DV model of Al-Salem

```

Procedure Bs3(var taumax:real; var aantst:integer;var taub:ttype;ugem,uorb,xmax:real);

```

```

var i:integer;
    filen:string;
    y1,y2,tauc,taumaxw,taugem,taugemab,x,y:real;

begin
  taumax:=0;
  writeln;
  write(' Filenaam van bodemschuifspanningsfile? ');
  readln(filen);
  write('Hoeveel punten wilt u inlezen? '); readln(aantst);
  assign(h,filen);
  reset(h);
  WRITELN(f);
  WRITELN(f,'Bodemschuifspanning ingelezen vanuit 1DV-model, ',filen);
  for i := 1 to aantst do begin
    read(h,x,y);
    readln(h,taub[i]);
    taub[i] := taub[i]*rho;
    taugem := taugem + taub[i];
    taugemab := taugemab + abs(taub[i]);
    if abs(taub[i]) >= taumax then taumax := abs(taub[i]);
  end;

```

```

end;
taugem := taugem/aantst;
taugemab := taugemab/aantst;
if keuzev = 't' then close(h);
fc := 2*sqrt(0.4/(ln(30*nivz/ks)));
fw := exp(-6 + 5.2*macht(xmax/ks,-0.19));
tauc := 0.5*rho*fc*abs(ugem)*ugem;
taumaxw := 0.5*rho*fw*abs(uorb)*uorb;
WRITELN(f);
WRITELN(f,' eerst is de absolute waarde gegeven daarna de dimensieloze');
WRITELN(f);
WRITELN(f,' TAUgem = ',taugem :7:4 , ' ',taugem/shfactor:7:4 );
WRITELN(f,' TAUgem,abs = ',taugemab:7:4 , ' ',taugemab/shfactor:7:4 );
WRITELN(f,' TAUmax = ',taumax :7:4 , ' ',taumax/shfactor:7:4 );
WRITELN(f,' TAUwave = ',taumaxw:7:4 , ' ',taumaxw/shfactor:7:4 );
WRITELN(f,' TAUcurrent = ',tauc :7:4 , ' ',tauc/shfactor:7:4 );
x := tauc/(tauc+taumaxw);
y1 := taugem/(tauc+taumaxw);
y2 := taumax/(tauc+taumaxw);
WRITELN(f,' x = ',x:6:4,' y1 = ',y1:6:4,' y2 = ',y2:6:4);
if keuze = '7' then writeln(qq,y1:10:5,y2:10:5);
close(h);
end;

```

## G.6 Modules to calculate sediment transport

### G.6.1 Transport calculated with Al-Salem's method

Procedure M1(u3:real);

```

begin
q := Am*u3;
WRITELN(f);
WRITELN(f,'Bodemtransport volgens Abdullah = ',q);
end;

```

### G.6.2 Transport calculated with the method of Ribberink and Al-Salem

Procedure M2(taub:ttype;aantstsch:integer);

```

var i:integer;
phis,uster,uster3:real;

begin
uster3 := 0;
for i := 1 to aantstsch do begin
uster := sqrt(abs(taub[i])/rho);
if taub[i] = 0 then uster3 := uster3 + macht(uster,3)
else uster3 := uster3 + macht(uster,3)*taub[i]/abs(taub[i]);
end;
uster3 := uster3/aantstsch;
phis := 4*uster3/(macht(Ws,3));
q := Ws*D50*4*uster3/(macht(Ws,3));
WRITELN(f);
WRITELN(f,'Bodemtransport volgens Abdullah & Ribberink = ',q,' ',phis);
end;

```

### G.6.3 Transport calculated with the method of Bailard

```

Procedure M3(utr,ucr,uorb,ugem,taumax:real);

var uhelpl,uhelp2,umax,delta,qb,qs,u3,u4,t,x,y,u,fcw:real;
    aantst,i:integer;

begin
  delta:=(rho-rho)/rho;
  u3:=0;
  u4:=0;
  uhelpl:=utr-ugem;
  uhelp2:=ucr+ugem;
  if uhelpl >= uhelp2 then umax:=uhelpl else umax:=uhelp2;
  fcw:=taumax/(0.5*rho*sqr(umax));
  if keuzev='t' then begin assign(h,velofile); reset(h); end;
  aantst:=round(periode/deltat);
  for i:=1 to aantst do begin
    t:=(i-1)*deltat;
    case keuzev of
      't':begin
        read(h,x,y);
        readln(h,u);
        end;
      's':u:=ugem+uorb*sin((2*pi/periode)*t);
      '2':u:=ugem+u1*cos((2*pi/periode)*t)+u2*cos(2*(2*pi/periode)*t);
    end;
    u3:=u3+u*u*u;
    u4:=u4+abs(u*u*u)*u;
  end;
  if keuzev='t' then close(h);
  u3:=u3/aantst;
  u4:=u4/aantst;
  qb:=(0.5*fcw*eb/(delta*g*tanfi))*u3;
  qs:=(0.5*fcw*es/(delta*g*Ws))*u4;
  q:=qb+qs;
  WRITELN(f);
  WRITELN(f,'Totaal transport volgens Bailard = ',q);
  WRITELN(f,' Bodemtransport = ',qb);
  WRITELN(f,' Suspensietransport = ',qs);
end;

```

### G.6.4 Transport calculated with the new method of Ribberink

```

Procedure M4(taub:type;aantstsch:integer);

var shieldsrep,phis,para,delta,shields:real;
    i:integer;

begin
  delta:=(rho-rho)/rho;
  para:=sqrt(delta*g*macht(D50,3));
  phis:=0;
  for i:=1 to aantstsch do begin
    shields:=taub[i]/((rho-rho)*g*D50);
    if abs(shields) >= shc then
      phis:=phis+m*macht((abs(shields)-shc),n)*(shields/abs(shields));
    end;
  phis:=phis/aantstsch;
  if phis >= 0 then shieldsrep:=shc+macht(phis/m,1/n)
  else shieldsrep:=-shc-macht(abs(phis)/m,1/n);
  q:=para*phis;
  WRITELN(f);
  WRITELN(f,'Bodemtransport volgens nieuw methode Ribberink = ',q,' ',phis);
  WRITELN(f,' shields-representatief = ',shieldsrep);
end;

```

### G.6.5 Transport calculated with the method of Dibajnia and Watanabe

```

Procedure M5(ugem,uorb:real);

var transport:double;
    omegac3,omegat3,omegaca3,omegata3,omegac,omegat,omegaca,omegata,delta,
    phis,wc,wt,uc,ut,uc2,ut2,Tc,Tt,t:real;
    tellerc,tellert,i:integer;

begin
if keuzev = 't' then begin
    assign(h,velofile);
    reset(h);
end;
aantstve:= round(periode/deltat);
delta:= (rhos-rho)/rho;
Tc := 0; Tt:=0; uc2:=0; ut2:=0; tellerc := 0; tellert :=0;
for i := 1 to aantstve do begin
    t := (i -1)*deltat;
    case keuzev of
    't':begin
        read(h,x,y);
        readln(h,u);
        end;
    's':u := ugem + uorb*sin((2*pi/periode)*t);
    '2':u := u0 + u1*cos((2*pi/periode)*t) + u2*cos(2*(2*pi/periode)*t);
    end;
    if u > 0 then begin
        Tc := Tc + deltat;
        tellerc := tellerc+1;
        uc2 := uc2 + sqrt(u);
    end
    else begin
        Tt := Tt + deltat;
        tellert := tellert+1;
        ut2 := ut2 + sqrt(u);
    end;
end;
uc2 := (2/tellerc)*uc2;
ut2 := (2/tellert)*ut2;
uc := sqrt(uc2);
ut := sqrt(ut2);
wc := 0.5*uc2/(delta*g*Ws*Tc);
wt := 0.5*ut2/(delta*g*Ws*Tt);
if wc <= 1 then begin
    omegac := 2*wc*Ws*Tc/D50;
    omegaca := 0;
end
else begin
    omegac := 2*Ws*Tc/D50;
    omegaca := 2*(wc-1)*Ws*Tc/D50;
end;
if wt <= 1 then begin
    omegat := 2*wt*Ws*Tt/D50;
    omegata := 0;
end
else begin
    omegat := 2*Ws*Tt/D50;
    omegata := 2*(wt-1)*Ws*Tt/D50;
end;
if keuzev = 't' then close(h);
omegac3 := sqrt(omegac)*omegac;
omegat3 := sqrt(omegat)*omegat;
omegaca3 := sqrt(omegaca)*omegaca;
omegata3 := sqrt(omegata)*omegata;

transport:= (uc*Tc*(omegac3 + omegata3) - (ut*Tt*(omegat3 + omegaca3)));
transport := transport/((uc+ut)*periode);
phis := 0.001* macht(abs(transport),0.55)*transport/abs(transport);
q := Ws*D50*phis;

```

```
WRITELN(f);  
WRITELN(f,'Totaaltransport volgens Watanabe = ',q,' ',phis);  
WRITELN(f,' Ωc = ',omegac:6:2,' Ωc'' = ',omegaca:6:2);  
WRITELN(f,' Ωt = ',omegat:6:2,' Ωt'' = ',omegata:6:2);  
WRITELN(xyz,Naam:10,' Ωc = ',omegac:6:2,' Ωc'' = ',omegaca:6:2,' Ωt = ',omegat:6:2,' Ωt'' = ',omegata:6:2 )  
end;
```



## References

- Al-Salem, A.A. (1993)  
"Sediment transport in oscillatory boundary layers under sheetflow conditions".  
Ph.D. thesis Delft University of Technology.
- Bagnold, R.A. (1963)  
"Mechanics of marine sedimentation". The sea, Vol 3, Wiley-Interscience, New  
York, pp 507-528.
- Bagnold, R.A. (1966)  
"An approach to the sediment transport problem from general physics".  
Professional Paper 422-I, US Geological Survey, pp 1-37.
- Bailard, J.A. (1981)  
"An energetics total load sediment transport model for a plane sloping beach".  
Journal of Geophysical Research, Vol.86, C3, pp 2035-2043.
- Bosman, J.J. (1982)  
"Concentration measurement under oscillatory water motion". Report M1695,  
DELFT HYDRAULICS.
- Bosman, J.J. (1984)  
"Calibration of optical systems for sediment concentration measurements". Report  
R716, Part 5, DELFT HYDRAULICS.
- Bosman, J.J., Van der Velden, E.J.T.M. and Hulsbergen, C.H. (1987)  
"Sediment concentration measured by transverse suction system". Coastal  
engineering, 11, pp 353-370.
- Chen, Z. (1991)  
"Sediment concentrations and sediment transport due to action of waves and a  
current". Ph.D. thesis Delft University of Technology.
- Christoffersen, J.E. and Jonsson, I.G. (1985)  
"Bed friction and dissipation in a combined wave and current and wave motion",  
Ocean Engineering, 12(5): pp. 387-423.
- Dibajnia, M. and Watanabe, A. (1992)  
"Sheet flow under nonlinear waves and currents". Proceedings of the 23<sup>th</sup>  
Conference on Coastal Engineering, pp. 2015-2028.
- Dick, J.E. and Sleath, J. F. A. (1991)  
"Velocities and concentrations in oscillatory flow over beds of sediment". J. Fluid  
Mech., vol 223, pp 165-196.

- Dick, J.E. and Sleath, J. F. A. (1992)  
"Sediment transport in oscillatory sheet flow". *Journal of Geophysical Research* vol. 97, no C4, pp 5745-5758.
- Jonsson, I.G. (1966)  
"Wave boundary layers and friction factors", *Proceedings of the 10<sup>th</sup> Conference on Coastal Engineering*, pp. 127-148.
- Horikawa, K., Watanabe, A., and Katori, S. (1982)  
"Sediment transport under sheetflow condition". *Proceedings of the 18<sup>th</sup> Conference on Coastal Engineering*, pp. 1335-1352.
- Katapodi, I., Ribberink, J.S., Ruol, P., Koelewijn, R., Lodahl, C., Longo, S., Crosato, A., and Wallace, H. (1994)  
"Intra-wave sediment transport in an oscillatory flow superimposed on a mean current". *Data report H1570.10, Part III*.
- Prandtl, L. (1926)  
"On fully developed turbulence". *Proceedings 2<sup>nd</sup> International Congress of Applied Mechanics, Zurich*, pp 62-74.
- Ramadan, K.A.H. (1993)  
"Time-averaged sediment transport phenomena in combined wave-current flows". *Delft Hydraulics Report H1889.11, Part I*.
- Ribberink, J.S. (1989).  
"The large oscillating water tunnel. Technical specifications and performances". *Delft Hydraulics report H840, Part I*.
- Ribberink, J.S. and Al-Salem, A. (1992)  
"Time-dependent sediment transport phenomena in oscillatory boundary-layer flow under sheet flow conditions". *Delft Hydraulics report H840.20, Part VI*.
- Ribberink, J.S and Chen, Z. (1993)  
"Sediment transport of fine sand under asymmetric oscillatory flow". *Delft Hydraulics report H 840.20, Part VII*.
- Ribberink, J.S. (1994)  
"Time-averaged sediment transport phenomena in combined wave-current flows". *Delft Hydraulics Report H1889.11, Part II*.
- Ribberink, J.S. and Al-Salem, A. (1994)  
"Sediment transport in oscillatory boundary layers in case of rippled beds and sheet flow". *Journal of Geophysical research*, volume 99, no. C6, pp. 12.707-12.727.

- Rijn, L.C. van, 1993  
"Principles of sediment transport in rivers, estuaries and coastal seas". Aqua publications, Amsterdam.
- Sawamoto, M., and Yamashita, T. (1986)  
"Sediment transport rate due to wave action". Journal of Hydroscience and Hydraulic Engineering Vol. 4, No. 1, pp.1-15.
- Soulsby, R.L., Hamm, L., Klopman, G., Myrhaug, D., Simons, R.R., and Thomas, G.P. (1993)  
"Wave-current interaction within and outside the bottom boundary layer". Coastal engineering, 21, pp 41-69, Elsevier Science Publishers B.V., Amsterdam.
- Soulsby, R.L. and Ockenden, M.C. (1994)  
"Sediment transport by currents plus irregular waves". Report SR 237, HR Wallingford.
- Staub, C., Jonsson, I.G. and Svendsen, I.A. (1984)  
"Variation of sediment suspension in oscillatory flow". Proceedings of the 19<sup>th</sup> Conference on Coastal Engineering, pp. 2310-2321.
- Swart, D.H. (1974)  
"Offshore sediment transport and equilibrium beach profiles", doctorate dissertation, Delft University of Technology.
- Wilson, K.C. (1987)  
"Analysis of bed load motion at high shear stress". Journal of Hydraulic Engineering, ASCE, No.1.



## List of Symbols

Symbol	Units	Definition
$\langle \dots \rangle$	[..]	Time averaged
$\sim$	[..]	Wave-related part
$C'$	[-]	Chezy friction coefficient based on grain roughness (= $18^{10} \log(12h/k_s)$ )
$C_D$	[-]	Current drag coefficient
$D_{50}$	[mm]	Median grain diameter
$f_c$	[-]	Current friction factor
$f_c^+$	[-]	Enhanced current friction factor for combined wave-current flow
$f_{cw}$	[-]	Friction factor for combined wave-current flow
$f_w$	[-]	Wave friction factor
$f_w^+$	[-]	Enhanced wave friction factor for combined wave-current flow
$g$	[m/s <sup>2</sup> ]	Gravity acceleration
$h$	[m]	Waterdepth
$k_s$	[m]	Nikuradse bed-roughness height
$p$	[N/m <sup>2</sup> ]	Pressure
$q_b$	[m <sup>2</sup> /s]	Bed load transport rate in real volume per unit time and width
$q_s$	[m <sup>2</sup> /s]	Suspended load transport rate in real volume per unit time and width
$R$	[-]	Degree of asymmetry of the horizontal flow
$T$	[s]	Period of the oscillatory flow
$u$	[m/s]	Horizontal velocity
$u_b$	[m/s]	Velocity at level $z$ above the bed
$u_b(t)$	[m/s]	Near bed horizontal time dependent velocity of the combined wave-current motion
$\langle u_b \rangle$	[m/s]	Time averaged or mean current velocity
$\hat{u}$	[m/s]	Velocity amplitude of the oscillatory flow (without mean current)
$u_c$	[m/s]	Maximum horizontal velocity in wave direction
$u_t$	[m/s]	Maximum horizontal velocity opposite to the wave direction
$\langle u^3 \rangle$	[m <sup>3</sup> /s <sup>3</sup> ]	Third order velocity moment
$u_\infty$	[m/s]	Free stream velocity
$\bar{u}_b(t)$	[m/s]	Oscillatory component of the near bed velocity
$u_*$	[m/s]	Skin friction velocity ( $u_* = \sqrt{\tau/\rho}$ )
$v$	[m/s]	Depth-averaged current velocity
$x$	[m]	Horizontal coordinate (parallel to the tunnel)
$\hat{x}$	[m]	Amplitude of horizontal oscillatory flow  (sinusoidal $\hat{x} = \hat{u} \cdot T/2\pi$ )
$y$	[m]	Horizontal coordinate (perpendicular to the tunnel)
$W_s$	[m/s]	Fall velocity of sediment particles
$z$	[m]	Vertical coordinate
$z_0$	[m]	Zero velocity level

$\alpha$	[-]	Weighing factor used to calculate the bed shear stress according to Ribberink's formula
$\epsilon_b$	[-]	Bed load efficiency factor for Bailard's formula (= 0.1)
$\epsilon_s$	[-]	Suspended load efficiency factor for Bailard's formula (= 0.02)
$\phi$	[-]	Angle of internal friction of the element
$\phi$	[m/s]	Horizontal sediment flux
$\phi_{bd}$	[-]	Non-dimensional transport rate
$\theta'(t)$	[-]	Shields parameter based on skin-friction
$\theta_c$	[-]	Critical Shields parameter
$\tau$	[N/m <sup>2</sup> ]	Shear stress
$\tau_b$	[N/m <sup>2</sup> ]	Bed shear stress
$\tau_{b,max}$	[N/m <sup>2</sup> ]	Maximum bed shear stress
$\rho_s$	[kg/m <sup>3</sup> ]	Density of sand
$\rho$	[kg/m <sup>3</sup> ]	Density of water
$\Delta$	[-]	Relative density = $(\rho_s - \rho) / \rho$
$\nu$	[m <sup>2</sup> /s]	Kinematic viscosity of water
$\kappa$	[-]	Von Karman coefficient
$\nu_t$	[m <sup>2</sup> /s]	Turbulent eddy viscosity